LIBRARY
Michigan State
University

This is to certify that the
dissertation entitled

CATALYTIC MEMBRANES PREPARED BY ADSORPTION OF POLYELECTROLYTE/METAL NANOPARTICLE FILMS IN POROUS SUPPORTS

presented by

DAVID M. DOTZAUER

has been accepted towards fulfillment
of the requirements for the

Ph.D. degree in Chemistry

Major Professor's Signature

Date

MSU is an Affirmative Action/Equal Opportunity Employer

PLACE IN RETURN BOX to remove this checkout from your record.
TO AVOID FINES return on or before date due.
MAY BE RECALLED with earlier due date if requested.

DATE DUE	DATE DUE	DATE DUE

5/08 K:/Proj/Acc&Pres/CIRC/DateDue.indd

CATALYTIC MEMBRANES PREPARED BY ADSORPTION OF POLYELECTROLYTE/METAL NANOPARTICLE FILMS IN POROUS SUPPORTS

By

David M. Dotzauer

A DISSERTATION

Submitted to
Michigan State University
in partial fulfillment of the requirements
for the degree of

DOCTOR OF PHILOSOPHY

Chemistry

2009

ABSTRACT

CATALYTIC MEMBRANES PREPARED BY ADSORPTION OF POLYELECTROLYTE/METAL NANOPARTICLE FILMS IN POROUS SUPPORTS

By

David M. Dotzauer

Well-defined metal nanoparticles are attractive for catalytic applications because of their high specific surface area and unique electronic properties. However, the high surface energy of these particles often leads to their aggregation so the nanoparticles must be capped with a stabilizer or immobilized on a support. This dissertation demonstrates metal nanoparticle immobilization in porous membranes via layer-by-layer (LbL) adsorption of polyelectrolyte/metal nanoparticle films and the potential advantages of these membranes for catalytic applications including reduction of nitro compounds, hydrogenation, and wet air oxidation for wastewater treatment. The immobilization method utilizes electrostatic interactions to facilitate deposition of oppositely charged polyelectrolytes and nanoparticles, and controlled synthesis of the nanoparticles prior to their deposition allows tuning of the nanoparticle size and composition for specific catalytic processes. Nanoparticles can also be formed after film deposition by incorporating metal ions into the polyelectrolyte film and later reducing these metal ions to form nanoparticles with diameters of 2-4 nm.

LbL deposition of polyelectrolyte/Au nanoparticle films in porous alumina and polymer substrates yields catalytic membranes with a high density of well-separated Au nanoparticles in the membrane pores. These nanoparticles catalyze the reduction of nitroaromatic compounds by sodium borohydride with

rate constants that are the same as those for nanoparticles in solution. Moreover, the membranes selectively catalyze the reduction of nitro groups in compounds containing other reducible functionalities such as cyano, chloro, and styrenyl moieties. These membranes are particularly attractive for controlling product distributions through variation of solution fluxes.

Membrane catalysts also facilitate contact between reactants in gas/liquid reactions by operating as flow-through or interfacial contactors. LbL deposition of polyelectrolyte/Pd nanoparticle films in flat membranes yields flow-through contactors that effectively hydrogenate allyl alcohol to 1-propanol when flowing H_2-saturated solutions through these membranes. Hydrogen reacts completely after one pass of the solution through the modified membranes, and thus the reaction is limited by the solubility of H_2 in the reactant solution. The interfacial contactor configuration, in which a tubular membrane separates the gas and liquid phases, provides enhanced contact between the immobilized catalytic nanoparticles and the gas/liquid interface. Control over the catalyst location in such membranes is crucial for efficient use of noble metals. LbL adsorption of polyelectrolyte/Pt nanoparticle films in tubular ceramic membranes allows deposition of the catalytic nanoparticles only near the interior of tube, where the gas/liquid interface is typically located. In wet air oxidation of formic acid, acetic acid, and phenol, tubular membranes modified by LbL deposition showed 2 to 10 times higher specific activities than similar membranes modified by conventional impregnation techniques, presumably due to controlled deposition of the Pt nanoparticles in the membrane.

To my wife, Heather, for all her love and support

ACKNOWLEDGEMENTS

I'd first like to thank my advisor, Dr. Merlin Bruening, for being a great advisor over the last four years. He has offered guidance when needed, but has also forced me to think and work independently so that I may learn. I appreciate his patience, when things were not working, his lack of patience, when things were working, and his positive encouragement throughout the entire process.

I would like to express gratitude to past and present members in the Bruening group for their help and suggestions in the last four years. I am especially grateful to Dr. Somnath Bhattacharjee, Dr. Jinhua Dai, Dr. Lei Sun, and Dr. Lu Ouyang for their direct involvement in my research projects. I would also like to thank Ya Wen, Stephanie Koszalka, and Katie Worley for their contributions to this work.

I want to thank Dr. Sylvain Miachon for being my co-advisor and giving me the opportunity to work with him at the Institute for Researches on Catalysis and the Environment in Lyon, France. He was a remarkable colleague and will be greatly missed.

Thank you to the MSU Department of Chemistry, the National Science Foundation, and the American Chemical Society for funding my research and providing me with many great opportunities during my time at Michigan State.

Lastly, I want to give a special thank you to my family for all of their support through the years and especially my wife, Heather, for her continuous encouragement and understanding.

TABLE OF CONTENTS

LIST OF TABLES

LIST OF FIGURES

LIST OF SCHEMES

LIST OF ABBREVIATIONS

LbL.....layer-by-layer

PAA.....poly(acrylic acid)

PSS.....poly(styrene sulfonate)

PEI.....poly(ethylenimine)

PAH.....poly(allylamine hydrochloride)

PVP.....poly(vinylpyrrolidone)

PAMAM.....poly(amidoamine)

PPI.....poly(propylenimine)

MSA.....mercaptosuccinic acid

NP.....nanoparticle

AuNP.....gold nanoparticle

PdNP.....palladium nanoparticle

PtNP.....platinum nanoparticle

CVD.....chemical vapor deposition

TEM.....transmission electron microscopy

FESEM.....field-emission scanning electron microscopy

GC.....gas chromatography

GC-MS.....gas chromatography-mass spectrometry

TOC.....total organic carbon

HPLC.....high performance liquid chromatography

IC.....ion chromatography

ICP-OES.....inductively coupled plasma-optical emission spectroscopy

FAAS.....flame atomic absorption spectroscopy

FAES.....flame atomic emission spectroscopy

SAM.....self assembled monolayer

UV-Vis.....ultraviolet-visible

TOF.....turnover frequency

Chapter One: Introduction

1.1 Introduction to Catalysis

Catalysts are used in roughly 90% of chemical processes, so it is essential to produce catalytic materials that are efficient, reusable, and broadly applicable to a wide range of processes.[1] In general, the purpose of a catalyst is to make chemical processes more efficient by accelerating the rate at which chemical reactions proceed. Catalysts do not change the thermodynamics of a reaction, but rather they change the kinetics of a reaction. Hence they are only useful for reactions that are thermodynamically favorable. Typical catalytic reactions between two molecules involve three steps: binding of reactants to the catalyst, reaction, and separation of the product from the catalyst.[2] As figure 1.1 shows, by incorporating a catalyst, the reaction has become more complex, but much more energetically favorable.

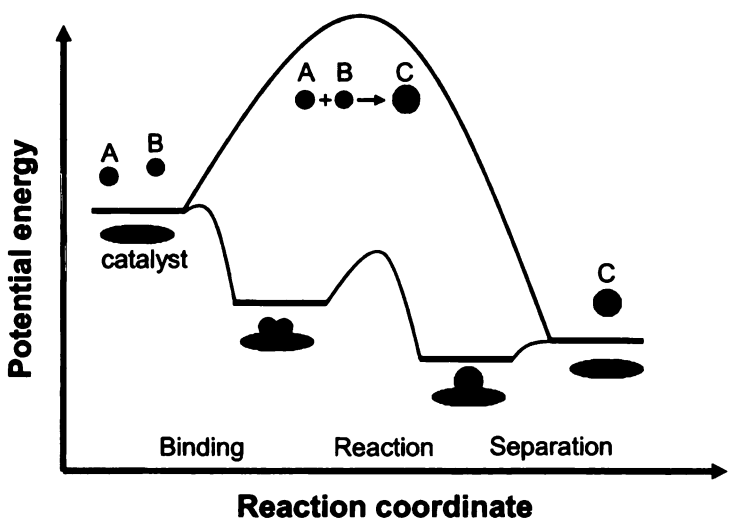

Figure 1.1 Potential energy diagram of a catalyzed and uncatalyzed reaction in which A and B react to form a single product, C. Figure adapted from Chorkendorff et al.[2]

Catalysts are frequently classified as enzymatic, homogeneous, or heterogeneous. Enzymatic catalysts are the most specific of the three types; they allow biological reactions to occur at the rates necessary for living systems to survive.[3] Homogeneous catalysts reside in the same phase as the reactants, and are often comprised of single molecules. Conversely, heterogeneous catalysts are solids, usually in the form of supported transition metals, which catalyze reactions of molecules in liquid or gaseous phases. As a result, heterogeneous catalysis takes place at an interface between a gas or liquid and a solid surface, where many different types of active sites may be involved in the reaction. The heterogeneity of the solid often leads to decreased selectivity.

Because homogeneous catalysts are most often individual molecules, the reactions typically take place on a single active site. Common advantages of homogeneous catalysts relative to heterogeneous systems include: higher selectivity and reproducibility, milder reaction conditions, ready chemical modification, and greater efficiency due to participation of all metal atoms in the catalytic reaction.[3] However, homogeneous catalysts are also more expensive, less robust, and more difficult to separate from reaction mixtures than heterogeneous catalysts. Thus, heterogeneous catalysts are still more widely used for industrial applications, while homogeneous catalysts are primarily employed for fine chemical synthesis.

Much of the ongoing research in heterogeneous catalysis focuses on bridging the gap between homogeneous and heterogeneous catalysts and overcoming the disadvantages described above. Specifically, interest in using

novel nanoparticles for catalysis has dramatically increased in the last decade because these materials have extremely high surface area to volume ratios that lead to efficient use of expensive metals. Many recent studies show that the properties of nanoparticles can be tuned to achieve high selectivity and efficient use of precious metals.[4-6] Thus, metal nanoparticle catalysts are increasingly being used in fine chemical synthesis and other reactions that historically relied on homogeneous catalysts.[7,8]

This dissertation discusses catalysis by supported noble metal nanoparticles with a specific focus on the use of porous membranes and polyelectrolyte multilayer films for nanoparticle immobilization. These catalysts exhibit excellent activities in a number of catalytic applications including reduction, hydrogenation, and oxidation reactions. The remainder of this chapter provides a review of recent work in the fields of nanoparticle catalysis and catalytic membranes to show the significance of this work. We first describe the most common catalyst supports and discuss the advantages and disadvantages of each material. We then discuss the benefits of using porous membranes as catalyst supports and describe the common types of catalytic membranes. A thorough discussion of traditional methods for in-situ and ex-situ incorporation of metal nanoparticles in porous supports follows, with special attention to formation of polyelectrolyte/metal nanoparticle films. Finally, a brief overview of the studies described in each of the remaining chapters is provided.

1.2 Nanoparticles and Catalysis

Metal nanoparticles were likely observed over 2500 years ago. For example, colloidal gold was used as early as the 5th century B.C. for coloring ruby glass and other ceramic materials.[9] In 1857, Faraday reported the formation of deep red solutions of colloidal gold by reduction of $AuCl_4^-$ using phosphorus in CS_2.[10] However, in the last 20 years, the study of metal nanoparticles has increased dramatically due to their unique size-related optical and electronic properties.[11-13] This interest is especially apparent in the field of catalysis because metal nanoparticles often show large increases in activity compared with their bulk metal counterparts.

Initial reports of nanoparticle catalysts include the use of silver nanoparticles for photography and platinum nanoparticles for the decomposition of hydrogen peroxide in the 1800's.[14] However, it wasn't until the work of Bond and Sermon[15,16] in the 1970's and Haruta[17-19] in the 1980's that researchers began showing interest in *controlled* nanoparticles for catalysis. This increased interest is partly due to the fact that these works showed that gold nanoparticles could be highly active catalysts even though bulk gold is typically an ineffective catalyst.[20,21] Haruta[22] and Goodman[6] later demonstrated that TiO_2-supported Au nanoparticles showed increased activity in CO oxidation when decreasing the nanoparticle diameter from 6 nm to 3 nm, but then showed decreased activity with nanoparticle diameters lower than 3 nm. This discovery led to an explosion of interest in trying to understand the mechanisms of reactions at nanoparticle

surfaces and in developing new methods to produce highly active and selective nanoparticle catalysts.[8,23-25]

From the numerous studies published on catalytic nanoparticles, it is clear that the most active nanoparticles have sizes on the order of 1 to 10 nm. However, the high surface energy of nanoparticles with diameters in this low nm range often leads to aggregation, which decreases the catalyst activity.[26-28] Stabilization of metal nanoparticles typically occurs through immobilization on a suitable support or addition of a stabilizing agent.

1.3 Common Nanoparticle Supports

The most effective catalyst supports should have high surface areas to facilitate loading of the catalyst. Thus, highly porous materials such as ceramics, metal oxides, carbonaceous materials, polymers, and a number of other materials are commonly used as catalyst supports. The properties of the support material often influence both the preparation of nanoparticle catalysts as well as their reactivity. Each support offers its own advantages for specific applications.

1.3.1 Metal Oxide Supports

Metal oxides are one of the most widely employed catalyst supports because they offer high thermal and chemical stability. When they are in the form of zeolites, they also have a well-defined pore structure and a high surface area. The surfaces of metal oxides can be easily functionalized, which simplifies

the procedure for catalyst deposition. The most common metal oxides used as catalyst supports are silica, alumina, titania, ceria, and zirconia.

Silica is commonly used in catalytic reactions that require mild temperatures, <300 °C, but at higher temperatures, it is less stable and can produce volatile hydroxides. Synthesis of silica materials occurs via sol-gel synthesis (composed of a network of silica spheres) or flame hydrolysis (fumed silica). The fumed silica has higher mechanical strength and can have surface areas as high as 300 m^2/g.[29] Alumina offers much higher thermal and mechanical stability than silica, and is thus the most widely used metal oxide in catalysis. Alumina exists in a number of forms, but the two most common are γ-alumina and α-alumina. γ-Alumina is a highly porous, amorphous material that offers surface areas as high as 300 m^2/g and pore sizes as small as 5 nm, whereas α-alumina is a nonporous, crystalline solid that has a relatively low surface area (3-5 m^2/g). However, α-alumina is highly stable even at temperatures as high as 1200 °C.[2]

Silica and alumina are typically classified as inert materials, but other metal oxide supports such as titania, ceria, and zirconia show reactive properties in certain reactions.[30-32] Thus, these latter materials have the potential to improve catalytic activity. For example, TiO_2 by itself exhibits excellent photocatalytic properties, but when it is used as a support for noble metal or transition metal nanoparticles, it shows enhanced activity and an increased effective wavelength range that extends into the visible region.[32]

1.3.2 Carbonaceous Supports

Carbon materials offer a variety of advantages as catalyst supports. Some carbon supports have surface areas as high as 1500 m^2/g and pore sizes less than 1 nm, but graphitic carbon has a relatively low surface area. Activated carbon materials containing functionalized surfaces can be prepared through several methods including ozone, plasma, or acid or base treatment.[33] This functionalization on the surface of carbon leads to more stable interactions between the catalytic nanoparticles and the support.

Most commercial carbon catalysts such as Pd/C or Pt/C use charcoal supports, and numerous studies examined these catalysts in hydrogenation, Suzuki, Heck, and C-C bond forming reactions.[34-38] Much of the current research with carbon supported catalysts focuses on developing novel carbon materials such as carbon nanotubes as catalyst supports.[39-42] Carbon nanotubes are unique substrates for nanoparticle immobilization because of their high surface area, unique physical properties and morphology, and high electrical conductivity. Moreover, their small size and hollow geometry facilitates the formation of small nanoparticles (typically 1 - 4 nm), which is ideal for catalysis.

1.3.3 Polymer Supports

As an alternative to traditional metal oxides and carbon, polymeric materials are attractive as nanoparticle supports because of their versatility. Many polymeric materials contain heteroatoms that can form complexes with metal nanoparticles, and the flexible structure of the polymers often makes them

particularly effective at stabilizing metal nanoparticles and preventing aggregation. Furthermore, the variety of functional groups available in polymeric materials is virtually unlimited. Some of the most common types of polymers used for nanoparticle immobilization include water soluble polyelectrolytes such as poly(vinylpyrrolidone) (PVP) and poly(ethylenimine) (PEI),[43-45] polymeric microspheres,[46,47] and ion exchange resins.[48-50] Figure 1.2 shows examples of each of these structures.

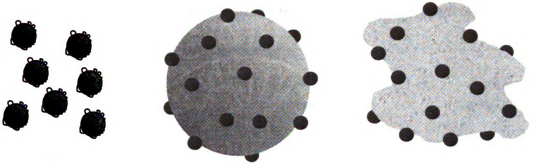

Figure 1.2 Schematic diagram of metal nanoparticles stabilized by a) polyelectrolytes b) a polymer microsphere and c) ion exchange resin.

Polyelectrolyte-stabilized nanoparticles are typically soluble in water and thus act similarly to homogeneous catalysts. The difficulty with using these systems lies in catalyst recovery and reuse, but changing solution conditions can sometimes force polyelectrolytes to precipitate out of solution.[51] Polymeric microspheres and ion exchange resins act similarly to traditional heterogeneous supports and are much easier to separate from the reaction mixture for catalyst recovery. However, polymer stabilizers suffer from a lack of stability at high temperature.

1.3.4 Dendrimer-Encapsulated Metal Nanoparticles

Dendrimers represent a special class of polymers that have a very uniform size distribution, as their polydispersity is ~ 1.[52] They are well-defined on a molecular level and often contain heteroatoms that can bind metal ions for nanoparticle synthesis. For example, poly(propylenimine) (PPI) and poly(amidoamine) (PAMAM) dendrimers contain multiple amine groups (Figure 1.3), and each tertiary amine can complex with metal ions. Subsequent reduction of these ions with $NaBH_4$ leads to the formation of metal nanoparticles that are encapsulated within the dendrimer (Figure 1.4).

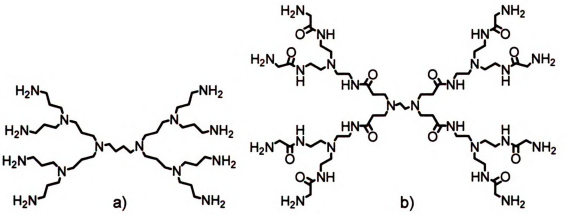

Figure 1.3 Chemical structure of a first generation a) PPI dendrimer and b) PAMAM dendrimer. Both dendrimers are commonly used for encapsulation of metal nanoparticles.

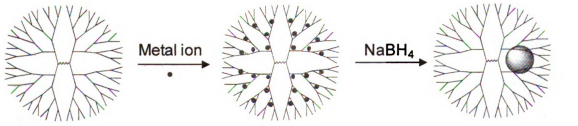

Figure 1.4 Schematic diagram showing the synthesis of metal nanoparticles encapsulated in a dendrimer structure.

In the past decade, a number of groups exploited the inherent properties of dendrimer-encapsulated nanoparticles for highly effective catalysis.[53-57] The well-defined structure of dendrimers allows the formation of metal nanoparticles with very narrow size distributions.[53,58,59] The caged structure of the dendrimers serves as a barrier to limit aggregation of particles, but it can also be used to selectively allow only certain molecules or certain functionalities to come in contact with the nanoparticles, thus making the catalyst more selective.[60,61] Dendrimer-encapsulated particles can be recovered and reused for additional catalytic reactions, but recovery often requires nanofiltration.[62]

1.4 Porous Membranes as Catalyst Supports

The most effective catalyst supports have a high surface area to promote catalyst loading and contact between the catalyst and the reactants. As mentioned above, high surface areas result from a highly porous structure with relatively small pore sizes, but small pores frequently exhibit high mass transport resistances during the catalytic reaction. In heterogeneous catalysis, there are generally five steps for every reaction: 1) transport of reactants to the catalyst, 2) adsorption of reactants on the catalyst, 3) reaction at the catalyst surface, 4) desorption of products from the catalyst, and 5) transport of products away from the catalyst. The middle three steps are chemical in nature and define the rate of the catalytic reaction under ideal circumstances where there is no mass transport limitation. However, diffusion of the reactants into and out of the pores of the support may be slow in comparison to the reaction rate at the catalyst surface. In

this case, the overall mass transport will limit the reaction rate, and such limitations are especially apparent for liquid phase reactions where the diffusion of reactants is slower than in the gas phase.

Several different reactor configurations are used for heterogeneous catalysis. Gas-phase reactions typically use fixed-bed or fluidized-bed reactor configurations. Fixed-bed reactors consist of catalyst particles packed in a column through which the gaseous reactants flow, while fluidized-bed reactors consist of fine catalyst powders that appear as a "fluid" because the gas is flowing upward through the tube with sufficient velocity to keep the particles in continuous motion. Liquid phase and gas/liquid reactions typically consist of a trickle-column, batch, or stirred tank reactor. The trickle-column reactor is similar to the reactors for gas phase reactions except the liquid phase passes downward through the column, and the gas phase either flows concurrently with the liquid down the bed or counter-currently up the bed. Batch and stirred-tank reactors are much more common in industry and require suspension of powder catalyst in the liquid by shaking or stirring and incorporation of gas in the case of gas/liquid reactions. All of these configurations can suffer from mass-transport limitations.

Porous membranes, which can consist of virtually any ceramic or polymer material, offer a support configuration that should provide several advantages over the conventional catalyst supports.[63] One of the motivations for using membranes as catalyst supports is the ability to catalyze reactions and perform separations at the same time. Also, membrane reactions can run continuously because the catalyst does not need to be separated from the reaction products,

unlike batch and stirred tank reactors. The internal pores of the membrane also provide a large surface area that permits a high loading of the catalytic material. Depending on the configuration of membrane reactors, they may provide a number of other advantages as well. Catalytic membranes are typically divided into three categories: extractors, distributors, and contactors (Figure 1.5), which are discussed below.

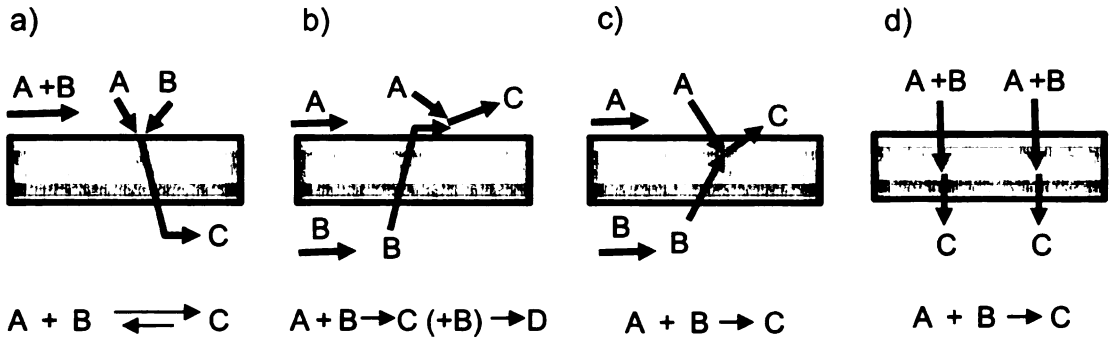

Figure 1.5 Schematic diagram of membranes operated as a) extractors, b) distributors, c) interfacial contactors, and d) flow-through contactors. The first three configurations involve tangential flow along the membrane surface, while the last configuration uses dead-end flow through the membrane pores.

1.4.1 Membrane Extractors

Membranes are generally not thought of as catalytic materials because they are widely used for separation processes such as reverse osmosis for water treatment, gas separations to produce high purity gases, and a number of other applications. However, in the late 1960's, researchers began trying to exploit the excellent separation capabilities of membranes for catalytic applications. The earliest work in this area employed membrane extractors to remove one or more of the products from the reaction to shift the equilibrium and increase conversion. When reactions are limited by equilibrium, the membrane can continuously and

selectively remove the product to shift the equilibrium (Figure 1.5a). An additional benefit of membrane extractors is the ability to decrease undesirable side reactions. After removal from the reaction mixture, the product can no longer react with starting materials to form unwanted byproducts. If the compound being removed is the end product, additional separation and purification steps will be less complicated and require less energy.

Many of the initial studies with membrane extractors involved beneficial hydrogen removal in reactions such as hydrocarbon dehydrogenation,[64,65] water-gas shift,[66] and methane steam reforming reactions.[67,68] These reactions were attractive targets because of the relative ease of selectively removing hydrogen by diffusion through Pd-based membranes or by Knudsen diffusion through membranes with large pore sizes.[69,70] Though removal of H_2 is the most common application of membrane extractors, membranes that selectively remove H_2O or O_2 have also been exploited.[71,72]

1.4.2 Membrane Distributors

Distributor membrane reactors provide controlled addition of a reactant to the reaction mixture to limit side reactions and provide higher selectivity for the desired product. This may occur by simply controlling the amount of a reactant that is introduced on one side of the membrane, or by selectively allowing one component from a mixture to pass through the membrane and undergo reaction. As an example, figure 1.5b demonstrates the reaction of two components, A and B, to yield a product, C without the continued formation of D. As component B

permeates through the membrane, it reacts with component A on the other side of the membrane to form product C. The reaction of B creates a concentration gradient within the membrane, which is the driving force for the continued permeation of B and subsequent reaction with A. Because B reacts with A immediately upon permeating through the membrane, very little side reactions occur to produce D. The most common example of this type of reaction is the partial oxidation of hydrocarbons.[73] In these reactions, O_2 reacts more easily with the partially oxidized species than the starting material. By controlling the addition of O_2 (B) to the hydrocarbon stream (A), complete oxidation can be limited.

1.4.3 Membrane Contactors

The newest form of catalytic membrane reactor is the membrane contactor, where the membrane acts as a support that brings the reactants into contact with the catalyst. In the case of extractors and distributors, the membrane is often catalytically inert and simply acts as a support with a fixed bed of catalyst on one side of the membrane. In that case, the membrane is solely responsible for the separation step, while the fixed catalyst bed is responsible for the reaction. Membrane contactors typically have catalyst deposited within the membrane pores, making them catalytically active, but they usually do not perform a separation function. Although they do not fulfill to requirements to be catalytic membrane reactors in the traditional sense (combining separation and reaction), most researchers in the field still

characterize them as a form of catalytic membrane reactor.[74] Membrane contactors are further classified into two categories in which the membrane acts as an interface between multiple phases (Figure 1.5c) or the membrane is utilized for dead-end flow where all the reactants pass through the catalytically active membrane pores (Figure 1.5d).

1.4.3.1 Interfacial Contactors

Interfacial contactors, which are also known as catalytic diffusers, use the membrane as a catalyst support to facilitate contact between reactants that are in multiple phases. The membrane can separate the two phases and cause enhanced contact between the catalyst and the reactants. The most common application for interfacial contactors is gas/liquid contacting for reactions such as hydrogenations or oxidations. A gas/liquid contactor typically has the gas on the side of the membrane that has larger pores and the liquid on the side that contains more of the catalyst, which is usually the skin layer. The gas and liquid solutes then diffuse to the catalyst surface and react. Flow of the liquid and gas facilitates transport of reactants and removal of products from the reaction zone. This configuration was successfully applied to oxidize organic acids to CO_2 and H_2O[75] and short chain alkanes to oxygenates.[76] A number of studies looked at the hydrogenation of unsaturated substrates including cinnemaldehyde,[77] methylenecyclohexane,[78] and sunflower seed oil,[79] with excellent success, in some cases achieving high selectivity for the desired product. There has also

been significant interest in using interfacial contactors for removal of nitrates from drinking water by hydrogenation.[70,80,81]

The interfacial contactor configuration is also beneficial for forming contact between two liquid phases. In processes such as solvent extraction, a membrane separates an aqueous phase from an organic phase.[82] Studies by Guibal and Vincent also used this configuration for contacting two reactants that are in the same phase but are separated by the membrane. These studies utilized chitosan hollow fiber membranes for nitrophenol reduction[83-85] and chlorophenol dehalogenation[86] by sodium formate. In these reactions, a solution of sodium formate flows by one side of the membrane while solutions of nitrophenol or chlorophenol flow by the opposite side of the membrane, and the concentration of sodium formate is much higher than the reduced species. The reactants diffuse into the pores from each side of the membrane and come into contact at the catalyst surface. However, if the reaction has fast kinetics, mass transport limitations may occur. Use of a flow-through mode can overcome mass transport limitations.

1.4.3.2 Flow-Through Contactors

Membranes operated as flow-through contactors act similarly to conventional fixed bed reactors. In traditional fixed bed reactors, the reactants need to diffuse into the pores of the support to react with the catalyst, but in flow-through membrane contactors, convective mass transport rapidly brings the reactants to the active surface of the immobilized catalyst (Figure 1.6). If the

pores are sufficiently small, radial diffusion will not limit reactions even at high flow rates where the contact time is very short. In this way, the pores of the membrane act as microreactors in which the reaction conversion can be controlled by simply adjusting the flow rate.[87] Flow-through contactors also have the advantage of constantly removing the products from the reaction zone. As a result, there will be less competition between products and reactants for active sites on the catalyst and a decreased possibility for the products to undergo side reactions or poison the catalyst surface.

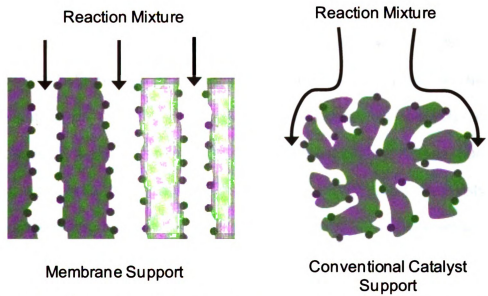

Figure 1.6 Schematic diagram showing the flow of reactants through a membrane operated as a flow-through contactor, and around a catalyst bead from a traditional fixed bed reactor.

The flow-through contactor configuration allows fine control over the residence time of reactants inside the membrane, which directly affects conversion. Even a single pass through the membrane yields nearly complete conversion in reactions such as volatile organic carbon (VOC) combustion or

photocatalytic oxidation of organic compounds.[88-90] However, a majority of previous experiments with flow-through contactors passed the reactant mixture through the membrane multiple times to obtain complete conversion. Many of these studies focused on gas-phase hydrogenation or oxidation reactions.[91] Flowing the gaseous mixture through the membrane very rapidly allows very short contact time, which results in partial hydrogenation of compounds such as acetylene, propyne, butadiene, and hexadiene.[92-95]

The flow-through configuration is also beneficial for gas/liquid reactions where a limited amount of gas is able to dissolve in the liquid phase. Thus with each pass, the liquid solution can again be resaturated with the gas. Schmidt and coworkers found that this strategy afforded high selectivity in the partial hydrogenation of a number of unsaturated organic compounds including cyclooctadiene, 1-octyne, phenyl acetylene, and geraniol.[96,97] Others had similar success with partial hydrogenation of sunflower oil[98-100] and α-methylstyrene[101] and hydrogenation of nitrate for water denitrification.[81,102] The overall success of membrane reactors in restricting the extent of reaction could make them quite valuable in a number of applications.

1.5 Formation of Metal Nanoparticles

Nanoparticles can be integrated into porous membranes via a number of different techniques, and this section describes the most common strategies for incorporating metal nanoparticle into porous supports. As figure 1.4 shows, reduction of metal ions with sodium borohydride to form the zerovalent metal is

one of the common methods for the preparation of supported metal nanoparticles. In general, formation of supported metal nanoparticles occurs by either in-situ or ex-situ methods. We first discuss in-situ formation in which nanoparticles are formed directly on the support, and then we present ex-situ methods that involve the formation of nanoparticles prior to immobilization on the porous support.

The first step in the in-situ formation of nanoparticles is binding of a metal precursor to the support via covalent, electrostatic, or other adsorptive interactions with the surface. Next a calcination step is sometimes required to remove any excess solvent. Finally, reduction of the metal precursor to the zerovalent state results in the formation of metal nanoparticles. This typically involves the use of a reducing agent such as H_2 at high temperatures or sodium borohydride. The size and shape of the nanoparticles depend on the amount of metal precursor that is initially bound to the support, and the morphology (ie. pore size and shape) of the support.

A variety of in-situ methods can be used to form supported metal nanoparticles. The most common methods are impregnation, deposition precipitation, coprecipitation, and chemical vapor deposition, which are described in detail below. However, other physical means to form supported nanoparticle catalysts include electrochemical reduction,[103] sonochemical reduction,[104,105] microwave irradiation,[106,107] and laser ablation,[108] but this is by no means an exhaustive list.

1.5.1 Impregnation

Impregnation techniques are probably the most widely used methods for forming catalytic metal nanoparticles on solid supports,[109,110] and the methods are often used to form metal nanoparticles in ceramic membranes.[111-113] In these techniques, the initial step simply involves "wetting" the solid support with a solution containing the metal precursor. Evaporation of the solvent leads to deposition of the metal precursor on the surface of the support, and subsequent calcination and reduction steps result in the formation of dispersed nanoparticles. The size of the nanoparticles can be controlled to some extent by varying the concentration of the metal precursor solution used to impregnate the support. This also controls the overall loading of metal on the support.

Various interactions can occur between the support surface and the metal precursor to facilitate adsorption. For example, supports composed of metal oxides like silica and alumina contain hydroxyl groups that serve as sites that anchor the metal precursor. These surface hydroxyl groups can also provide surface charge, depending on the pH of the solution and isoelectric point of the support. Thus ionic precursors may bind to the oppositely charged sites of the support, and this form of impregnation is also called ionic impregnation.

1.5.2 Deposition Precipitation

Similar to impregnation, deposition precipitation involves precipitation of a metal hydroxide or carbonate species on the surface of a support. This occurs by first dissolving a metal precursor in solution and then adding base to adjust

the pH of the solution and form a precipitate. The support surface provides nucleation sites for the deposition of the precipitate. Calcination and reduction of the metal precipitate yields supported metal nanoparticles.[114,115] This method can be problematic as it is essential to have efficient stirring to make sure the pH is homogeneous throughout the solution and the support and metal precursor are well-distributed. Hence the method is difficult to apply in porous membranes. Control over nanoparticle size is often difficult as deposition of the metal salt on the support is not homogeneous.[116] This inhomogeneity also leads to the formation of larger aggregates of particles in some locations.

1.5.3 Coprecipitation

Unlike impregnation and deposition precipitation techniques where the metal precursor is deposited onto the support, coprecipitation involves precipitation of the metal and support at the same time.[117] In this method, deposition of the metal during formation of the support and subsequent calcination and reduction allow the metal to deposit in the porous structure of the support. A number of studies looked at the coprecipitation of metals during sol-gel synthesis of silica[109,114,118] and during carbon activation.[119] Notably, co-precipitation with Ag yielded a silica support with evenly dispersed 3.5 nm diameter Ag nanoparticles, while impregnation yielded a support with unevenly distributed 15-18 nm diameter Ag nanoparticles.[118] Though coprecipitation can lead to a high dispersion of catalyst in the support materials, the incorporated

metal may also lead to decreased thermal and mechanical stability of the support, and some of the metal may not be accessible for catalysis.

Coprecipitation was recently used to form polymer-metal nanoparticle composites for catalysis.[120] In some cases the nanoparticles tend to form aggregates during reduction,[121] but studies by Mallick et al.[122,123] found that using Pd acetate as the oxidizing agent during polymerization of anthranilic acid or aminobenzoic acid resulted in formation of ~2 nm diameter Pd nanoparticles that were well-distributed and stabilized within the polymer matrix. These polymer-Pd nanoparticle composites showed high activity in ethylene hydrogenation reactions. Similar methods were used to incorporate metal nanoparticles into polymeric membranes by adding metal precursors to polymer solutions and reducing the metals during membrane synthesis.[95,96,124,125] Incorporation of metal nanoparticles during polymer membrane synthesis may lead to some heterogeneity in pore structure, but the main disadvantage of using coprecipitation to incorporate metal nanoparticles into the support material is that some of the nanoparticle surface is not accessible for catalysis, and the overall catalytic activity decreases. This is often a concern when using expensive metals that need to be utilized efficiently, so this process is more beneficial for incorporation of relatively cheap catalyst materials.

1.5.4 Chemical Vapor Deposition

Chemical vapor deposition (CVD) is attractive for producing well-dispersed catalysts with a narrow size distribution. In general, CVD involves the deposition

of a metal precursor from the vapor phase onto a support under high vacuum conditions in the presence of a reducing agent. The main advantage of this method lies in the potential to control the nanoparticle size for a given metal loading by adjusting the amount of precursor deposited on the surface prior to reduction. [126] Compared to the conventional wet impregnation methods, the absence of solvent favors the uniform distribution of the metal precursor inside the pores of the support and eliminates the drying step during which the metal can redistribute.[127] CVD can modify a wide variety of support materials including carbon nanofibers.[126,128] This technique is also an excellent method for forming a thin Pd layer on the surface of membranes that serve as extractors for hydrocarbon dehydrogenation[70] or interfacial contactors for hydrogenation reactions.[80]

1.5.5 Synthesis of Unsupported Metal Nanoparticles

To date, one of the biggest limitations of using in-situ methods to form supported metal nanoparticles is the difficulty of producing metal nanoparticles with a uniform size distribution. Ex-situ preparation of metal nanoparticles that are stable in solution has the potential to yield much more uniform particle shapes and sizes. In solution, the nucleation and growth of nanoparticles can occur freely without the vagaries characteristic of heterogeneous processes.

A variety of chemistries are available for stabilizing metal nanoparticles in solution. These unsupported metal nanoparticles typically form by the reduction of metal ions in the presence of a ligand or other stabilizing agent that can bind to

the surface of the newly formed particle and terminate growth. The stabilizing agent offers control over nanoparticle size and polydispersity. Figure 1.7 demonstrates that a charged stabilizing ligand on the surface of the nanoparticles produces an electric double layer that causes particle-particle repulsion and minimizes particle agglomeration.[129] Choice of ligand is important in nanoparticle synthesis as it provides control over surface functional groups and the solvent compatibility of the nanoparticles. Citrate, thiols, amines, and phosphines are the most common stabilizing agents used in metal nanoparticle synthesis.

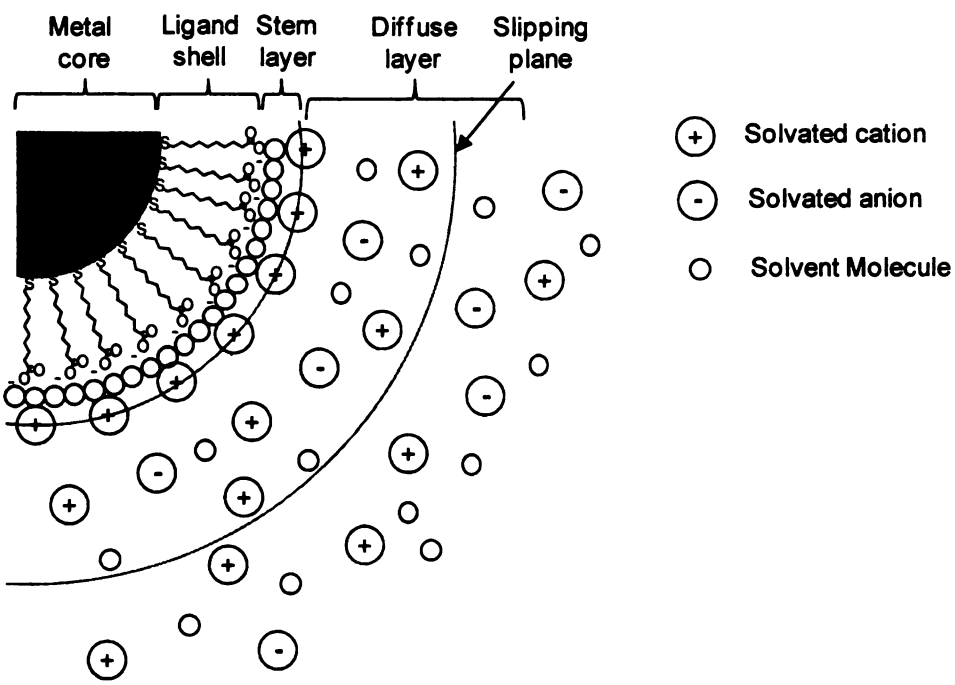

Figure 1.7 Schematic diagram of the electric double-layer structure surrounding a nanoparticle stabilized with charged ligands. In this figure mercaptoundecanoic acid is the stabilizing ligand.

Citrate reduction, which was pioneered by Turkevich in the 1950's, yields nearly monodisperse, water soluble Au nanoparticles that can range in size from 8 to 100 nm.[130-132] This technique utilizes citrate as both the reducing agent and

the stabilizing agent. Upon reducing the Au(III) to Au(0) (scheme 1.1), excess citrate stabilizes the Au nanoparticles to terminate particle growth.[133] Thus, a layer of citrate anions forms at the surface of the nanoparticles, leading to a net negative charge that allows the nanoparticles to remain separated.

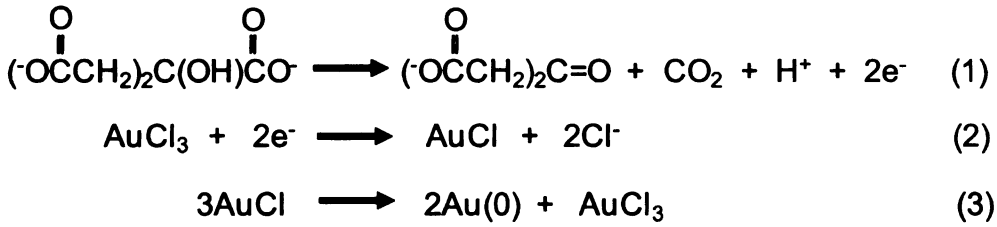

Scheme 1.1 Series of reactions believed to occur during the citrate reduction of $AuCl_3$ to form Au nanoparticles.

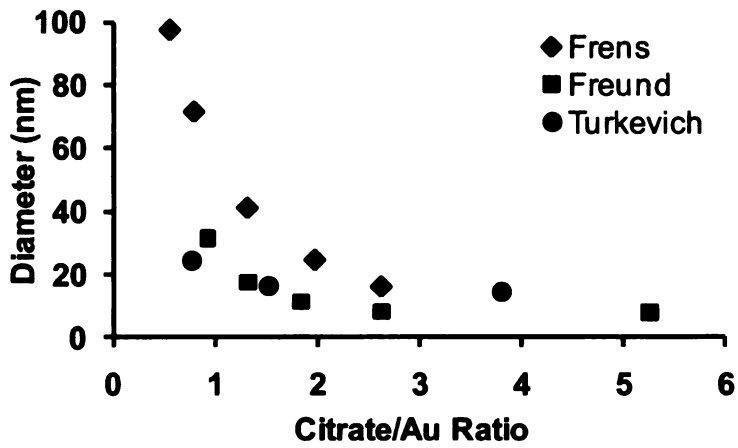

Figure 1.8 Variation of Au nanoparticle size with molar ratio of the initial concentration of citrate and Au salt.[131,134,135]

Variation of the molar ratio of the citrate to Au in the solution affords fine control over nanoparticle diameter (Figure 1.8).[131,133-136] Moreover, the citrate method is quite adaptable as it has been used for formation of aqueous solutions of Pd,[47,137,138] Pt,[139,140] and Ag[141,142] nanoparticles. Although the citrate reduction method is simple and versatile, a number of other methods have been developed

to improve nanoparticle stability, change surface functional groups, and produce nanoparticles with smaller diameters.

In the early 1990's, Brust and coworkers developed a nanoparticle synthesis in which a dodecanethiol stabilizer was added to the metal precursor solution during reduction by $NaBH_4$.[143,144] This method initially yielded organic-soluble Au nanoparticles with diameters in the range of 2 to 8 nm. Subsequent studies with other thiol capping agents produced particles with a wider range of sizes and surface functionalities.[145] Kimura and Kunitake demonstrated that careful selection of thiol ligands can also yield water-soluble nanoparticles.[146,147] This method was later extended to the synthesis of thiol-stabilized Pt nanoparticles.[148]

When nanoparticles are coated with strong stabilizing agents such as thiols, additional surface functionalization can be very difficult, and catalytic activity will also be low. These drawbacks of thiol stabilizers led researchers to look to alternative stabilizing ligands such as amines. Amine-stabilized nanoparticles can be prepared by simply substituting an appropriate amine for the thiol.[149] This method has been used for synthesis of Au, Pt, and Ag nanoparticles in organic solvents,[150,151] and a similar method for synthesizing water-soluble Au nanoparticles has also been demonstrated.[152] In some cases amines can be used as both the reducing and stabilizing agent during nanoparticle synthesis.[153] Triphenylphosphine is another stabilizing ligand that has advantages over thiol ligands because it is a weak stabilizing ligand and can

easily undergo ligand-exchange reactions to functionalize the nanoparticle surface.[154-156]

All of these methods of nanoparticle synthesis involve the generation of metal nanoparticles from molecular precursors in the presence of reducing agents and stabilizing agents. Other methods of nanoparticle fabrication include laser ablation and sonochemical, electrochemical, and microwave syntheses.[145] In all cases, the resulting nanoparticles are soluble in a specific solvent and can be used directly to perform catalytic reactions. Thus the nanoparticles in these systems act as semi-homogeneous catalysts and demonstrate some of the advantages of molecular catalysts even though they are actually solid materials. As we mentioned previously, the difficulty in using the as-prepared nanoparticles directly for catalysis lies in the catalyst recovery step. Immobilization of the metal nanoparticles onto a suitable support, which is presented in the next section, facilitates catalyst recovery and reuse.

1.5.6 Surface Modification with Preformed Metal Nanoparticles

The ability to synthesize metal nanoparticles prior to immobilization on a support affords much more control over nanoparticle size and surface functionality than the methods for in-situ formation (sections 1.5.1 to 1.5.4) of supported metal nanoparticles. Ex-situ formation can lead to the development of more selective or reactive catalysts that can be tuned to a specific process. Assembly of metal nanoparticles on surfaces is often driven by electrostatic interactions or covalent bonding between the chemical functionalities of a metal

nanoparticle and a surface. Chemical modification of the substrate may be needed to create interactions with the metal nanoparticles, and such modification can be achieved through a variety of methods. Surfaces modified with amine- or carboxylate-terminated self assembled monolayers (SAMs) of functionalized thiols are capable of capturing metal nanoparticles capped by various types of charged stabilizing ligands. The extent of nanoparticle adsorption varies with the strength of the interaction between the nanoparticles and the surface. Silanization is another common method for surface functionalization, and Chaudret and Schmid reacted porous alumina membranes with alkoxysilanes and subsequently adsorbed several noble metal clusters or colloids.[157] These membranes catalyzed the gas phase hydrogenation of 1,3-butadiene and CO oxidation.[91,92] Sehayek and coworkers modified porous alumina membranes with aminopropyltrimethoxysilane prior to deposition of citrate-stabilized Au and Pd nanoparticles. However, this procedure led to aggregated nanoparticles that formed nanotube structures (the intended result of that study) rather than the well-separated nanoparticles that are efficient catalysts.[138,158].

The methods of nanoparticle immobilization discussed above lead to the immobilization of a monolayer of metal nanoparticles. But in some catalytic applications it would be useful to increase the nanoparticle loading by immobilizing multiple layers of nanoparticles. The next section introduces the method of layer-by-layer (LbL) assembly as a simple and effective method for incorporating metal nanoparticles into catalyst supports.

1.6 Layer-by-Layer Assembly of Polyelectrolyte Multilayer Films

The LbL method, which was pioneered by Decher in the early 1990's, typically involves alternating adsorption of polycations and polyanions and can be simply carried out on nearly any substrate that will support adsorption of an initial layer of polymer.[159-162] The adsorption of the first polymer layer is usually driven by strong electrostatic attraction between the charged surface and the initial polyelectrolyte. The many charged groups on the polyelectrolyte can overcompensate the charge on the support surface to present an excess charge for subsequent adsorption of an oppositely charged polyelectrolyte. The excess surface charge of each layer also acts to repel the adsorption of additional similarly charged polyelectrolyte molecules, limiting deposition to a single "layer". Subsequent addition of an oppositely charged polyelectrolyte results in the formation of one bilayer on the support surface (Figure 1.9). This process can be repeated multiple times to form films with the desired thickness.

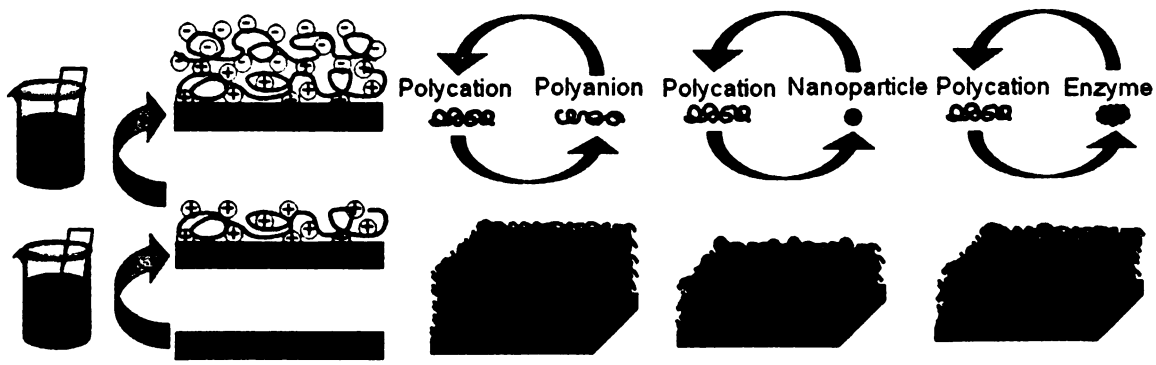

Figure 1.9 Schematic drawing of layer-by-layer deposition by alternating adsorption of polyanions and polycations. The rinsing between each deposition step is not shown. These films can incorporate a wide variety of functional materials including metal nanoparticles and enzymes.

The adsorption of a polyelectrolyte on a surface is an entropy driven process.[163] For each polyelectrolyte that adsorbs on the surface, many counter ions are released into solution. Thus, adsorption of a single polyelectrolyte layer should release a sufficient number of counterions to cause a large increase in entropy.

The properties of polyelectrolyte multilayer films can easily be tailored to fit specific applications by changing the pH, salt concentration, or solvent composition of polyelectrolyte deposition solutions. For films containing weak polyelectrolytes, changing the solution pH greatly affects film thickness because the degree of protonation (and therefore charge density) will change according to the solution pH.[164] For example, Rubner and coworkers determined that the thickness of films containing poly(acrylic acid) (PAA) and poly(allylamine hydrochloride) (PAH) is highly dependent on pH. When deposition solutions had a pH of 7, the thickness of 1 layer was ~5 Å, whereas the layer thickness increased to 80 Å when the solutions were adjusted to a pH of 5.[165] Likewise, changes in ionic strength can lead to dramatic changes in film thickness. When the polyelectrolyte solution has a high salt concentration, the salt ions screen the charges on the polyelectrolyte to give a more coiled polyelectrolyte structure that forms a thicker film.[165-167] Conversely, decreasing the ionic strength leads to less charge screening, and the polyelectrolytes stretch out and form relatively thin films with few loops and coils.

The LbL method is not limited to simple polymers, but can be used for many charged species including biomolecules,[168-173] dendrimers,[174,175] carbon

nanotubes,[176-178] metal oxide particles,[179-182] and metal nanoparticles,[183-189] (see Figure 1.9). Metal nanoparticles can even be incorporated into multilayer films by in-situ methods of reduction,[5,190,191] which typically involve the addition of a metal salt to the polyelectrolyte during deposition and subsequent reduction of the metal ions to form nanoparticles stabilized by the polyelectrolyte film. While most LbL applications primarily use electrostatic attraction as the driving force for film formation, there are many other interactions that can initiate deposition, including hydrogen bonding[192-195] and covalent bonding.[182,196,197] In general, there simply needs to be some form of interaction between the materials that are incorporated into the thin film structure.

Given the vast range of materials that can form multilayer films, LbL deposition is an excellent way to produce films that can be tuned to specific processes, such as catalysis.[5,185,198-200] Although LbL assembly is most easily applied to flat surfaces, it can also occur in porous and irregular structures. Thus, LbL assembly of films containing preformed metal nanoparticles is an ideal method for modifying porous supports to make highly effective catalysts.

1.7 Scope of this work

Adaptation of Layer-by-layer adsorption to membrane modification occurs by exposing porous membranes to alternating polyanion and polycation solutions, with water rinses after each deposition step. Previous and on-going research in the Bruening group involves film deposition primarily on top of the support.[201-203] In such work, only the top portion of the membrane is in contact

with the polyelectrolyte solutions, and because the membranes have small surface pores (~20 nm), the solution does not enter into the pores and thus modifies only the top of the membrane.

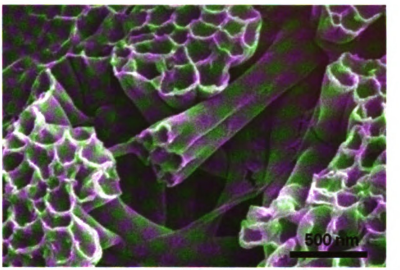

Figure 1.10 FESEM image of a cross-linked $[PAA/PAH]_3$ film that was deposited in the interior pores of an anodized alumina membrane (0.2 μm pore size). The alumina membrane was dissolved prior to imaging the polymer nanotubes.

The deposition of polyelectrolyte films in the interior of membranes simply requires the flow of the polyelectrolyte solutions through membranes with relatively large pores (typically 200 nm or larger). Figure 1.10 shows polyelectrolyte tubes that were formed by depositing a PAA/PAH film in porous alumina, crosslinking via amide formation,[204] and dissolving the alumina[205] in 3 M sodium hydroxide. The image clearly shows the formation of hollow polymeric tubes that still allow convective flow of solution through the membrane. Ai and Caruso separately demonstrated the formation of similar polyelectrolyte tubes even without cross-linking of polyelectrolytes.[206,207]

This dissertation discusses the use of LbL deposition to modify porous membrane and powder supports with metal nanoparticle-containing thin films, and the subsequent use of these supports for heterogeneous catalysis. The next three chapters each focus on a specific application. Chapter 2 presents the use of Au nanoparticle-containing membranes for catalyzing the reduction of nitroaromatic compounds by sodium borohydride. These studies show the effect of functional group, solution flow rate, and membrane structure on conversion in membrane reactions. This chapter also presents the characterization of Au nanoparticle-containing polyelectrolyte films on aluminum wafers, alumina powder, and in porous membranes. Chapter 3 discusses the application of Pd-containing supports for hydrogenation of a variety of substrates and demonstrates the use of flat disk-shaped membranes as flow-through contactors for gas/liquid reactions. Experiments with Pd-containing alumina powder catalysts show the effect of nanoparticle size on reaction selectivity. Chapter 4 discusses the use of Pt nanoparticle-containing supports for the wet air oxidation of several model compounds and demonstrates the use of tubular ceramic membranes as interfacial contactors. This work compares LbL deposition of catalytic nanoparticles with catalytic membranes prepared by other procedures. Chapter 5 discusses some conclusions and future directions for this work as well as some of the challenges that should be addressed. Overall, this dissertation shows that the LbL method yields catalytically active support materials that effectively catalyze reduction, hydrogenation, and oxidation reactions.

1.8 References

(1) Adams, C. J. *North American Catalysis Society*, http://www.nacatsoc.org/edu_info.asp Accessed June 4, 2009.

(2) Chorkendorff, I.; Niemantsverdriet, J. W. *Concepts of Modern Catalysis and Kinetics*; Wiley-VCH: Weinheim, Germany, 2003.

(3) Swiegers, G. F. *Mechanical Catalysis: Methods of Heterogeneous, Homogeneous, and Enzymatic Catalysis*; John Wiley & Sons, Inc.: Hoboken, New Jersey, 2008.

(4) Corma, A.; Serna, P. *Science* **2006**, *313*, 332-334.

(5) Kidambi, S.; Dai, J.; Li, J.; Bruening, M. L. *J. Am. Chem. Soc.* **2004**, *126*, 2658-2659.

(6) Valden, M.; Lai, X.; Goodman, D. W. *Science* **1998**, *281*, 1647-1650.

(7) Augustine, R. L. *Heterogeneous Catalysis for the Synthetic Chemist*; Marcel Dekker, Inc.: New York, New York, 1996.

(8) Astruc, D.; Lu, F.; Aranzaes, J. R. *Angew. Chem. Int. Ed.* **2005**, *44*, 7852-7872.

(9) Daniel, M.-C.; Astruc, D. *Chem. Rev.* **2004**, *104*, 293-346.

(10) Faraday, M. *Philos. Trans. R. Soc. London* **1857**, *147*, 145-181.

(11) Zhao, J.; Bradbury, C. R.; Fermin, D. J. *J. Phys. Chem. C* **2008**, *112*, 6832-6841.

(12) Zhou, W. P.; Lewera, A.; Larsen, R.; Masel, R. I.; Bagus, P. S.; Wieckowski, A. *J. Phys. Chem. B* **2006**, *110*, 13393-13398.

(13) Akamatsu, K.; Deki, S. *J. Mater. Chem.* **1997**, *7*, 1773-1777.

(14) Schmid, G. *Clusters and Colloids*; Wiley-VCH: Weinheim, Germany, 1994.

(15) Bond, G. C.; Sermon, P. A.; Webb, G.; Buchanan, D. A.; Wells, P. B. *J. Chem. Soc., Chem. Commun.* **1973**, 444-5.

(16) Bond, G. C.; Sermon, P. A. *Gold Bulletin* **1973**, *6*, 102-105.

(17) Haruta, M.; Kobayashi, T.; Sano, H.; Yamada, N. *Chem. Lett.* **1987**, 405-8.

(18) Haruta, M.; Tsubota, S.; Kobayashi, T.; Kageyama, H.; Genet, M. J.; Delmon, B. *J. Catal.* **1993**, *144*, 175-192.

(19) Haruta, M.; Yamada, N.; Kobayashi, T.; Iijima, S. *J. Catal.* **1989**, *115*, 301-309.

(20) Hammer, B.; Norskov, J. K. *Nature* **1995**, *376*, 238-240.

(21) Haruta, M. *Chem. Rec.* **2003**, *3*, 75-87.

(22) Bamwenda, G. R.; Tsubota, S.; Nakamura, T.; Haruta, M. *Catal. Lett.* **1997**, *44*, 83-87.

(23) Shiju, N. R.; Guliants, V. V. *Appl. Catal., A* **2009**, *356*, 1-17.

(24) Corma, A.; Garcia, H. *Top. Catal.* **2008**, *48*, 8-31.

(25) Zecchina, A.; Groppo, E.; Bordiga, S. *Chem. Eur. J.* **2007**, *13*, 2440-2460.

(26) Mirkin, C. A. *Small* **2005**, *1*, 14-16.

(27) Doyle, A. M.; Shaikhutdinov, S. K.; Jackson, S. D.; Freund, H.-J. *Angew. Chem. Int. Ed.* **2003**, *42*, 5240-5243.

(28) Schmid, G.; Maihack, V.; Lantermann, F.; Peschel, S. *J. Chem. Soc., Dalton Trans.* **1996**, 589 - 595.

(29) Jacobsen, H.; Kleinshmit, P. In *Handbook of Heterogeneous Catalysis*; Ertl, G., Knözinger, H., Weitkamp, J., Eds.; VCH: Weinheim, Germany, 1997.

(30) Qian, K.; Lv, S.; Xiao, X.; Sun, H.; Lu, J.; Luo, M.; Huang, W. *J. Mol. Catal. A: Chem.* **2009**, *306*, 40-47.

(31) Boaro, M.; Vicario, M.; Llorca, J.; De Leitenburg, C.; Dolcetti, G.; Trovarelli, A. *Appl. Catal., B* **2009**, *88*, 272-282.

(32) Han, F.; Kambala, V. S. R.; Srinivasan, M.; Rajarathnam, D.; Naidu, R. *Appl. Catal., A* **2009**, *359*, 25-40.

(33) Tasis, D.; Tagmatarchis, N.; Bianco, A.; Prato, M. *Chem. Rev.* **2006**, *106*, 1105-1136.

(34) Toebes, M. L.; Van Dillen, J. A.; De Jong, K. P. *J. Mol. Catal. A: Chem.* **2001**, *173*, 75-98.

(35) Leblond, C. R.; Andrews, A. T.; Sun, Y.; Sowa, J. R., Jr. *Org. Lett.* **2001**, *3*, 1555-1557.

(36) Kohler, K.; Heidenreich, R. G.; Krauter, J. G. E.; Pietsch, J. *Chem. Eur. J.* **2002**, *8*, 622-631.

(37) Toshima, N.; Shiraishi, Y.; Teranishi, T.; Miyake, M.; Tominaga, T.; Watanabe, H.; Brijoux, W.; Bonnemann, H.; Schmid, G. *Appl. Organomet. Chem.* **2001**, *15*, 178-196.

(38) Reetz, M. T.; Schulenburg, H.; Lopez, M.; Spliethoff, B.; Tesche, B. *Chimia* **2004**, *58*, 896-899.

(39) Wildgoose, G. G.; Banks, C. E.; Compton, R. G. *Small* **2006**, *2*, 182-193.

(40) Pan, X.; Bao, X. *Chem. Commun.* **2008**, 6271-6281.

(41) Wang, C.; Guo, S.; Pan, X.; Chen, W.; Bao, X. *J. Mater. Chem.* **2008**, *18*, 5782-5786.

(42) Endo, M.; Kim, Y. A.; Ezaka, M.; Osada, K.; Yanagisawa, T.; Hayashi, T.; Terrones, M.; Dresselhaus, M. S. *Nano Lett.* **2003**, *3*, 723-726.

(43) Sun, X. P.; Zhang, Z. L.; Zhang, B. L.; Dong, X. D.; Dong, S. J.; Wang, E. K. *Chin. Chem. Lett.* **2003**, *14*, 866-869.

(44) Tsunoyama, H.; Ichikuni, N.; Tsukuda, T. *Langmuir* **2008**, *24*, 11327-11330.

(45) Tsunoyama, H.; Sakurai, H.; Negishi, Y.; Tsukuda, T. *J. Am. Chem. Soc.* **2005**, *127*, 9374-9375.

(46) Liu, W.; Yang, X.; Huang, W. *J. Colloid Interface Sci.* **2006**, *304*, 160-165.

(47) Dokoutchaev, A.; James, J. T.; Koene, S. C.; Pathak, S.; Prakash, G. K. S.; Thompson, M. E. *Chem. Mater.* **1999**, *11*, 2389-2399.

(48) Jana, S.; Ghosh, S. K.; Nath, S.; Pande, S.; Praharaj, S.; Panigrahi, S.; Basu, S.; Endo, T.; Pal, T. *Appl. Catal., A* **2006**, *313*, 41-48.

(49) Shi, F.; Zhang, Q.; Ma, Y.; He, Y.; Deng, Y. *J. Am. Chem. Soc.* **2005**, *127*, 4182-4183.

(50) Ishida, T.; Haruta, M. *Angew. Chem. Int. Ed.* **2007**, *46*, 7154-7156.

(51) Wittmer, J.; Johner, A.; Joanny, J. F. *J. Phys. II* **1995**, *5*, 635-654.

(52) Tomalia, D. A.; Naylor, A. M.; Goddard, W. A. *Angew. Chem.* **1990**, *102*, 119-57.

(53) Kim, Y.-G.; Oh, S.-K.; Crooks, R. M. *Chem. Mater.* **2004**, *16*, 167-172.

(54) Niu, Y.; Crooks, R. M. *Comptes Rendus Chimie* **2003**, *6*, 1049-1059.

(55) Balogh, L.; Tomalia, D. A. *J. Am. Chem. Soc.* **1998**, *120*, 7355-7356.

(56) Esumi, K.; Isono, R.; Yoshimura, T. *Langmuir* **2004**, *20*, 237-243.

(57) Hayakawa, K.; Yoshimura, T.; Esumi, K. *Langmuir* **2003**, *19*, 5517-5521.

(58) Zhao, M.; Crooks, R. M. *Adv. Mater.* **1999**, *11*, 217-220.

(59) Zhao, M.; Sun, L.; Crooks, R. M. *J. Am. Chem. Soc.* **1998**, *120*, 4877-4878.

(60) Niu, Y.; Yeung, L. K.; Crooks, R. M. *J. Am. Chem. Soc.* **2001**, *123*, 6840-6846.

(61) Oh, S.-K.; Niu, Y.; Crooks, R. M. *Langmuir* **2005**, *21*, 10209-10213.

(62) Andres, R.; De Jesus, E.; Flores, J. C. *New J. Chem.* **2007**, *31*, 1161-1191.

(63) Armor, J. N. *Catal. Today* **1995**, *25*, 199-207.

(64) Yildirim, Y.; Gobina, E.; Hughes, R. *J. Membr. Sci.* **1997**, *135*, 107-115.

(65) Collins, J. P.; Schwartz, R. W.; Sehgal, R.; Ward, T. L.; Brinker, C. J.; Hagen, G. P.; Udovich, C. A. *Ind. Eng. Chem. Res.* **1996**, *35*, 4398-4405.

(66) Uemiya, S.; Sato, N.; Ando, H.; Kikuchi, E. *Ind. Eng. Chem. Res.* **1991**, *30*, 585-589.

(67) Shu, J.; Grandjean, B. P. A.; Kaliaguine, S. *Appl. Catal., A* **1994**, *119*, 305-325.

(68) Hsiung, T. H.; Christman, D. D.; Hunter, E. J.; Homyak, A. R. *AIChE J.* **1999**, *45*, 204-208.

(69) Dalmon, J.-A. In *Handbook of Heterogeneous Catalysis*; Ertl, G., Knozinger, H., Weitkamp, J., Eds.; Wiley-VCH: Weinheim, Germany, 1997; Vol. 3, p 1387-1398.

(70) Dittmeyer, R.; Höllein, V.; Daub, K. *J. Mol. Catal. A: Chem.* **2001**, *173*, 135-184.

(71) Lipnizki, F.; Field, R. W.; Ten, P.-K. *J. Membr. Sci.* **1999**, *153*, 183-210.

(72) Dixon, A. G. *Specialist Periodical Reports: Catalysis* **1999**, *14*, 40-92.

(73) Marcano, J. G. S.; Tsotsis, T. T. *Catalytic Membranes and Membrane Reactors*; Wiley-VCH: Weinheim, Germany, 2002.

(74) Dittmeyer, R.; Svajda, K.; Reif, M. *Top. Catal.* **2004**, *29*, 3-27.

(75) Miachon, S.; Perez, V.; Crehan, G.; Torp, E.; Raeder, H.; Bredesen, R.; Dalmon, J. A. *Catal. Today* **2003**, *82*, 75-81.

(76) Espro, C.; Arena, F.; Frusteri, F.; Parmaliana, A. *Catal. Today* **2001**, *67*, 247-256.

(77) Pan, X. L.; Liu, B. J.; Xiong, G. X.; Sheng, S. S.; Liu, J.; Yang, W. S. *Catal. Lett.* **2000**, *66*, 125-128.

(78) Bottino, A.; Capannelli, G.; Comite, A.; Di Felice, R. *Desalination* **2002**, *144*, 411-416.

(79) Veldsink, J. W. *J. Am. Oil Chem. Soc.* **2001**, *78*, 443-446.

(80) Daub, K.; Wunder, V. K.; Dittmeyer, R. *Catal. Today* **2001**, *67*, 257-272.

(81) Reif, M.; Dittmeyer, R. *Catal. Today* **2003**, *82*, 3-14.

(82) Gabelman, A.; Hwang, S.-T. *J. Membr. Sci.* **1999**, *159*, 61-106.

(83) Guibal, E.; Vincent, T. *J. Environ. Manage.* **2004**, *71*, 15-23.

(84) Vincent, T.; Guibal, E. *Environ. Sci. Technol.* **2004**, *38*, 4233-4240.

(85) Vincent, T.; Guibal, E. *Langmuir* **2003**, *19*, 8475-8483.

(86) Vincent, T.; Spinelli, S.; Guibal, E. *Ind. Eng. Chem. Res.* **2003**, *42*, 5968-5976.

(87) Westermann, T.; Melin, T. *Chem. Eng. Process.* **2009**, *48*, 17-28.

(88) Pina, M. P.; Menéndez, M.; Santamaría, J. *Appl. Catal., B* **1996**, *11*, L19-L27.

(89) Maira, A. J.; Lau, W. N.; Lee, C. Y.; Yue, P. L.; Chan, C. K.; Yeung, K. L. *Chem. Eng. Sci.* **2003**, *58*, 959-962.

(90) Tsuru, T.; Kan-No, T.; Yoshioka, T.; Asaeda, M. *Catal. Today* **2003**, *82*, 41-48.

(91) Kormann, H.-P.; Schmid, G.; Pelzer, K.; Philippot, K.; Chaudret, B. *Z. Anorg. Allg. Chem.* **2004**, *630*, 1913-1918.

(92) Pelzer, K.; Philippot, K.; Chaudret, B.; Meyer-Zaika, W.; Schmid, G. *Z. Anorg. Allg. Chem.* **2003**, *629*, 1217-1222.

(93) Lange, C.; Storck, S.; Tesche, B.; Maier, W. F. *J. Catal.* **1998**, *175*, 280-293.

(94) Lambert, C.; Gonzalez, R. *Catal. Lett.* **1999**, *57*, 1-7.

(95) Gröschel, L.; Haidar, R.; Beyer, A.; Coelfen, H.; Frank, B.; Schomäcker, R. *Ind. Eng. Chem. Res.* **2005**, *44*, 9064-9070.

(96) Schmidt, A.; Haidar, R.; Schomäcker, R. *Catal. Today* **2005**, *104*, 305-312.

(97) Schmidt, A.; Wolf, A.; Warsitz, R.; Dittmeyer, R.; Urbanczyk, D.; Voigt, I.; Fischer, G.; Schomäcker, R. *AIChE J.* **2008**, *54*, 258-268.

(98) Schmidt, A.; Schomäcker, R. *J. Mol. Catal. A: Chem.* **2007**, *271*, 192-199.

(99) Bengtson, G.; Fritsch, D. *Desalination* **2006**, *200*, 666-667.

(100) D. Fritsch, G. B. *Adv. Eng. Mater.* **2006**, *8*, 386-389.

(101) Purnama, H.; Kurr, P.; Schmidt, A.; Schomäcker, R.; Voigt, I.; Wolf, A.; Warsitz, R. *AIChE J.* **2006**, *52*, 2805-2811.

(102) Ilinich, O. M.; Gribov, E. N.; Simonov, P. A. *Catal. Today* **2003**, *82*, 49-56.

(103) Dominguez-Dominguez, S.; Arias-Pardilla, J.; Berenguer-Murcia, A.; Morallon, E.; Cazorla-Amoros, D. *J. Appl. Electrochem.* **2008**, *38*, 259-268.

(104) Haas, I.; Gedanken, A. *Chem. Commun.* **2008**, 1795-1797.

(105) Gedanken, A. *Ultrason. Sonochem.* **2004**, *11*, 47-55.

(106) Glaspell, G.; Hassan, H. M. A.; Elzatahry, A.; Abdalsayed, V.; El-Shall, M. S. *Top. Catal.* **2008**, *47*, 22-31.

(107) Glaspell, G.; Fuoco, L.; El-Shall, M. S. *J. Phys. Chem. B* **2005**, *109*, 17350-17355.

(108) Savastenko, N.; Volpp, H. R.; Gerlach, O.; Strehlau, W. *J. Nanopart. Res.* **2008**, *10*, 277-287.

(109) Barau, A.; Budarin, V.; Caragheorgheopol, A.; Luque, R.; Macquarrie, D. J.; Prelle, A.; Teodorescu, V. S.; Zaharescu, M. *Catal. Lett.* **2008**, *124*, 204-214.

(110) Campelo, J. M.; Lee, A. F.; Luque, R.; Luna, D.; Marinas, J. M.; Romero, A. A. *Chem. Eur. J.* **2008**, *14*, 5988-5995.

(111) Perego, C.; Villa, P. *Catal. Today* **1997**, *34*, 281-305.

(112) Uzio, D.; Miachon, S.; Dalmon, J.-A. *Catal. Today* **2003**, *82*, 67-74.

(113) Perez, V.; Miachon, S.; Dalmon, J.-A.; Bredesen, R.; Pettersen, G.; Raeder, H.; Simon, C. *Sep. Purif. Technol.* **2001**, *25*, 33-38.

(114) Akolekar, D. B.; Bhargava, S. K.; Foran, G.; Takahashi, M. *J. Mol. Catal. A: Chem.* **2005**, *238*, 78-87.

(115) Centeno, M. A.; Portales, C.; Carrizosa, I.; Odriozola, J. A. *Catal. Lett.* **2005**, *102*, 289-297.

(116) Date, M.; Okumura, M.; Tsubota, S.; Haruta, M. *Angew. Chem. Int. Ed.* **2004**, *43*, 2129-2132.

(117) Tsubota, S.; Haruta, M.; Kobayashi, T.; Ueda, A.; Nakahara, Y. *Stud. Surf. Sci. Catal.* **1991**, *63*, 695-704.

(118) Liu, H.; Ma, D.; Blackley, R. A.; Zhou, W.; Bao, X. *Chem. Commun.* **2008**, 2677-2679.

(119) Bekyarova, E.; Kaneko, K. *Adv. Mater.* **2000**, *12*, 1625-1628.

(120) Xu, C.; Ouyang, C.; Jia, R.; Li, Y.; Wang, X. *J. Appl. Polym. Sci.* **2009**, *111*, 1763-1768.

(121) Hasik, M.; Turek, W.; Nyczyk, A.; Stochmal, E.; Bernasik, A.; Sniechota, A.; Soltysek, A. *Catal. Lett.* **2009**, *127*, 304-311.

(122) Mallick, K.; Mondal, K.; Witcomb, M.; Scurrell, M. *J. Mater. Sci.* **2008**, *43*, 6289-6295.

(123) Scalzullo, S.; Mondal, K.; Witcomb, M.; Deshmukh, A.; Scurrell, M.; Mallick, K. *Nanotechnology* **2008**, *19*, 075708/1-075708/8.

(124) Meyer, D. E.; Bhattacharyya, D. *J. Phys. Chem. B* **2007**, *111*, 7142-7154.

(125) Meyer, D. E.; Wood, K.; Bachas, L. G.; Bhattacharyya, D. *Environ. Prog.* **2004**, *23*, 232-242.

(126) Serp, P.; Kalck, P.; Feurer, R. *Chem. Rev.* **2002**, *102*, 3085-3128.

(127) Okumura, M.; Nakamura, S.; Tsubota, S.; Nakamura, T.; Azuma, M.; Haruta, M. *Catal. Lett.* **1998**, *51*, 53-58.

(128) Liang, C.; Xia, W.; Soltani-Ahmadi, H.; Schlueter, O.; Fischer, R. A.; Muhler, M. *Chem. Commun.* **2005**, 282-284.

(129) Laaksonen, T.; Ahonen, P.; Johans, C.; Kontturi, K. *ChemPhysChem* **2006** *7*, 2143 - 2149.

(130) Kimling, J.; Maier, M.; Okenve, B.; Kotaidis, V.; Ballot, H.; Plech, A. *J. Phys. Chem. B* **2006**, *110*, 15700-15707.

(131) Turkevich, J.; Stevenson, P. C.; Hillier, J. *Discussions of the Faraday Society* **1951**, *No. 11*, 55-75.

(132) Turkevich, J.; Stevenson, P. C.; Hillier, J. *J. Phys. Chem.* **1953**, *57*, 670-673.

(133) Kumar, S.; Gandhi, K. S.; Kumar, R. *Ind. Eng. Chem. Res.* **2007**, *46*, 3128-3136.

(134) Frens, G. *Nature Physical Science* **1973**, *241*, 20-22.

(135) Freund, P. L.; Spiro, M. *J. Phys. Chem.* **1985**, *89*, 1074-1077.

(136) Chow, M. K.; Zukoski, C. F. *J. Colloid Interface Sci.* **1994**, *165*, 97-109.

(137) Turkevich, J.; Kim, G. *Science* **1970**, *169*, 873-9.

(138) Sehayek, T.; Lahav, M.; Popovitz-Biro, R.; Vaskevich, A.; Rubinstein, I. *Chem. Mater.* **2005**, *17*, 3743-3748.

(139) Turkevich, J.; Miner, R. S., Jr.; Babenkova, L. *J. Phys. Chem.* **1986**, *90*, 4765-7.

(140) Brugger, P. A.; Cuendet, P.; Graetzel, M. *J. Am. Chem. Soc.* **1981**, *103*, 2923-7.

(141) Pillai, Z. S.; Kamat, P. V. *J. Phys. Chem. B* **2004**, *108*, 945-951.

(142) Lee, P. C.; Meisel, D. *J. Phys. Chem.* **1982**, *86*, 3391-3395.

(143) Brust, M.; Walker, M.; Bethell, D.; Schiffrin, D. J.; Whyman, R. *J. Chem. Soc., Chem. Commun.* **1994**, 801-2.

(144) Brust, M.; Fink, J.; Bethell, D.; Schiffrin, D. J.; Kiely, C. *J. Chem. Soc., Chem. Commun.* **1995**, 1655-1657.

(145) Dahl, J. A.; Maddux, B. L. S.; Hutchison, J. E. *Chem. Rev.* **2007**, *107*, 2228-2269.

(146) Chen, S.; Kimura, K. *Langmuir* **1999**, *15*, 1075-1082.

(147) Yonezawa, T.; Sutoh, M.; Kunitake, T. *Chem. Lett.* **1997**, 619-621.

(148) Chen, S.; Kimura, K. *J. Phys. Chem. B* **2001**, *105*, 5397-5403.

(149) Leff, D. V.; Brandt, L.; Heath, J. R. *Langmuir* **1996**, *12*, 4723-4730.

(150) Jana, N. R.; Peng, X. *J. Am. Chem. Soc.* **2003**, *125*, 14280-14281.

(151) Hiramatsu, H.; Osterloh, F. E. *Chem. Mater.* **2004**, *16*, 2509-2511.

(152) Aslam, M.; Fu, L.; Su, M.; Vijayamohanan, K.; Dravid, V. P. *J. Mater. Chem.* **2004**, *14*, 1795 - 1797.

(153) Newman, J. D. S.; Blanchard, G. J. *Langmuir* **2006**, *22*, 5882-5887.

(154) Weare, W. W.; Reed, S. M.; Warner, M. G.; Hutchison, J. E. *J. Am. Chem. Soc.* **2000**, *122*, 12890-12891.

(155) Warner, M. G.; Reed, S. M.; Hutchison, J. E. *Chem. Mater.* **2000**, *12*, 3316-3320.

(156) Brown, L. O.; Hutchison, J. E. *J. Am. Chem. Soc.* **1999**, *121*, 882-883.

(157) Braunstein, P.; Kormann, H.-P.; Meyer-Zaika, W.; Pugin, R.; Schmid, G. *Chem. Eur. J.* **2000**, *6*, 4637-4646.

(158) Lahav, M.; Sehayek, T.; Vaskevich, A.; Rubinstein, I. *Angew. Chem. Int. Ed.* **2003**, *42*, 5576-5579.

(159) Decher, G.; Schlenoff, J. B. *Multilayer Thin Films: Sequential Assembly of Nanocomposite Materials*; Wiley-VCH: Weinheim, Germany, 2003.

(160) Decher, G.; Schmitt, J. *Thin Solid Films* **1992**, *210/211*, 831-835.

(161) Benkirane-Jessel, N.; Lavalle, P.; Ball, V.; Ogier, J.; Senger, B.; Picart, C.; Schaaf, P.; Voegel, J.-C.; Decher, G. *Macromol. Eng.* **2007**, *2*, 1249-1305.

(162) Decher, G. *Science* **1997**, *277*, 1232-1237.

(163) Arys, X.; Jonas, A. M.; Laschewsky, A.; Legras, R. In *Supramolecular Polymers*; Ciferri, A., Ed.; CRC Press: 2005, p 651-710.

(164) Rubner, M. F. In *Multilayer Thin Films*; Decher, G., Schlenoff, J. B., Eds. 2003, p 133-154.

(165) Shiratori, S. S.; Rubner, M. F. *Macromolecules* **2000**, *33*, 4213-4219.

(166) Ruths, J.; Essler, F.; Decher, G.; Riegler, H. *Langmuir* **2000**, *16*, 8871-8878.

(167) Kurth, D. G.; Volkmer, D.; Klitzing, R. V. In *Multilayer Thin Films*; Decher, G., Schlenoff, J. B., Eds.; Wiley-VCH: Weinheim, Germany, 2003.

(168) Porcel, C. H.; Izquierdo, A.; Ball, V.; Decher, G.; Voegel, J. C.; Schaaf, P. *Langmuir* **2005**, *21*, 800-802.

(169) Picart, C.; Lavalle, P.; Hubert, P.; Cuisinier, F. J. G.; Decher, G.; Schaaf, P.; Voegel, J. C. *Langmuir* **2001**, *17*, 7414-7424.

(170) Ladam, G.; Schaaf, P.; Cuisinier, F. J. G.; Decher, G.; Voegel, J.-C. *Langmuir* **2001**, *17*, 878-882.

(171) Cavalieri, F.; Postma, A.; Lee, L.; Caruso, F. *ACS Nano* **2009**, *3*, 234-240.

(172) Johnston, A. P. R.; Read, E. S.; Caruso, F. *Nano Lett.* **2005**, *5*, 953-956.

(173) Wang, Y.; Caruso, F. *Chem. Mater.* **2005**, *17*, 953-961.

(174) Bergbreiter, D. E.; Franchina, J. G.; Kabza, K. *Macromolecules* **1999**, *32*, 4993-4998.

(175) Zhao, M.; Liu, Y.; Crooks, R. M.; Bergbreiter, D. E. *J. Am. Chem. Soc.* **1999**, *121*, 923-930.

(176) Srivastava, S.; Kotov, N. A. *Acc. Chem. Res.* **2008**, *41*, 1831-1841.

(177) Qin, S.; Qin, D.; Ford, W. T.; Zhang, Y.; Kotov, N. A. *Chem. Mater.* **2005**, *17*, 2131-2135.

(178) Lee, S. W.; Kim, B.-S.; Chen, S.; Shao-Horn, Y.; Hammond, P. T. *J. Am. Chem. Soc.* **2009**, *131*, 671-679.

(179) Lee, D.; Gemici, Z.; Rubner, M. F.; Cohen, R. E. *Langmuir* **2007**, *23*, 8833-8837.

(180) Lee, D.; Rubner, M. F.; Cohen, R. E. *Nano Lett.* **2006**, *6*, 2305-2312.

(181) Lee, D.; Omolade, D.; Cohen, R. E.; Rubner, M. F. *Chem. Mater.* **2007**, *19*, 1427-1433.

(182) Ichinose, I.; Kawakami, T.; Kunitaki, T. *Adv. Mater.* **1998**, *10*, 535-539.

(183) Chen, H.; Dong, S. *Talanta* **2007**, *71*, 1752-1756.

(184) Chirea, M.; Garcia-Morales, V.; Manzanares, J. A.; Pereira, C.; Gulaboski, R.; Silva, F. *J. Phys. Chem. B* **2005**, *109*, 21808-21817.

(185) Chirea, M.; Pereira, C. M.; Silva, F. *J. Phys. Chem. C* **2007**, *111*, 9255-9266.

(186) Yang, M.; Yang, Y.; Yang, H.; Shen, G.; Yu, R. *Biomaterials* **2005**, *27*, 246-255.

(187) Srivastava, S.; Ball, V.; Podsiadlo, P.; Lee, J.; Ho, P.; Kotov, N. A. *J. Am. Chem. Soc.* **2008**, *130*, 3748-3749.

(188) Malikova, N.; Pastoriza-Santos, I.; Schierhorn, M.; Kotov, N. A.; Liz-Marzan, L. M. *Langmuir* **2002**, *18*, 3694-3697.

(189) Lee, D.; Cohen, R. E.; Rubner, M. F. *Langmuir* **2005**, *21*, 9651-9659.

(190) Joly, S.; Kane, R.; Radzilowski, L.; Wang, T.; Wu, A.; Cohen, R. E.; Thomas, E. L.; Rubner, M. F. *Langmuir* **2000**, *16*, 1354-1359.

(191) Dai, J.; Bruening, M. L. *Nano Lett.* **2002**, *2*, 497-501.

(192) Yang, S. Y.; Lee, D.; Cohen, R. E.; Rubner, M. F. *Langmuir* **2004**, *20*, 5978-5981.

(193) Kim, B.-S.; Park, S. W.; Hammond, P. T. *ACS Nano* **2008**, *2*, 386-392.

(194) Delongchamp, D. M.; Hammond, P. T. *Langmuir* **2004**, *20*, 5403-5411.

(195) Bergbreiter, D. E.; Tao, G.; Franchina, J. G.; Sussman, L. *Macromolecules* **2001**, *34*, 3018-3023.

(196) Sun, J.; Wu, T.; Liu, F.; Wang, Z.; Zhang, X.; Shen, J. *Langmuir* **2000**, *16*, 4620-4624.

(197) Kohli, P.; Blanchard, G. J. *Langmuir* **2000**, *16*, 8518-8524.

(198) Kidambi, S.; Bruening, M. L. *Chem. Mater.* **2005**, *17*, 301-307.

(199) Yu, A.; Liang, Z.; Caruso, F. *Chem. Mater.* **2005**, *17*, 171-175.

(200) Bhattacharjee, S.; Bruening, M. L. *Langmuir* **2008**, *24*, 2916-2920.

(201) Malaisamy, R.; Bruening, M. L. *Langmuir* **2005**, *21*, 10587-10592.

(202) Stanton, B. W.; Harris, J. J.; Miller, M. D.; Bruening, M. L. *Langmuir* **2003**, *19*, 7038-7042.

(203) Bruening, M. In *Multilayer Thin Films*; Decher, G., Schlenoff, J. B., Eds. 2003, p 487-510.

(204) Harris, J. J.; Derose, P. M.; Bruening, M. L. *J. Am. Chem. Soc.* **1999**, *121*, 1978-1979.

(205) Martin, C. R. *Science* **1994**, *266*, 1961-6.

(206) Ai, S.; Lu, G.; He, Q.; Li, J. *J. Am. Chem. Soc.* **2003**, *125*, 11140-11141.

(207) Liang, Z.; Susha, A. S.; Yu, A.; Caruso, F. *Adv. Mater.* **2003**, *15*, 1849-1853.

Some of the text and figures contained in chapter two appeared in the following publications.
Dotzauer, D. M.; Dai, J.; Sun, L.; Bruening, M. L. *Nano Lett.* **2006**, *6*, 2268-2272.
Dotzauer, D. M.; Bhattacharjee, S.; Wen, Y.; Bruening, M. L. *Langmuir* **2009**, *25*, 1865-1871.

Chapter 2: Catalytic Reduction of Nitroaromatic Compounds with Au-Nanoparticle Containing Membranes

2.1 Introduction

The reduction of aromatic nitro compounds to the corresponding amines is important in synthetic chemistry because aromatic amines are frequent intermediates in the production of pharmaceuticals, agrochemicals, polymers, dyes, and other fine chemicals.[1-6] A variety of methods exist for nitro group reduction, including direct hydrogenation,[7-12] catalytic transfer hydrogenation,[13-15] and photocatalytic,[16] electrochemical,[17,18] enzymatic,[19-21] and hydride reduction.[22] In each case, transformation to the amine likely occurs via formation of nitroso and hydroxylamine intermediates.[17] Furthermore, under basic conditions, additional azo, azoxy, and hydrazo intermediates may also form (Scheme 2.1).[23]

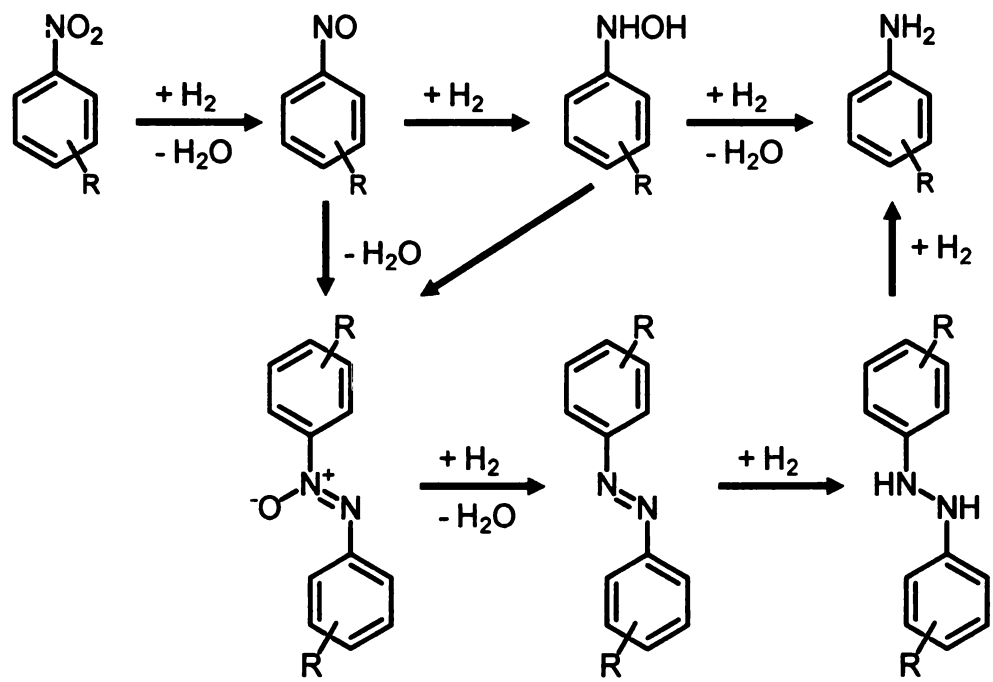

Scheme 2.1 Formation of functionalized anilines from the parent nitro compound via hydrogenation with multiple reduction pathways.

If reactions of these intermediates occur too slowly, they may accumulate.[24-26] Thus, it is important to develop reactions that lead to rapid formation of amine compounds.

Hydrogenation of simple aromatic nitro compounds readily occurs with traditional commercial catalysts and can often be carried out easily at large scales.[24] However, the selective hydrogenation of nitro groups in the presence of other reducible functional groups is more challenging. Reduction of these other functional groups can occur during any one of the intermediate steps in the transformation to the amine. Therefore, effective nitro-hydrogenation catalysts should be active toward each step in the nitro reduction but inactive toward reduction of other functional groups such as C=C, C≡C, C≡N, C=O, and Cl.

Recently, a number of studies focused on the development of noble metal nanoparticle catalysts and methods that can provide high selectivity for the amine product while maintaining high yields. Studies by Serna et al. show that titania-supported AuNPs provide selectivity for nitro group reduction in the presence of C=C, C=O, and C≡N functional groups.[27-29] Chen et al. also used supported AuNPs to demonstrate selective reduction for a number of nitroaromatic compounds.[30] Gold is sometimes chosen as a catalyst material because it can effectively catalyze the reduction of the nitro group, albeit under relatively high temperature, whereas it is much less active than traditional platinum or palladium catalysts in the hydrogenation of other reducible functional groups.[31] This may be partly because NO_2 adsorbs molecularly to the surface of Au and dissociatively to Pt or Pd surfaces.[32] Nevertheless, the high

temperature/pressure and relatively long reaction times for nitro hydrogenation with gold catalysts limit the application of these materials.[27]

Carbon nanofiber-supported Pt and Pd nanoparticles catalyze selective hydrogenation of aromatic nitro groups in halogenated compounds, but these catalysts are less selective in the presence of other reducible functional groups.[33] Ranu et al. use Cu nanoparticles and ammonium formate in ethylene glycol for reduction of aromatic nitro compounds with high chemoselectivity. However, these reactions also take place under high temperature (120 °C) and long reaction times (8-12 h).[14]

A number of studies also examine the reduction of nitroaromatic compounds by sodium borohydride in reactions facilitated by nanoparticles in solution[34-36] and on polymeric supports.[37-44] These studies mainly discuss the catalytic reduction of 4-nitrophenol, however, and do not show whether these catalyst systems can selectively reduce nitro groups in compounds containing other reducible functional groups. More recent research investigated the use of Au[45] and Ni[46] clusters as chemoselective catalysts in the reduction of nitroaromatic compounds with sodium borohydride, but these clusters are difficult to prepare.

This chapter examines the use of Au nanoparticle-containing membranes as catalysts for the reduction of aromatic nitro groups. We begin by discussing the preparation and characterization of Au nanoparticle-containing films. The catalytic reduction of 4-nitrophenol to 4-aminophenol by sodium borohydride was used as a test reaction to investigate the kinetics of membrane reactions.

Controlling the flow rate and therefore residence time in membrane reactions allows excellent control over conversion. Remarkably, Au nanoparticles contained in membranes exhibit the same activity as unsupported Au nanoparticles in solution. Furthermore, additional studies looking at the reduction of nitro groups in the presence of a variety of reducible and non-reducible functional groups demonstrate the ability to control product formation in membrane reactions.

2.2 Experimental Methods

2.2.1 Materials

Anodisc aluminum oxide membranes (25 mm disks with 0.2 μm diameter pores) and Nuclepore track-etched polycarbonate membranes (25 mm disks with 0.2 μm diameter pores) were purchased from Whatman. Nylon membranes (25 mm disks with nominal 0.45 μm diameter pores) were purchased from Millipore. Nitroaromatic compounds, $HAuCl_4$, sodium citrate, sodium borohydride, aluminum oxide (100 mesh), poly(allylamine hydrochloride) (PAH, M_w = 15,000), poly(ethylenimine) (PEI, branched, M_w = 25,000), and poly(sodium styrene sulfonate) (PSS, M_w = 70,000) were reagent grade and used as received from Sigma-Aldrich. Poly(acrylic acid) (PAA, M_w = 5,000) was obtained from Polysciences. All solutions were prepared with deionized water (18.2 MΩ) obtained from a Milli-Q (Millipore) purification system.

2.2.2 Modification of Aluminum Wafers with Polyelectrolyte/AuNP Films

Gold nanoparticles with an average diameter of 12 nm were prepared according to the citrate reduction method described in the literature.[47,48] In a 250 mL round bottom flask equipped with a condenser, 100 mL of aqueous $HAuCl_4$ (1.0 mM) was heated to boiling under vigorous stirring, and 10 mL of a heated sodium citrate (38.8 mM) was added to this solution under continued stirring. Immediately after adding the sodium citrate, the solution turned from faint yellow to colorless. After 15 seconds, the color changed to light blue, then dark blue, and finally to red after about 45 seconds. The mixture was boiled while stirring for 15 minutes to allow the reaction to go to completion, and then removed from heat and stirred for an additional 10 minutes. The resulting AuNP solutions were stored in an amber bottle at 5 °C until use.

Al-coated Si wafers (200 nm Al on Si(100) wafers) were first cleaned in a UV/ozone cleaner (Boekel) for 15 min. For film formation, a bare aluminum wafer was immersed in an aqueous solution containing 0.02 M PAA and 0.5 M NaCl (pH adjusted to 4.5 with 1.0 M NaOH) for 5 min (molarities of polyelectrolytes are always given with respect to the repeating unit). The aluminum substrate was rinsed with deionized water for 1 min before exposure to a solution containing 0.5 M NaCl and either 0.02 M PAH (pH adjusted to 4.5 with 0.1 M HCl) or 0.02 M PEI (pH adjusted to 9.0 with 1.0 M HCl) for 5 min, followed by another water rinse for 1 min. The substrate was then immersed for 5 min in the as-prepared AuNP solution for adsorption of a layer of AuNPs and finally

rinsed for 1 min in deionized water. Alternating exposure to polycation and AuNP solutions was repeated until the desired number of bilayers was deposited.

2.2.3 Modification of Aluminum Oxide Powder with Polyelectrolyte/AuNP Films

To prepare heterogeneous catalysts for use in a conventional batch reactor, alumina powder was modified with AuNPs using LbL deposition of a polyelectrolyte/AuNP film as shown in Figure 2.1. This catalyst preparation procedure was developed from a previous method for in-situ preparation of Pd nanoparticles in polyelectrolyte multilayer films.[49,50] In a 100-mL flask, 7.5 g of 100 mesh alumina was added to 50 mL of a pH 4.5 solution containing 0.02 M PAA and 0.5 M NaCl, and then stirred vigorously for 10 min. The alumina was then allowed to settle and the supernatant was decanted. To remove excess polyelectrolyte, the alumina particles were washed 4 times by adding 50 mL of deionized water, stirring, letting the alumina settle, and decanting the water. Next, 50 mL of a pH 4.5 solution containing 0.02 M PAH and 0.5 M NaCl was added to the alumina, and this mixture was stirred for 10 min, after which the particles were washed as described above.

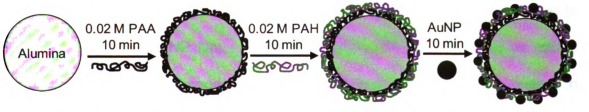

Figure 2.1 Schematic diagram of the deposition of polyelectrolyte/AuNP films on alumina powder.

To deposit the AuNPs, 15 mL of the as-prepared AuNP solution was diluted to 60 mL with deionized water, and this solution was added to the PAA/PAH-modified alumina and stirred for 10 min. The alumina was then allowed to settle and rinsed 4 times with water as described above. After decanting the final water rinse, the resulting powder was dried under vacuum for 8 hours to remove residual water. The final gold loading was 0.4 mg Au per g of alumina powder as determined by flame atomic absorption spectroscopy (FAAS, Varian SpectrAA-200).

2.2.4 Modification of Disk-Shaped Membranes with Polyelectrolyte/AuNP Films

Anodized alumina membranes were pretreated in a UV/ozone cleaner for 15 min prior to modification with polyelectrolyte films. During film formation, the membranes were placed in an Amicon 8010 ultrafiltration cell, and all solutions were passed through the membranes using a peristaltic pump (Cole Parmer Masterflex C/L) attached to the permeate side of the Amicon cell. For alumina membrane modification, solutions of PAA (10-15 mL), water (40 mL), PAH (10-15 mL), water (40 mL), citrate-stabilized AuNPs, and water (40 mL) were sequentially passed through the membranes at a flux of ~ 0.02 mL/cm^2-sec to deposit a PAA/PAH/AuNP film. Additional PAH/AuNP bilayers could be added by simply alternating passage of the PAH and AuNP solutions with rinsing in between. The polyelectrolyte deposition solutions had the same composition as those used for modification of alumina powder. Polycarbonate and nylon

membrane modification involved the same process, except a solution containing 0.02 M PSS (pH not adjusted) and 0.5 M NaCl was used to deposit the precursor polyanion layer because PSS likely adheres better than PAA to polymeric membranes.[51] For each membrane type, the as-prepared AuNP solution was diluted by a factor of 10 to 20 and passed through the membrane until the AuNPs were no longer adhering to the polyelectrolyte layer, i.e., the solution exiting the membrane exhibited the same red color as the solution entering the membrane. For some experiments, PEI solution was used in place of PAH solution during the deposition process.

2.2.5 Characterization of Polyelectrolyte/AuNP Films

Citrate-stabilized AuNPs were characterized by UV-Vis spectrophotometry (Perkin Elmer Lambda 40) and transmission electron microscopy (JEM-2200FS microscope). TEM samples of Au nanoparticles were prepared by diluting the as-prepared AuNP solution by a factor of 10 and placing a 2 μL drop of the resulting solution on a carbon-coated copper TEM grid and letting the solvent evaporate. The thicknesses of PAA/[PAH/AuNP]$_x$ and PAA/[PEI/AuNP]$_x$ films on Al wafers were determined by ellipsometry using a J. A. Woollam model M-44 rotating analyzer ellipsometer. Au deposition was also confirmed by specular reflectance UV-Vis spectroscopy.

Aluminum wafer and membrane samples were imaged using a Hitachi S-4700 II field-emission scanning electron microscope (FESEM). Prior to imaging, membrane samples were fractured (alumina was broken with tweezers,

polycarbonate was simply torn, and nylon was fractured in liquid nitrogen with tweezers) to reveal a cross-section and coated with 5 to 10 nm of Au with a Pelco SC-7 sputter coater. No sample preparation was necessary for imaging of AuNP-containing films on Al wafers. To determine the AuNP content in membrane and alumina-powder samples, aqua regia (3 parts HCl, 1 part HNO_3) was used to dissolve the Au, and these solutions were diluted and analyzed by FAAS.

2.2.6 Catalytic Reactions with As-Prepared Au Nanoparticles and Nanoparticles Supported on Alumina Powder

Homogeneous catalytic reactions with the as-prepared AuNPs allowed comparison of the unsupported AuNP activity with the activities of alumina powder- and membrane-supported AuNPs. In a typical reaction, 20 µL of the as-prepared AuNP solution was added to 3 mL of a solution containing 0.1 mM nitro compound and 10 mM $NaBH_4$ in a quartz cuvette. Samples were analyzed by UV-Vis spectrophotometry either by scanning a range of wavelengths during regular time intervals or monitoring the absorbance at a specific wavelength continuously. In some cases, the reactions took place in a reaction flask with 20 to 50 mL volumes under continuous stirring, and sample aliquots were collected and analyzed immediately by UV-Vis.

In a typical slurry reaction using alumina powder-supported AuNPs, 75 mg of catalyst was added to 60 mL of an aqueous solution containing 0.1 to 5 mM nitro compound and a 100-fold excess of $NaBH_4$, and the mixture was stirred

vigorously at room temperature to suspend the catalyst. The use of a high excess of $NaBH_4$ ensures that its concentration remains essentially constant during the reaction, which allows the assumption of pseudo first order kinetics with respect to the nitro compound. Samples of the reaction mixture were collected at specific time intervals and filtered through cotton prior to analysis by UV-Vis spectrophotometry and/or gas chromatography-mass spectrometry (GC-MS, Hewlett-Packard G1800B GCD system with a HP-5MS column). For GC-MS analysis, 3 mL of sample was extracted three times into 1 mL portions of diethyl ether, which were then combined. In all reactions, the MS response was assumed to be the same for reactants, intermediates, and products. (This assumption was confirmed in the case of nitrobenzene, aniline, and nitrosobenzene, but due to the limited availability of other nitroso species it was not confirmed with other compounds.) The ratios of peak areas from the chromatograms were used to determine the percent of each substrate in the reaction mixture. Identification of intermediate species was confirmed by comparison with a mass spectrum library. Azoxy intermediates appeared at low levels in some reactions and small amounts of azo and azoxy species may have formed in other cases,[52,53] but these compounds might not readily elute from the column. To prove that the extraction was efficient at collecting all reaction products, the aqueous portion that remained after ether extraction was analyzed by UV-Vis spectrophotometry from 200 to 600 nm.

2.2.7 Catalytic Reactions with Au Nanoparticle-Containing Membranes

To perform reduction reactions with the AuNP-containing membranes, a room-temperature, aqueous solution containing 0.1 to 5 mM nitro compound and a 100-fold excess of $NaBH_4$ was passed through the membrane using either a peristaltic pump (Figure 2.2a) or pressure supplied by nitrogen gas on the feed side of the membrane (Figure 2.2b). Samples were analyzed by UV-Vis spectrophotometry and/or GC-MS to determine the extent of the reaction as described above. In the experiments that examined the effect of temperature on membrane reactions, the solution was first heated in a silicon oil bath or cooled in an ice bath to achieve the desired temperature, and then the solution passed through the membrane as in a typical experiment. From the beginning to the end of these experiments, the solution temperature fluctuated by only 1 to 2 °C

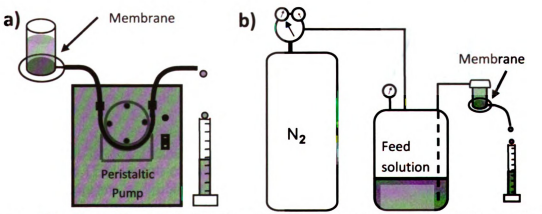

Figure 2.2 Experimental apparatuses used for performing catalytic reactions with membranes at a) low flow rates, and b) higher flow rates.

2.3 Results and Discussion

2.3.1 Characterization

2.3.1.1 Au Nanoparticle Characterization

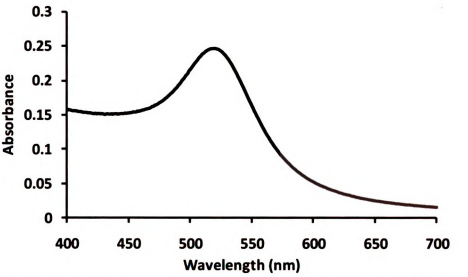

Figure 2.3 UV-Vis spectrum of a 0.12 mM Au nanoparticle solution showing a maximum absorbance at 517 nm. Molarity is given with respect to Au atoms.

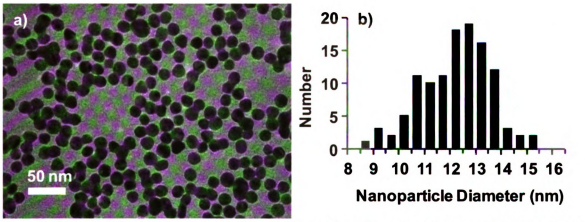

Figure 2.4 a) TEM image of citrate-stabilized AuNPs on a carbon-coated copper grid. b) Histogram of AuNP diameters taken from several TEM images. The average particle diameter is 12 ± 1 nm.

Au nanoparticles prepared according to the citrate reduction method[48] exhibited a bright red color with an absorbance maximum at 517 nm (Figure 2.3), which suggests a AuNP size of 10 to 15 nm.[54,55] A red shift in the absorbance maximum would indicate that some nanoparticle aggregation occurred or that the

size of the nanoparticles was larger than expected.[56] Further analysis by TEM showed a monodisperse size distribution with an average nanoparticle diameter of 12 ± 1 nm (Figure 2.4).

2.3.1.2 Characterization of Polyelectrolyte/AuNP Films on Aluminum

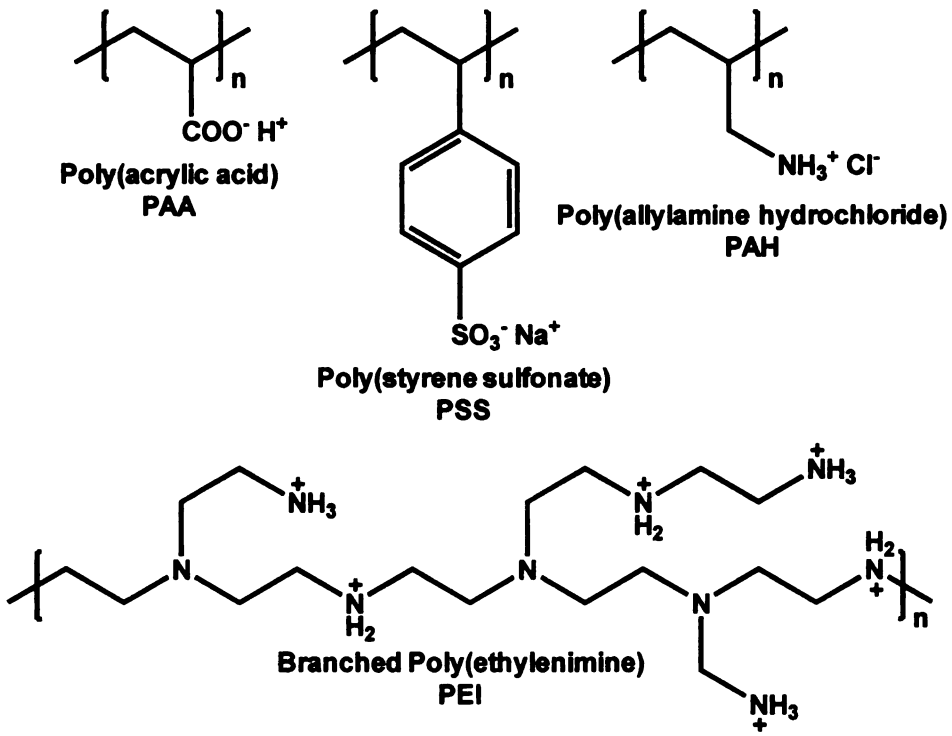

Figure 2.5 Structures of polyelectrolytes used in this work.

This study employed PAA or PSS as the polyanion and PAH or PEI as the polycation (Figure 2.5) for multilayer film formation because these are the most frequently used polyelectrolytes in layer-by-layer film formation.[57-61] The polyelectrolytes in a particular film have a large impact on the amount of nanoparticle adsorption that takes place. For example, films containing branched PEI should be thicker and thus have more sites for nanoparticle adsorption than films containing PAH. This increased thickness with the PEI-containing film is

likely due to the highly branched structure of PEI compared to the linear structure of PAH. The polyanion also plays an important role in nanoparticle adsorption. In studies involving polymeric substrates, PSS is the best choices for the precursor polyelectrolyte because it adheres well to polymer surfaces. If PAA is used instead, almost no polyelectrolyte adsorption takes place, and this leads to very thin films that would not bind much Au.

Prior to depositing polyelectrolyte/AuNP films in membranes, we deposited these coatings on Al-coated Si wafers for characterization. We first used ellipsometry to determine the thickness of $[PAA/PAH]_x$ and $[PEI/PAA]_x$ films. In the case of $[PEI/PAA]_x$, PEI was deposited at a pH of 9 because the aluminum/aluminum oxide surface is negatively charged at this pH,[62] so it is not necessary to start with an initial PAA layer. In contrast, we deposited PAH at a pH of 4.5, so adsorption of $[PAA/PAH]_x$ films began with PAA. At this deposition pH, the PAH is partially protonated yielding films with thicknesses of several nm, which are desired for this application.[57] Ellipsometry demonstrates uniform, stepwise growth of both types of films (Figure 2.6). The thickness increase after the addition of each bilayer, with the exception of the initial bilayer, was approximately 4 nm and 5 nm for PAA/PAH and PEI/PAA films, respectively, which agrees with previous reports.[57,63]

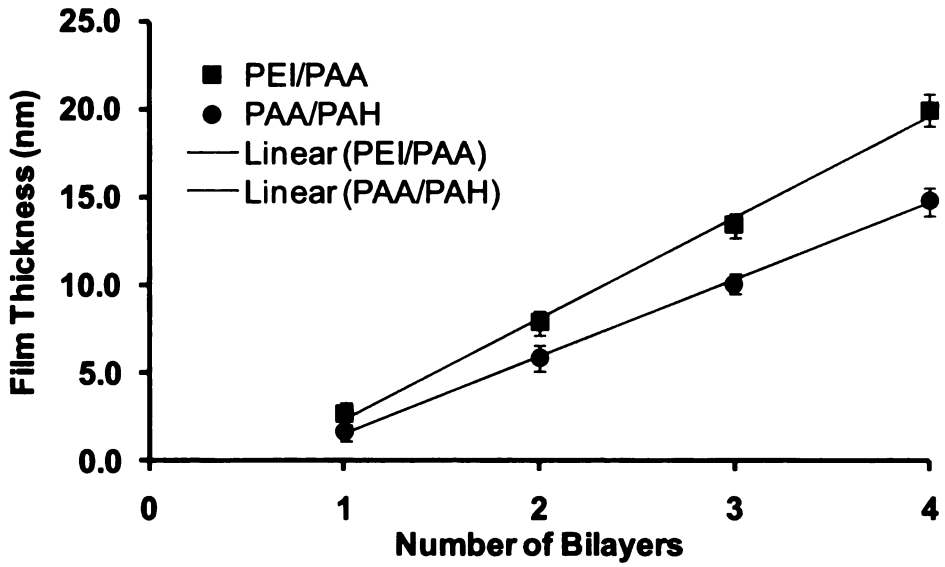

Figure 2.6 Ellipsometric thicknesses for multilayered $[PEI/PAA]_x$ (squares) and $[PAA/PAH]_x$ (circles) films deposited on Al-coated Si wafers.

Determination of the ellipsometric thickness of thin films containing non-transparent Au nanoparticles is inherently much less accurate than measurement of polymer films which have a uniform refractive index. Thus, the deposition of Au nanoparticles was confirmed with UV-Vis and SEM analysis of the $PAA/[PAH/AuNP]_x$ films. Specular reflectance UV-Vis spectrophotometry of films on Al-coated Si wafers showed that a wafer coated with a PAA/PAH bilayer had almost no absorbance from 400 – 700 nm (Figure 2.7). On the other hand, a wafer coated with a PAA/PAH/AuNP film showed a peak absorbance at 517 nm, which is consistent with the UV-Vis spectrum of the as-prepared Au nanoparticles (Figure 2.4). Additionally, FESEM images of Al wafers coated with $PAA/[PAH/AuNP]_x$ films demonstrate that Au nanoparticles deposited uniformly on the Al wafer and remained well-separated (Figure 2.8). Images of films containing 2 and 3 PAH/AuNP bilayers (Figure 2.8c and 2.8d) show an increased

density of Au nanoparticles in the films, confirming that the LbL modification increased the Au loading with each deposition step. In the film containing 3 PAH/AuNP bilayers (Figure 2.8d), the Au nanoparticles appeared to form chains of 3 to 5 nanoparticles. However, since these images represent dry films, it is possible that the nanoparticles were still well-separated when the films were immersed in solution. When in solution, polyelectrolytes often undergo swelling,[59] which allows the AuNPs to have some mobility. The AuNPs may also have been somewhat separated in the z direction.

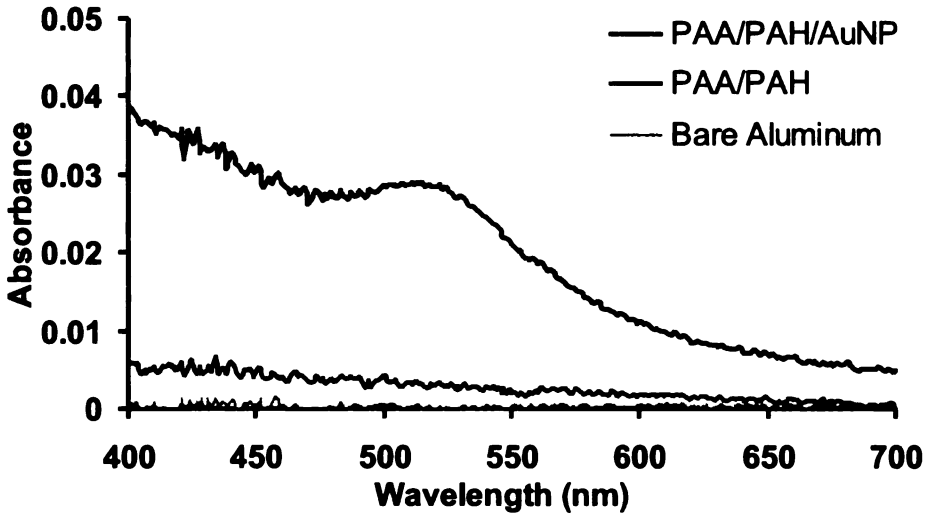

Figure 2.7 Specular reflectance UV-Vis spectra of an Al-coated Si wafer before (light gray line) and after (dark gray line) deposition of a PAA/PAH layer and subsequent adsorption of Au nanoparticles (black line).

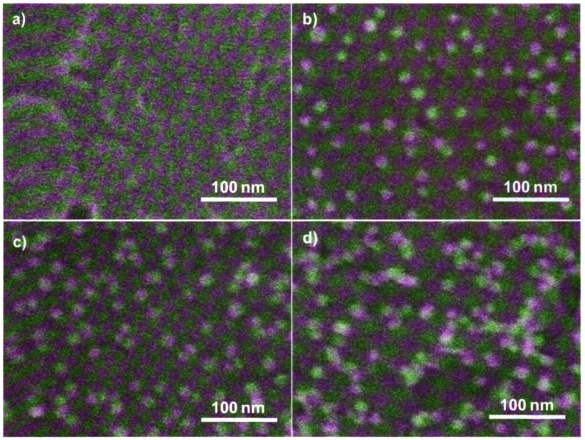

Figure 2.8 FESEM images of Al-coated Si wafers after deposition of a) PAA/PAH b) PAA/[PAH/AuNP]$_1$ c) PAA/[PAH/AuNP]$_2$ and d) PAA/[PAH/AuNP]$_3$ films.

2.3.1.2 Characterization of Polyelectrolyte/AuNP Films in Membranes

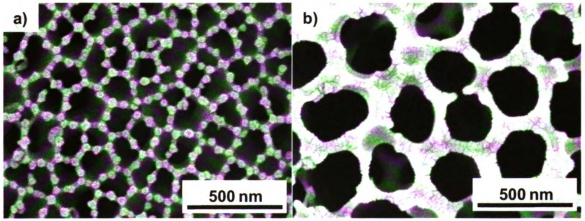

Figure 2.9 FESEM images of the a) skin layer and b) support layer of a commercially available anodized alumina membrane.

We chose to first modify anodized alumina membranes because they have a well-defined cylindrical pore structure, are mechanically stable, and can be easily functionalized.[64-66] The anodized alumina membranes used in this work were 60 μm thick with a 5 μm thick skin layer. The skin layer was highly branched and had pores with ~200 nm diameters (Figure 2.9a). The support layer of the membranes contained slightly larger pores (~230 nm diameter) that were cylindrical through the length of the membrane (Figure 2.9b). During modification of the membranes, we flowed solutions from the support side of the membrane to the skin layer side because the larger pore sizes in the support were less susceptible to cake layer formation on the membrane surface.

Alumina membranes should be positively charged when exposed to the citrate-stabilized AuNP solution (pH 6), but no visible adsorption of AuNPs occurred when flowing the Au nanoparticle solution through an untreated alumina membrane. Deposition of the AuNPs in the membrane required adsorption of an underlying PAA/PAH bilayer. PAA was chosen as the polyanion layer because in addition to electrostatic interactions with the positively charged alumina surface, the carboxylate groups could also coordinate strongly with the aluminum oxide. Subsequent addition of a polycation layer provided the highly positively charged surface needed for adsorption of citrate-stabilized nanoparticles. Furthermore, the amine groups of PAH and PEI most likely coordinated with AuNPs to enhance the adsorption of the particles onto the membrane surface. Figure 2.10 shows FESEM images of an alumina membrane before and after coating with a

PAA/PAH/AuNP film. The images clearly show the presence of the adsorbed Au nanoparticles.

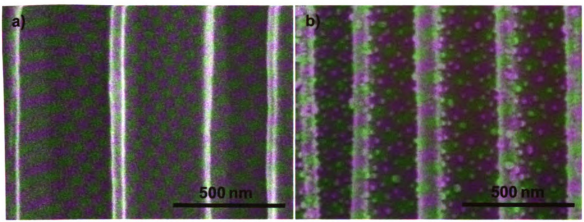

Figure 2.10 FESEM images of cross-sections of anodized alumina membranes a) before and b) after modification with a PAA/PAH/AuNP film.

After deposition of 1 PAA/PAH bilayer, adsorption of AuNPs yielded a red membrane, and the first 90 mL of a red 0.045 mM AuNP solution (concentration is given with respect to gold atoms) exited a PAA/PAH-modified membrane as a colorless liquid. UV-Vis spectrophotometry of the AuNP solution exiting the membrane demonstrated that >99% of the nanoparticles adsorbed to the membrane during modification. Once most of the adsorption sites became filled with AuNPs, the particles passed through the membrane, and the concentration of AuNPs in the permeate solution increased, as shown by UV-Vis spectrophotometry (Figure 2.11). Typically during membrane modification, the nanoparticle deposition step was considered complete once the permeate solution exhibited a red color that was easily visible.

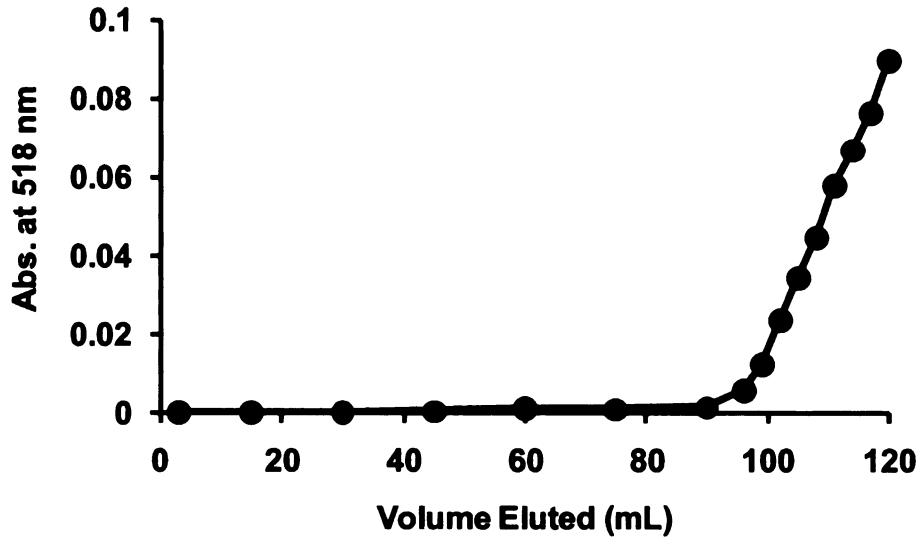

Figure 2.11 Plot of absorbance at 518 nm vs. volume eluted during deposition of Au nanoparticles in a PAA/PAH-modified alumina membrane. The Au concentration in the nanoparticle feed solution was 0.045 mM, which corresponds to an absorbance of 0.163 at 518 nm.

Dissolution of the adsorbed nanoparticles in aqua regia and analysis of this solution using FAAS revealed that the gold loading in porous alumina modified with one layer of PAA/PAH/AuNP was (4.9 ± 0.2) x 10^{-6} mol of Au per membrane. (The exposed surface area of the top of the 60 μm-thick membranes was 2.8 cm^2.) Assuming a porosity of 30% and a pore diameter of 0.23 μm, this gold loading corresponds to 5.5 x 10^{-9} mol Au per cm^2 of internal (pore) surface area. For a nanoparticle diameter of ~12 nm, this value is equivalent to 620 nanoparticles/ μm^2, which is reasonably consistent with the density of ~500 nanoparticles/ μm^2 seen in SEM images such as Figure 2.10b.

Multiple PAH/AuNP bilayers were deposited by continued alternating adsorption of PAH and AuNPs. For membranes modified with 2 and 3 total PAH/AuNP bilayers, the gold loading was 8.3 ± 0.2 μmol and 11.4 ± 0.6 μmol of

Au per membrane, respectively. Enhanced Au loading with adsorption of more layers confirms the layer-by-layer deposition. The FESEM image in Figure 2.12a corroborates the higher loading of AuNPs in the membrane with an additional PAH/AuNP bilayer. Porous alumina membranes were also modified through direct adsorption of PEI/AuNP bilayers (Figure 2.12b). In this case, the pH of the PEI deposition solution was 9, which allowed the polycation to adsorb directly to the alumina surface without the need for adsorption of a precursor PAA layer. Gold coverages were 9.2 ± 0.9, 17 ± 2, and 24 ± 3 μmol per membrane for alumina modified with 1, 2, and 3 PEI/AuNP bilayers, respectively. Deposition of PEI at pH 9 on a PAA precursor layer resulted in a surface that allowed similarly high AuNP adsorption.

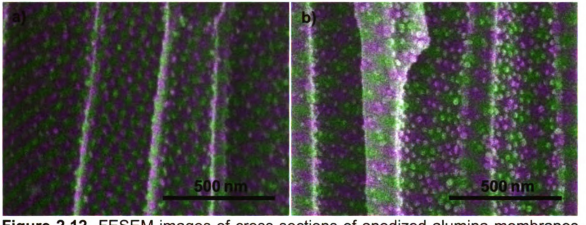

Figure 2.12 FESEM images of cross sections of anodized alumina membranes after modification with a) PAA/$[PAH/AuNP]_2$ and b) PEI/AuNP films.

One concern with LbL formation of polyelectrolyte/nanoparticle multilayer films in porous membranes is the possibility of plugging the pores. To confirm that the pores were still open after addition of each layer, we measured the flux of pure water through the membrane at a constant pressure. Furthermore, the

thickness of each layer was estimated by using the Hagen-Poiseuille equation for laminar flow through a tube with a circular cross-section, equation 2.1:

$$Q = \frac{\pi r^4}{8\mu}\frac{\Delta P}{l} \qquad (2.1)$$

where Q is the volumetric flow rate, r is the membrane pore radius, μ is the viscosity of water, ΔP is the pressure drop across the membrane, and l is the membrane thickness. Hence, by assuming that each pore is a cylindrical tube extending across the length of the membrane with an initial pore diameter of 230 nm, the decrease in flux and thus pore radius could be related to an increase in film thickness.

Interestingly, during deposition of each layer, the flux declined significantly after PAH deposition, and recovered slightly after AuNP deposition (Figure 2.13). This change in flux is likely due to the fact that the polyelectrolyte multilayer films

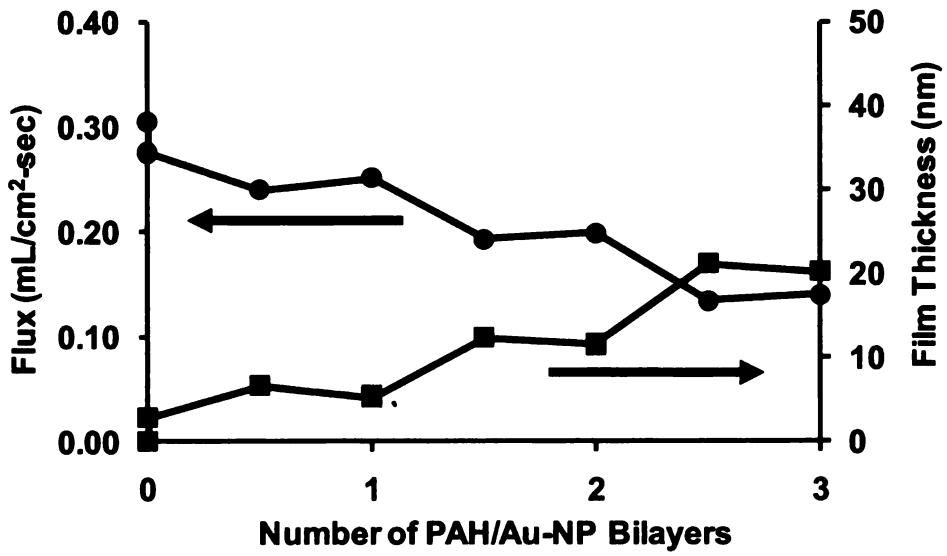

Figure 2.13 Plot of pure water flux and estimated film thickness vs. number of PAH/AuNP bilayers during modification of an alumina membrane. The pure water flux was measured at a constant pressure of 1.4 bar. The values for flux and film thickness after deposition of PAA are displayed as 0 PAH/AuNP bilayers.

undergo more swelling when the terminating layer is PAH. When terminating with a AuNP layer, the flux most likely increased because the PAH was bound to the nanoparticles and underwent less swelling into the solution. The overall estimated thickness of a PAA/[PAH/AuNP]$_3$ film was approximately 20 nm, which is consistent with the results seen for ellipsometric thickness measurements on Al-coated Si wafers.

To demonstrate the versatility of the LbL technique for membrane modification, we also deposited polyelectrolyte/AuNP films in polycarbonate track etched membranes containing nominal pore sizes of 0.2 μm and nylon membranes containing nominal pore sizes of 0.45 μm. Figure 2.14 shows FESEM images of the tops of unmodified polycarbonate and nylon membranes. Like the 60 μm thick porous alumina, track-etched polycarbonate membranes (Figure 2.14a) contain cylindrical pores, but the polycarbonate membrane thicknesses (~10 μm) and pore densities (10-15%) are relatively low. As a result, less gold was immobilized within the polycarbonate membranes. In contrast, the nylon membranes (Figure 2.14b) are thicker (150 μm) than alumina membranes and have a high pore density (~70%) in their sponge-like structure. In spite of the different structures, however, FESEM images show that the LbL technique deposited a dense layer of well-separated metal nanoparticles in both polycarbonate and nylon membranes (Figure 2.15).

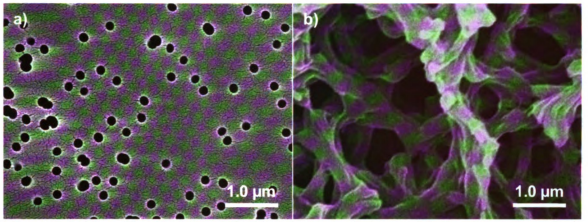

Figure 2.14 Top-down FESEM images of unmodified a) track-etched polycarbonate and b) nylon membranes.

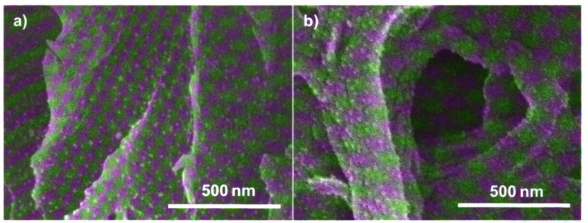

Figure 2.15 Cross-sectional FESEM images of polymer membranes modified with PSS/PAH/AuNP films. a) polycarbonate and b) nylon.

The amount of gold deposited in a polyanion/PAH/AuNP layer is 0.81, 4.9, and 9.1 µmoles for polycarbonate, alumina, and nylon membranes, respectively, and these values reflect the different surface areas of the membranes. Calculated porous surface areas of polycarbonate and alumina membranes are 62 and 890 cm^2/ membrane, assuming pore radii of 100 and 115 nm and porosities of 0.1 and 0.3 for polycarbonate and alumina, respectively. In the case of the nylon membrane, N_2 adsorption measurements showed a surface area of

1900 cm^2/ membrane. From these surface areas, the gold loading was 2.6, 1.1, and 0.95 μg/ cm^2 for polycarbonate, alumina, and nylon membranes, respectively. The polycarbonate had a somewhat higher loading than the other membranes, which might be due to differences in the interactions between the polyelectrolyte film and the substrate, or an underestimation of the polycarbonate membrane surface area.

2.3.2 Catalytic Reduction of 4-Nitrophenol with Au Nanoparticles in Solution

Reduction of 4-nitrophenol to 4-aminophenol in the presence of $NaBH_4$ (Scheme 2.2) provides a rapid, easily characterized reaction for examining the catalytic activity of nanoparticles immobilized in membranes. The reduction does not occur at a measurable rate in the absence of a catalyst and is readily monitored with UV/Vis spectrophotometry. In basic solution, the 4-nitrophenolate ion shows a strong absorbance maximum at 400 nm, and the rate of reduction is easily monitored by the disappearance of this peak (Figure 2.16). The gradual appearance of a peak at 298 nm shows the corresponding production of 4-aminophenol.

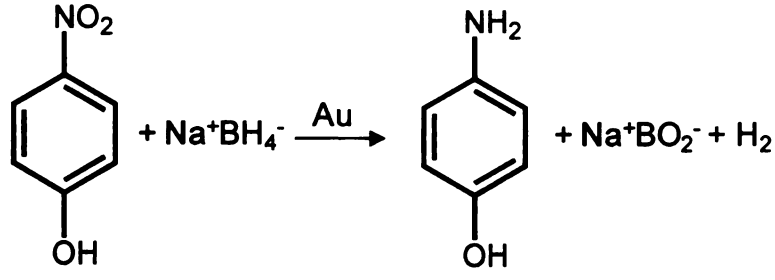

Scheme 2.2 Au-catalyzed reduction of 4-nitrophenol by $NaBH_4$.

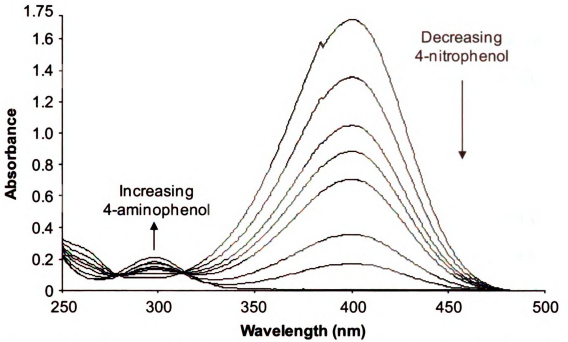

Figure 2.16 UV/Vis spectra demonstrating the catalytic reduction of 3 mL of 0.1 mM 4-nitrophenol in 10 mM $NaBH_4$ to form 4-aminophenol over time. Spectra were collected in 4 minute time intervals after addition of 20 µL of as-prepared AuNPs.

As a control experiment, the as-prepared citrate-stabilized Au nanoparticles (without immobilization in a film or on a support) were used for the catalytic reduction of 4-nitrophenol. In these experiments, the $NaBH_4$ was in >100 fold excess of 4-nitrophenol to ensure that the reaction followed pseudo-first order kinetics with respect to the 4-nitrophenol concentration according to equation 2.2:

$$\frac{dC}{dt} = -k_{app}C \qquad (2.2)$$

where C is the molar concentration of 4-nitrophenol at time t, and k_{app} is the apparent first order rate constant for the reaction.

To facilitate comparison of different nanoparticle systems, the batch reaction rate constants were normalized to the total surface area of the nanoparticles in the system divided by the solution volume according to equation 2.3:

$$\frac{dC}{dt} = -k_{norm}\frac{A}{V_{soln}}C \qquad (2.3)$$

where A is the total surface area of nanoparticles in the system in cm^2 and V_{soln} is the volume of the solution in cm^3 used in the reaction. Previous batch reactions that employed Pt, Au, or Ag nanoparticles dispersed in solution produced normalized rate constants, k_{norm}, ranging from 0.0005 to 0.055 cm/sec, and showed some variation with particle size.[36,38,41,43,67] These values were calculated from the apparent rate constants reported in the literature. The total surface area was calculated from the given diameters assuming that the nanoparticles were spherical, and volumes were determined from the experimental parameters.

For our reactions with AuNPs in solution, the solution was continuously stirred, and the rate constant was determined by collecting samples every 4 minutes and measuring the absorbance at 400 nm. The plot in Figure 2.17 conforms well to a linear fit suggesting that the reaction was indeed first order with respect to the concentration of 4-nitrophenol. The citrate-stabilized AuNPs used in this work exhibited a normalized rate constant, k_{norm}, of 0.014 ± 0.002 cm/sec. Thus, the activities of the citrate-stabilized AuNPs were in the same range as other nanoparticle systems previously reported in the literature.

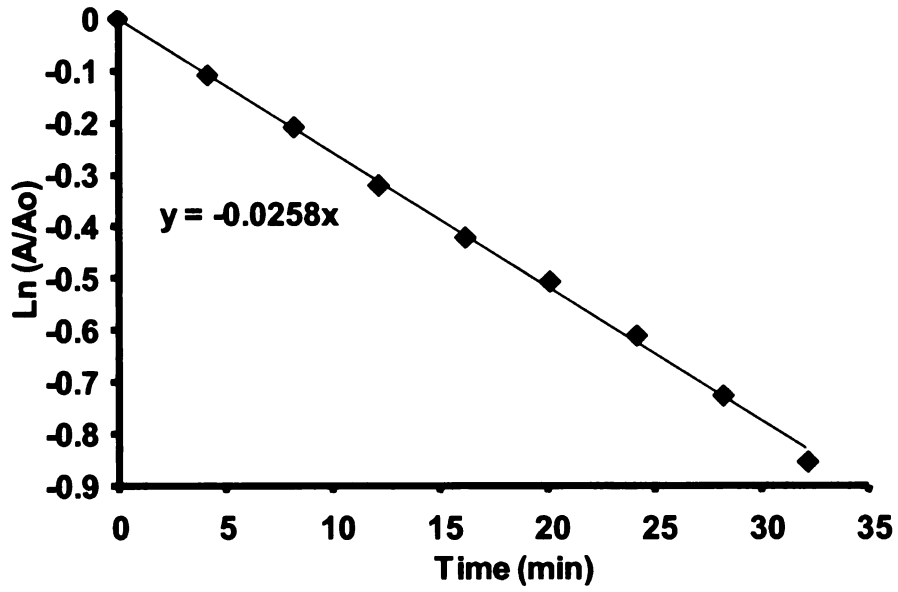

Figure 2.17 Plot of $\ln(A/A_o)$ vs. time for the reduction of 4-nitrophenol with $NaBH_4$ catalyzed by Au-nanoparticles in solution. A is the absorbance of the solution at 400 nm during the reaction and A_o is the initial absorbance of the solution. [4-nitrophenol] = 0.085 mM, [$NaBH_4$] = 12 mM, and [Au] = 5.9×10^{-4} mM.

2.3.3 Catalytic Reduction of 4-Nitrophenol with Membrane-Supported Au Nanoparticles

To the best of our knowledge, this was the first investigation of the reduction of 4-nitrophenol via flow-through catalytic membranes, and Au nanoparticle-containing membranes showed remarkable conversions of 4-nitrophenol to 4-aminophenol at high flow rates. Passage of a solution containing 0.1 mM 4-nitrophenol and 10 mM $NaBH_4$ through a PAA/PAH/AuNP modified alumina membrane at a rate of 0.29 mL/cm^2-sec resulted in reduction of greater than 99% of the 4-nitrophenol (Figure 2.18). Similarly high conversions occurred with 4-nitrophenol concentrations as high as 5 mM, provided that $NaBH_4$ was in at least a 50-fold excess. At such high conversions, the reaction

was essentially mass-flow limited even at these high fluxes. The solution flux of 0.29 mL/cm^2-sec corresponds to a residence time within the membrane of only 6.1 msec and a linear velocity of 0.98 cm/sec.

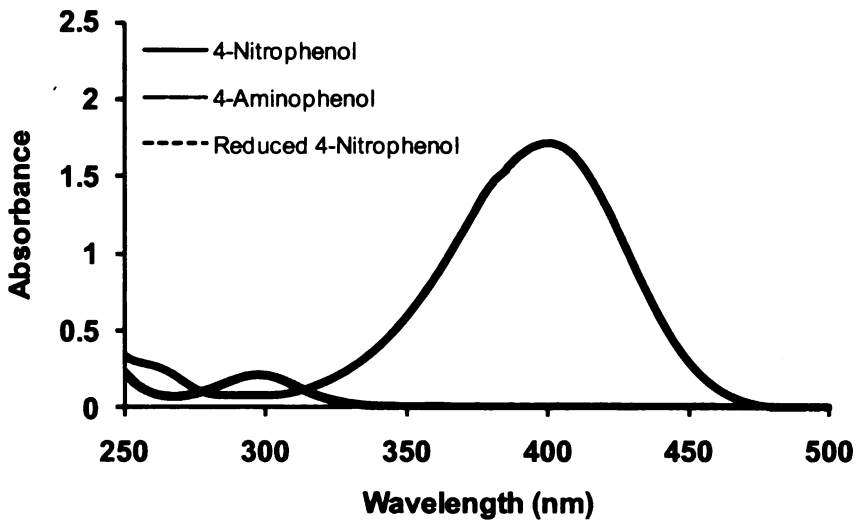

Figure 2.18 UV-VIS absorbance spectra of a 0.1 mM solution of 4-nitrophenol containing 10 mM $NaBH_4$ before (solid black line) and after (solid gray line) passing through a membrane modified with a PAA/PAH/AuNP film at a flux of 0.29 mL/cm^2-sec. The spectrum of a 0.1 mM 4-aminophenol solution containing 10 mM $NaBH_4$ is also shown as a reference (dotted black line that overlaps the gray line).

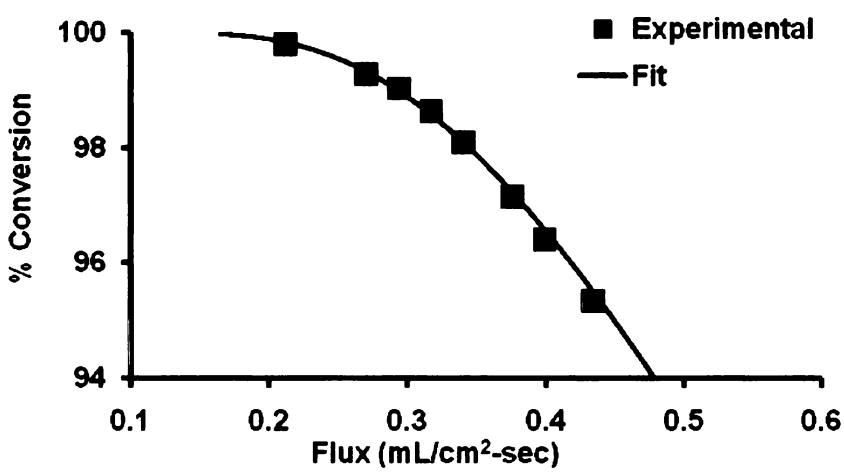

Figure 2.19 Plot of 4-nitrophenol reduction percentage vs. flow rate of a 0.4 mM 4-nitrophenol solution through a porous alumina membrane containing a PAA/PAH/AuNP film. [$NaBH_4$] = 20 mM.

At higher fluxes, conversion declined slightly as would be expected. Still, as Figure 2.19 shows, conversion was greater than 95% at fluxes as high as 0.44 mL/cm^2-sec (residence time of 4.1 msec). The maximum flux in this system was practically limited to about 0.53 mL/cm^2-sec because higher applied pressures resulted in membrane fracture.

The data in figure 2.19 conform well to a simple first-order kinetic model of the reaction, in which we assume that the membrane acts as a plug flow reactor. In a plug of solution flowing through a porous membrane, reduction of 4-nitrophenol occurs with pseudo first-order kinetics according to equation 2.4,

$$\frac{dC_{plug}}{dt} = -k_{mem}\frac{A}{V_{pores}}C_{plug} \qquad (2.4)$$

where C_{plug} is the molar concentration of 4-nitrophenol in the plug of solution at a given time, t, k_{mem} is the normalized, pseudo first order heterogeneous rate constant, A is the surface area of the nanoparticles in the membrane, and V_{pores} is the volume of the pores in the membrane. The use of nanoparticle surface area and membrane pore volume in the equation allowed the direct comparison between k_{mem} and k_{norm} for solution reactions.

Integration of the rate law in equation 2.4 yields the fractional conversion of the nitro group as a function of residence time in the membrane, t_{res}, as shown in equation 2.5.

$$conversion = 1 - exp\left[\frac{-k_{mem}t_{res}A}{V_{pores}}\right] \qquad (2.5)$$

Noting that residence time is equal to $l\varepsilon/F$, where l is membrane thickness, ε is membrane porosity, and F is the solution flux through the membrane; and that

V_{pores} is $V_{mem}\varepsilon$ where V_{mem} is the volume of the membrane including porous and nonporous regions, equation 2.5 can be rewritten as shown in equation 2.6,

$$conversion = 1 - exp\left[\frac{-k_{mem} lA}{V_{mem} F}\right] \qquad (2.6)$$

in quantities that are relatively easy to determine. We calculated the nanoparticle surface area, A, from the gold loading in the membrane, assuming that the nanoparticles had a diameter of 12 nm with all of the surface area accessible. The fit of equation 2.6 to the data in Figure 2.19 was excellent and yielded a rate constant (k_{mem}) for this system of 0.018 ± 0.002 cm/sec, which was essentially the same within experimental uncertainty as the value for nanoparticles in solution (0.014 ± 0.002 cm/sec). This shows that immobilization of nanoparticles did not restrict access to catalytic sites or alter catalytic activities.

Most reductions were performed with a 50 to 100-fold excess of $NaBH_4$ with respect to 4-nitrophenol to allow the concentration of BH_4^- to remain essentially constant throughout the reaction. When the $NaBH_4$ concentration was lower than a 50-fold excess, the reaction conversion became dependent on both the 4-nitrophenol and $NaBH_4$ concentrations. In Figure 2.20, all parameters in the reduction were held constant except for the $NaBH_4$ concentration, which was in 63, 50, 35, and 25-fold excess with respect to the 4-nitrophenol concentration of 0.8 mM. The figure shows that only about 90% of 4-nitrophenol was reduced with a 25-fold excess of $NaBH_4$, while at a 50-fold excess of $NaBH_4$, > 99% of the 4-nitrophenol was reduced. Excesses of $NaBH_4$ > 50-fold did not significantly enhance the fraction of 4-nitrophenol reduced.

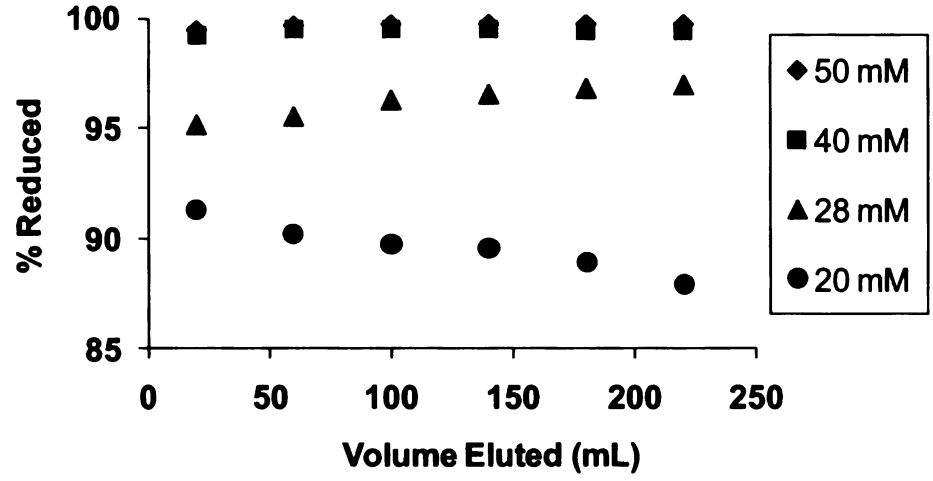

Figure 2.20 Effect of $NaBH_4$ concentration on the percent reduction of 4-nitrophenol achieved by flowing $NaBH_4$/4-nitrophenol solutions through an alumina membrane modified with a PAA/PAH/AuNP film. Conditions: [4-nitrophenol] = 0.8 mM, flux = 0.28 mL/cm^2-sec.

2.3.3.1 4-Nitrophenol Reduction as a Function of Film Composition

Adding a PAH capping layer to adsorbed films had little impact on the reactivity of underlying nanoparticles. For reductions using a 4-nitrophenol concentration of 0.4 mM and $NaBH_4$ concentration of 20 mM, membranes terminated with PAH gave essentially the same percent reduction of 4-nitrophenol as membranes terminated with a AuNP layer (Figure 2.21). Since the percent reduction was >99% in both cases, membranes with and without a PAH capping layer were also used for reductions with only a 25-fold excess of $NaBH_4$. In this experiment, membranes coated with a PAH capping layer still showed similar activity to membranes without a capping layer, which supports the hypothesis that the polyelectrolyte film does not hinder access of the reactants to the active sites of the AuNPs.

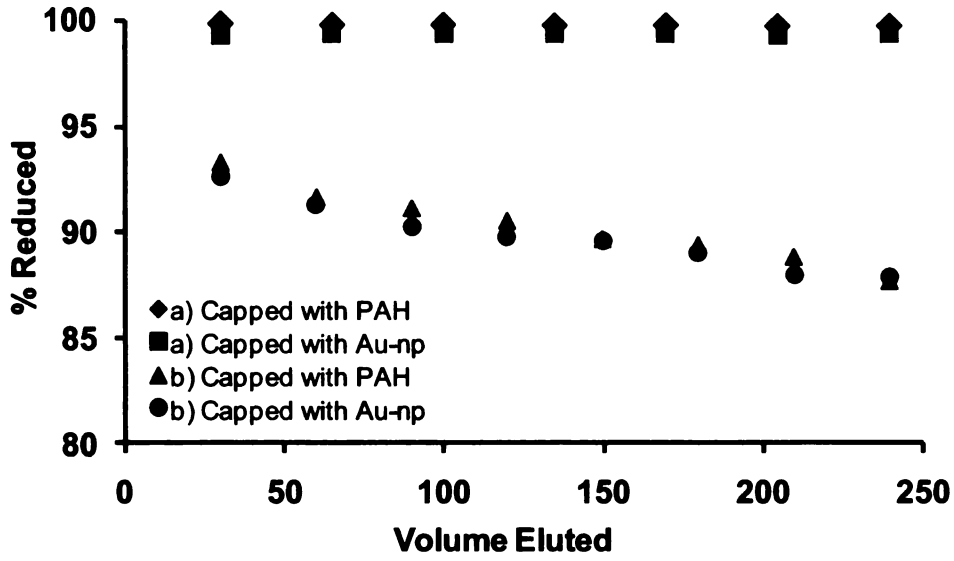

Figure 2.21 Comparison of 4-nitrophenol reduction in membranes modified by adsorption of PAA/PAH/AuNP and PAA/PAH/AuNP/PAH films when [4-nitrophenol] = a) 0.4 mM, and b) 0.8 mM. Other conditions: [$NaBH_4$] = 20 mM, flux = 0.28 mL/cm^2-sec.

Increasing the number of AuNPs adsorbed in the membrane should improve conversion in the membrane reactor. However, since conversion of 4-nitrophenol to 4-aminophenol was nearly 100% even with a single layer of adsorbed nanoparticles, we initially decreased reaction rates to study the effect of additional PAH/AuNP bilayers on the reaction. To do this, we reduced the initial $NaBH_4$ excess from 50-fold to 25-fold relative to 4-nitrophenol. Table 2.1 shows that under these conditions at a flux of 0.30 mL/cm^2-sec, conversion increased from 89 to 98% on going from 1 to 3 adsorbed PAH/AuNP bilayers in the membrane. This supports the hypothesis that a higher Au loading leads to higher activity.

Table 2.1 Au loading, percent 4-nitrophenol reduction, and rate constant vs. the number of PAH/AuNP bilayers contained in PAA/[PAH/AuNP]$_x$ films deposited in porous alumina membranes employed for flow-through reactions.

Number of Bilayers	Au Loading (μmoles)	% of 4-Nitrophenol Reduced[a]	Rate Constant (k_{mem}) (cm/sec)[b]
1	4.9 ± 0.2	88.8 ± 0.9	0.018 ± 0.002
2	8.3 ± 0.2	94.1 ± 0.3	0.018 ± 0.002
3	11.4 ± 0.6	98.3 ± 0.5	-[c]

[a][4-nitrophenol] = 0.8 mM, [$NaBH_4$] = 20 mM, flux = 0.30 mL/cm^2-sec.
[b][4-nitrophenol] = 0.4 mM, [$NaBH_4$] = 20 mM, flux varied between 0.20 mL/cm^2-sec and 0.55 mL/cm^2-sec.
[c]The high conversion did not allow determination of a rate constant.

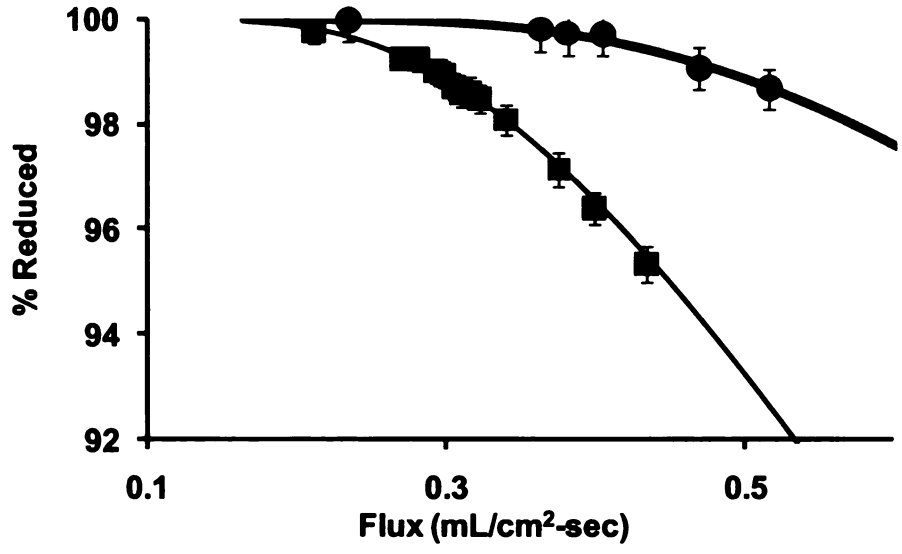

Figure 2.22 Plot of percent conversion vs. flux for membranes containing 1 and 2 PAH/AuNP bilayers. The curves represent a first-order reaction model with rate constants (k_{mem}) of 0.0018 cm/sec for each membrane. (Rate constants are normalized to the nanoparticle surface area in each membrane.) Conditions: [4-nitrophenol] = 0.4 mM, [$NaBH_4$] = 20 mM.

Unfortunately, the use of a 25-fold excess of $NaBH_4$ does not always result in first-order kinetics. However, even with a 50-fold excess of $NaBH_4$,

measurement of percent conversion vs. flow rate showed that the overall activity of the membrane improves on going from 1 to 2 PAH/AuNP bilayers (Figure 2.22). Furthermore, the calculated rate constant, k_{mem}, which was normalized to the total surface area of the nanoparticles in the membrane, was unchanged by depositing an additional PAH/AuNP layer (Table 2.1). This suggests that k_{mem} was not affected by the number of layers deposited and that interior nanoparticles were readily accessible to both 4-nitrophenol and BH_4^-. Because of very high conversions, we could not determine the value of k_{mem} for membranes containing 3 PAH/AuNP bilayers.

Membranes modified with PEI/AuNP films showed catalytic activities similar to those of membranes containing PAA/PAH/AuNP coatings. The reduction of 4-nitrophenol was greater than 99% even at fluxes of 0.30 mL/cm^2-sec, and the % conversion increased as a function of layer number for PEI/AuNP films when using a 25-fold excess of $NaBH_4$. However, the higher gold loading and consequently higher conversions with PEI/AuNP coatings made it difficult to determine rate constants for membranes modified with these films.

2.3.3.2 Comparison of the Catalytic Activities of Nanoparticles in Alumina, Nylon, and Polycarbonate Membranes

To further demonstrate the generality of LbL polyelectrolyte/metal nanoparticle adsorption for forming catalytic membranes, we compared the catalytic activity of nanoparticles in alumina, nylon, and polycarbonate membranes. As Figure 2.23a shows, at sufficiently low flow rates all three types

of membranes catalyzed reduction of more than 99% of the 4-nitrophenol in a solution containing 1 mM 4-nitrophenol and 100 mM $NaBH_4$. Comparison of the membranes at identical fluxes was not possible because the low porosity and relatively low burst pressure (0.7 atm) of the polycarbonate membranes greatly limited flux through these membranes. In contrast, because the nylon membranes are much more porous than polycarbonate membranes, higher flow rates were obtained in the reduction reactions. In fact, PSS/PAH/AuNP modified nylon membranes reduced more than 99% of 4-nitrophenol in a 1 mM solution at fluxes as high as 0.70 mL/cm^2-sec. However, nylon membranes also have a lower burst pressure (2.3 atm) than alumina membranes (4.3 atm), which still limits the amount of pressure that can be applied.

As Figure 2.23a shows, the conversion of 4-nitrophenol to 4-aminophenol decreased with increasing solution flux for all three types of porous membrane substrates coated with a AuNP-containing film. If it were reasonable to compare conversions at a given flux, they would decrease in the order nylon > alumina >

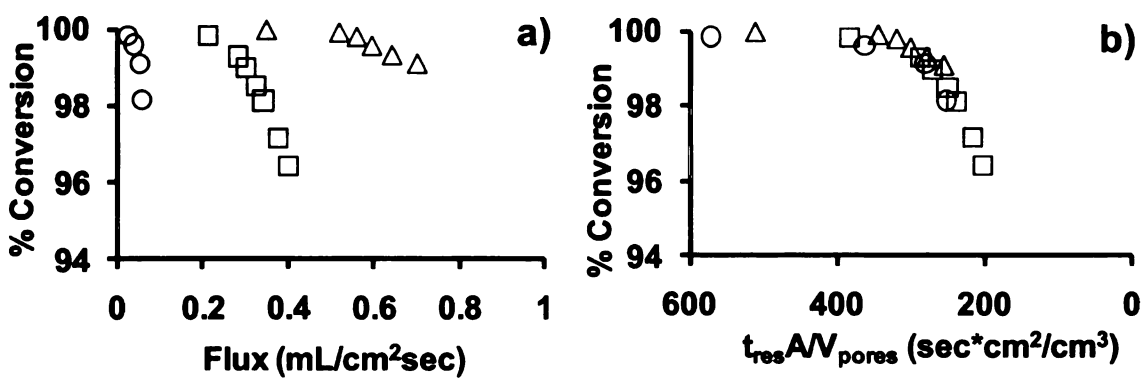

Figure 2.23 Plot of conversion vs. a) flux and b) residence time multiplied by the AuNP surface area per membrane pore volume ($t_{res}A/V_{pores}$) in the reduction of 4-nitrophenol to 4-aminophenol using membranes modified with a polyanion/PAH/AuNP film. In both plots, O = polycarbonate, □ = alumina, △= nylon. Conditions: [4-nitrophenol] = 1 mM, [$NaBH_4$] = 100 mM.

polycarbonate. Because the membranes had different thicknesses and gold loadings, however, an appropriate comparison of the catalytic activities of different membranes needed to account for the membrane geometry and reaction kinetics.

Replotting the conversions in Figure 2.23a as a function of the product of residence time and nanoparticle surface area per membrane pore volume, $t_{res}A/V_{pores}$, which is equivalent to $Al/(V_{mem}F)$, shows that the three membranes behaved similarly (Figure 2.23b). Put another way, fitting of the data in Figure 2.23a to equation 2.5 gives values of k_{mem} that differ by less than 20% among the three membranes. The k_{mem} values are 0.017, 0.015, and 0.018 cm/sec for alumina, track-etched polycarbonate, and nylon membranes, respectively. Thus, the catalytic activity of the nanoparticles in the different membranes is quite similar. Nylon membranes give the highest conversions because they are the thickest of the three substrates, and conversions with alumina are higher than with polycarbonate membranes because the polycarbonate is thinner and also has a lower porosity than alumina.

2.3.4 Effect of Substituent Groups on the Reduction of Nitroaromatic Compounds

2.3.4.1 Reduction of Compounds with Single Reaction Products

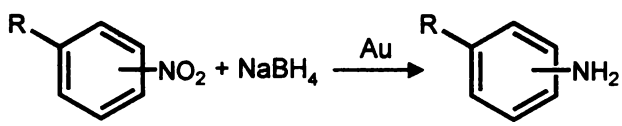

R = H, OH, NH_2, CH_3, CN, Cl, $CH=CH_2$

Scheme 2.3 Au-catalyzed reduction of nitroaromatic compounds by $NaBH_4$.

Table 2.2 Rate constants for reduction of nitrophenol and nitroaniline. The reactions were catalyzed by PAA/PAH/AuNP films in porous alumina membranes (k_{mem}) and on alumina powder (k_{slurry}).

Compound	k_{mem} (cm/sec)	k_{slurry} (cm/sec)
4-Nitrophenol	0.018 ± 0.003	0.020 ± 0.004
2-Nitrophenol	0.015 ± 0.003	0.016 ± 0.003
4-Nitroaniline	0.023 ± 0.004	0.022 ± 0.005
2-Nitroaniline	0.018 ± 0.004	0.015 ± 0.003

One of the goals of this work was to determine the effects of substituent composition and position on the reduction of nitrobenzene derivatives. To do this, we reduced the compounds in Scheme 2.3 using alumina membranes modified with 1 layer PAA/PAH/AuNP films. The reduction of 2- or 4-nitrophenol gave the corresponding amine as the only observed product, so k_{mem} was determined by measuring nitro group conversion as a function of flux and fitting the data to equation 2.5. The same was true for the reduction of 2- and 4-nitroaniline. Table 2.2 shows that the values of k_{mem} were nearly the same for these 4 compounds. Thus, the hydroxyl and amino groups influenced the nitro reduction to nearly the same degree, and the effect of substituent position (*ortho* versus *para*) was also small.

For comparison, we performed conventional slurry reactions with catalytic nanoparticles on micron-sized alumina. For these reactions, the pseudo first order rate constant, k_{slurry}, was calculated by modeling conversion versus time, t, with equation 2.7.

$$conversion = 1 - exp\left[\frac{-k_{slurry} A t}{V_{solution}}\right] \qquad (2.7)$$

As Table 2.2 shows, within experimental error, the rate constants for the slurry and membrane reactions were the same. Thus the nanoparticle catalytic properties are independent of the substrate on which they are deposited.

2.3.4.2 Reduction of Compounds with Multiple Reaction Products

Table 2.3 presents the product distributions for the membrane-catalyzed reduction of several substituted nitroaromatic compounds. In contrast to hydroxyl or amino functionalized nitroaromatics, reduction of 2- and 4-nitrotoluene yielded a mixture of the amino and nitroso forms of each compound.

Table 2.3 Product distributions in membrane-catalyzed reductions of nitroaromatic compounds at two different solution fluxes. The membranes consisted of porous alumina modified with PAA/PAH/AuNP films.

Compound	Flux = 0.015 mL/cm^2-sec			Flux = 0.15 mL/cm^2-sec		
	% NO_2	% NO[a]	%NH_2	% NO_2	% NO[a]	%NH_2
4-Nitrophenol	<1	-	>99	1	-	99
2-Nitrophenol	<1	-	>99	1	-	99
4-Nitroaniline	<1	-	>99	1	-	99
2-Nitroaniline	<1	-	>99	1	-	99
4-Nitrotoluene	<1	23	76	3	44	53
2-Nitrotoluene	<1	19	80	2	40	58
Nitrobenzene	3	24	73	4	47	49
2-Nitro-*m*-xylene	2	5	93	5	23	72

[a]Uncertainties in these values are about 2%.

Slurry reactions provided a better window into reduction kinetics because the reaction occurred on a longer time scale due to the large solution volume. Figure 2.24 shows the temporal composition of slurry mixtures during the reduction of several of the substituted nitroaromatic compounds. For 4-

nitrophenol (figure 2.24a) and 4-nitroaniline (figure 2.24b), the reduction of the nitro species was accompanied by the corresponding formation of the amino species. Similar plots were obtained in the reduction of 2-nitrophenol and 2-nitroaniline. For 4-nitrotoluene (Figure 2.24c), the initial rapid formation of both the amino and nitroso species followed by slow reduction of the nitroso compound to the amine suggests that there were two pathways to the amine in this reaction. Similar trends occurred for 2-nitrotoluene (Figure 2.24d) and nitrobenzene (Figure 2.24e). The most likely explanation for the absence of the nitroso product after reduction of hydroxyl or amino functionalized nitroaromatics is that the electron-donating hydroxyl and amino substituents inhibited reduction to the nitroso functionality. The overall reduction of the nitro group was actually slower for 4-nitrophenol than 4-nitrotoluene, perhaps because of inhibition of nitrosophenol formation in reduction of 4-nitrophenol. It is possible that the hydroxyl and amino groups increased the rate of reduction of the nitroso group (so nitroso compounds are not observed) while decreasing the overall rate of nitro reduction, but this seems improbable.

In both slurry (Figure 2.24f) and membrane (Table 2.3) reductions, 2-nitro-*m*-xylene showed less formation of the nitroso compound than 2- and 4-nitrotoluene, presumably because of additional electron donation by the second methyl group. However, the overall conversion of the nitro compound was lower for 2-nitro-*m*-xylene than for 2- and 4-nitrotoluene, which may be partly due to steric hindrance caused by the two methyl groups.

The formation of nitroso intermediates is consistent with a hydrogenation pathway where nitroso and hydroxylamine species form in a direct pathway to the amine.[17] Other studies have proposed several pathways in which the nitroso

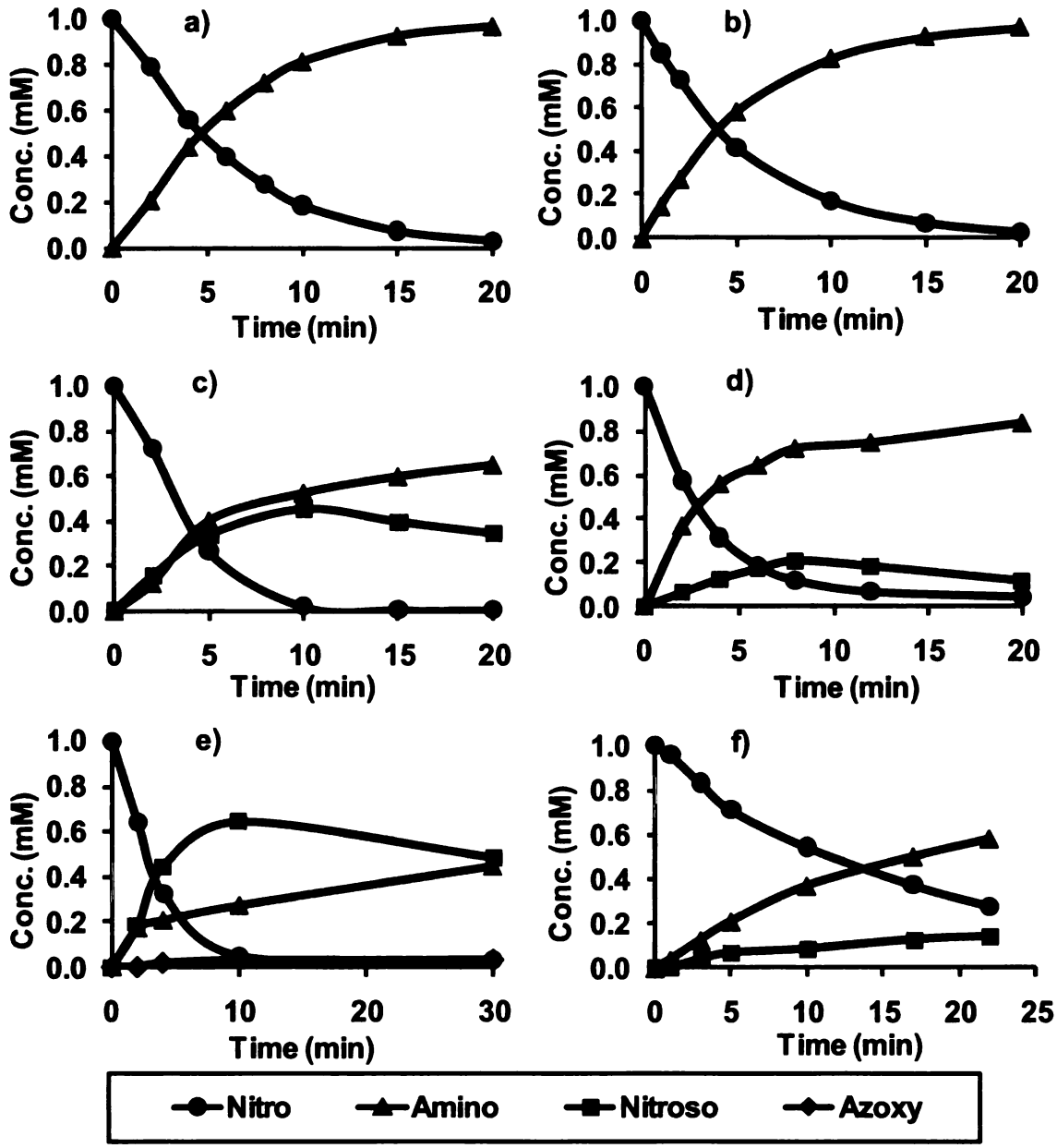

Figure 2.24 Slurry reaction profiles for reduction of a) 4-nitrophenol, b) 4-nitroaniline, c) 4-nitrotoluene, d) 2-nitrotoluene, e) nitrobenzene, and f) 2-nitro-*m*-xylene with $NaBH_4$ using alumina powder modified with a PAA/PAH/AuNP film as a catalyst. For each reaction, circles represent the starting nitro compound, triangles represent the amine product, squares represent the nitroso product, and diamonds represent the azoxy product.

species is not an intermediate in the reaction, but rather a product that may result from side reactions.[52,53] Litvić et al. also observed the formation of nitroso, hydroxylamino, and diazo intermediates in the reduction of several nitroaromatic compounds with Raney nickel and sodium borohydride.[46] In the membrane systems, the increased amounts of the nitroso compound at shorter reaction times (higher flow rates) suggest that it is an intermediate to the formation of the amine rather than a side product; however, the data for slurry reactions provide evidence for an additional, more rapid pathway to the amine that does not go through a nitroso intermediate.

2.3.4.3 Effect of Flux on Product Distributions

Table 2.3 indicates that solution flux, which is inversely related to residence time within the membrane, can be used to control conversion in membrane reactions. As the solution flux through nanoparticle-modified alumina membranes increased, the ratio of the amine to nitroso product decreased. To further investigate this trend, we determined the product distribution for reduction of 2-nitrotoluene as a function of the flux through nylon, polycarbonate, and alumina membranes. Figure 2.25a shows the percentage of each compound in the product stream for all three membrane types. Similar to Figure 2.23, when product composition was plotted as a function of the residence time multiplied by the AuNP surface area per pore volume ($t_{res}A/V_{pores}$), the product compositions from the different membranes were comparable (Figure 2.25b).

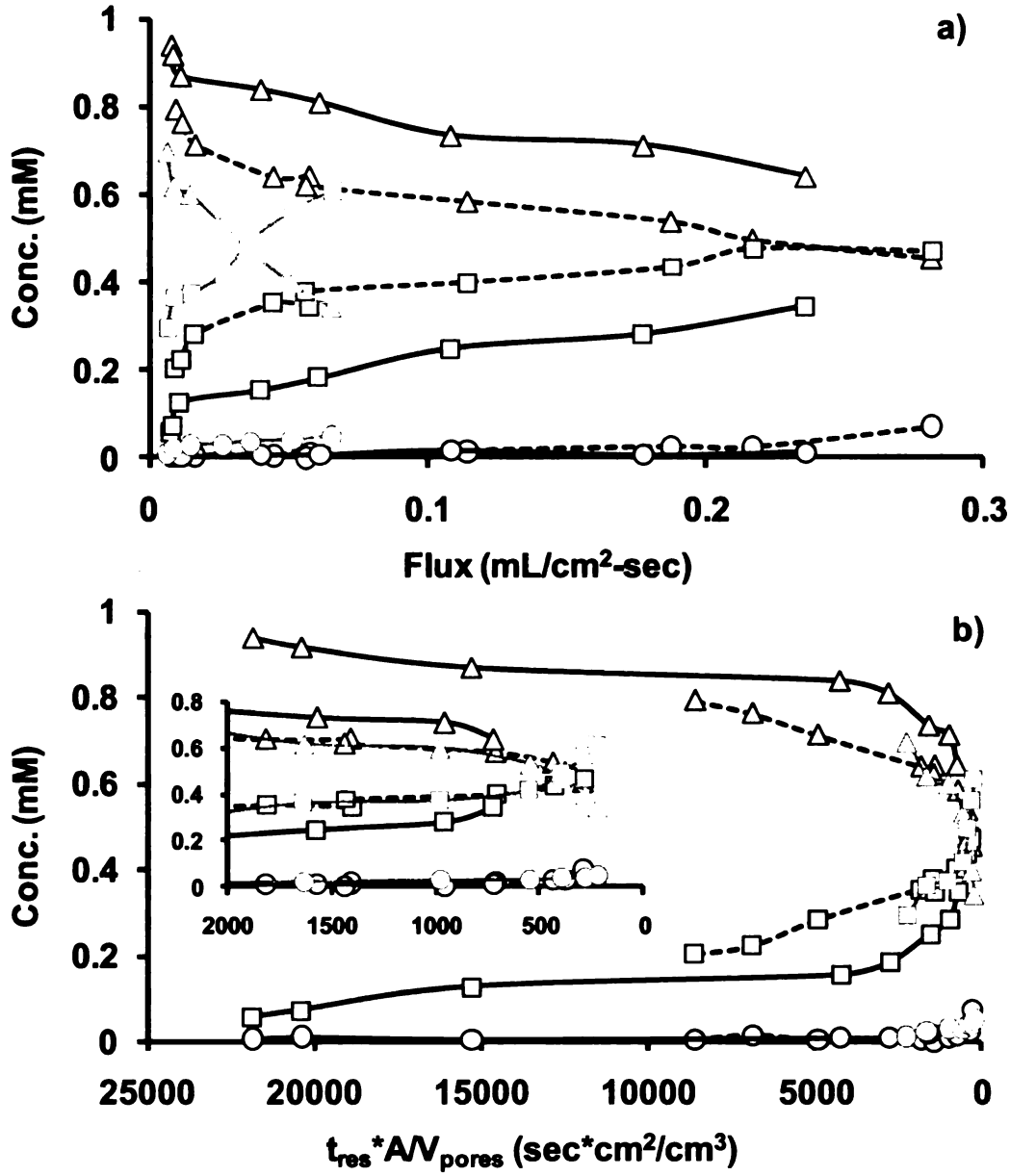

Figure 2.25 Plot of effluent composition as a function of a) flux and b) residence time multiplied by nanoparticle surface area per pore volume ($t_{res}A/V_{pores}$) in the reduction of 2-nitrotoluene using AuNP-containing membranes. In both diagrams: △ = amine, □ = nitroso, ○ = nitro, solid black line = nylon membrane, dotted black line = alumina membrane, and solid gray line = polycarbonate membrane. The inset in Figure b shows an expanded plot of the data at the right of this figure.

Most importantly, Figure 2.25 demonstrates the control over product composition provided by variation of flux, or alternatively residence time. Remarkably, Figure 2.25a shows that the yield of 2-aminotoluene was 94% at low fluxes through nylon membranes (solid black line) and only 34% at relatively high fluxes through polycarbonate membranes (solid gray line). Moreover, the yield of the nitroso compound was higher at low values of $t_{res}A/V_{pores}$, as one would expect, and the conversion to the nitroso compound ranged from 5% at high values of $t_{res}A/V_{pores}$ to 61% at the lowest values of $t_{res}A/V_{pores}$. Increased fluxes (or lower residence times) might produce even larger fractions of the nitroso compound; however, the amount of unreacted starting material might also increase at these higher fluxes. Unfortunately, fluxes are currently limited by the strength of the membranes. When rate constants for the formation of an intermediate and for the subsequent conversion to product are even more disparate, it should be possible to obtain the intermediate in even higher yield. Overall, fine control over residence time makes membranes attractive for selective product formation.

2.3.4.4 Selectivity in Reactions with Multiple Reducible Functional Groups

We investigated catalytic reduction of cyano, chloro, and styrenyl functionalized nitroaromatic compounds to determine whether AuNPs can selectively catalyze nitro group reduction in the presence of other reducible functional groups. As Table 2.4 shows, the reaction with $NaBH_4$ resulted in reduction of 2% or less of cyano, styrenyl, and chloro groups at conversions of

Table 2.4 Product distributions in the membrane-catalyzed reduction of nitroaromatic compounds containing other reducible functional groups. The reactions employed a gold nanoparticle-modified alumina membrane and a flux of 0.015 mL/cm^2-sec.

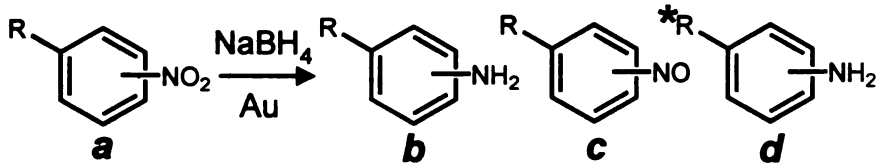

Compound (R)	% *a*	% *b*	% *c*	% *d*
4-Nitrobenzonitrile (CN)	<1	>97	-	2
2-Nitrobenzonitrile (CN)	<1	>98	-	1
1,4-Chloronitrobenzene (Cl)	2	92	6	-
1,2-Chloronitrobenzene (Cl)	2	93	5	-
3-Nitrostyrene (-CH=CH$_2$)	1	85	13	<1

*R = reduced form of R-group.

98% or more of the nitro groups to amino or nitroso products. In the catalytic reduction of 2- and 4-nitrobenzonitrile, no nitroso product formed, whereas reductions of 1,2-chloronitrobenzene, 1,4-chloronitrobenzene, and 3-nitrostyrene gave small amounts of the nitroso compound, but the amine was still the major product at this flux. Thus, selective reduction of the nitro group is feasible.

2.3.4.5 Catalytic Reduction of Nitrocyclohexane

The ability to reduce both aromatic and aliphatic nitro groups[68,69] without changing the catalyst system is important in synthetic organic chemistry, but is often quite difficult to achieve. To determine whether membrane-catalyzed reduction by $NaBH_4$ could be extended to aliphatic nitro groups, we attempted reduction of nitrocyclohexane. Passage of a solution of nitrocyclohexane and sodium borohydride through a gold nanoparticle-containing alumina membrane at 0.020 mL/cm^2-sec yielded greater than 95% reduction of the nitro group, but

the product was a mixture of cyclohexanone oxime and cyclohexanamine (Scheme 2.4).

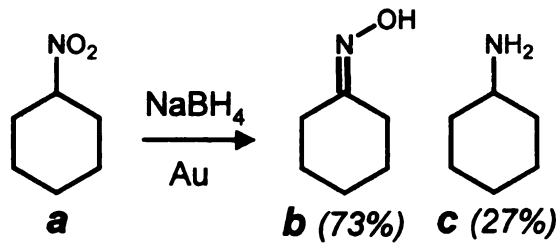

Scheme 2.4 Reduction of nitrocyclohexane catalyzed by a Au nanoparticle-containing alumina membrane with a solution flux of 0.020 mL/cm^2-sec.

2.3.4.6 Effect of Temperature on Reaction Rates and Product Distributions

Temperature provides another variable for controlling reaction rates and product distributions. Panigrahi, et al. demonstrated that when catalyzed with 20 nm Au nanoparticles, the rate of reduction of 4-nitrophenol with sodium borohydride exhibits Arrhenius behavior.[67] We tested the effect of temperature on the reduction of 4-nitrophenol, 4-nitrotoluene, and 1,4-chloronitrobenzene in slurry reactions catalyzed by alumina powder modified with AuNP-containing films. The results of these experiments were consistent with the data of Panigrahi, et al. and are shown in Figure 2.26.

Though it appears that the reductions of 4-nitrotoluene and 1,4-chloronitrobenzene were slightly faster than the reduction of 4-nitropheneol, it should be noted that during reduction of 4-nitrotoluene and 1,4-chloronitrobenzene, nitroso intermediates appeared. In the case of 1,4-chloronitrobenzene, a small amount of the azoxy species also formed. The complete conversion to the amine was actually faster for 4-nitrophenol. For each compound, the reactions showed Arrhenius behavior (Figures 2.26b, d, and f).

The activation energies determined from these plots were 27, 62, and 59 kJ/mol for 4-nitrophenol, 4-nitrotoluene, and 1,4-chloronitrobenzene respectively, but in the case of reduction of 4-nitrotoluene and 1,4-chloronitrobenzene, these activation energies represent a composite value for formation of different reaction products.

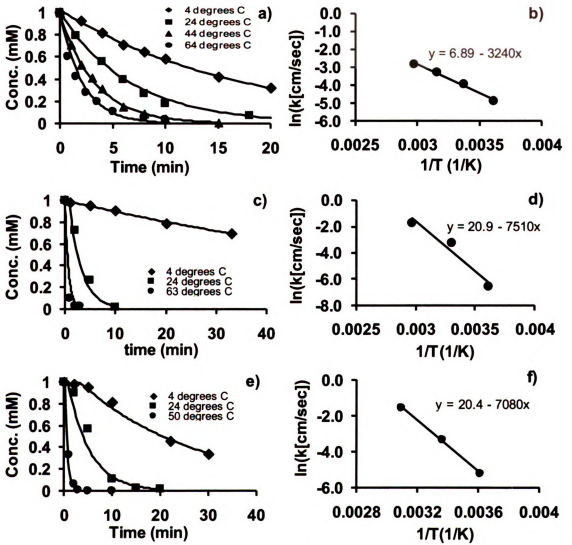

Figure 2.26 Slurry reaction profiles and corresponding Arrhenius plots for the reduction of a,b) 4-nitrophenol, c,d) 4-nitrotoluene, and e,f) 1,4-chloronitrobenzene by $NaBH_4$ at different temperatures. The reaction was catalyzed by alumina powder modified with a PAA/PAH/AuNP film. The lines in a, c, and e are fits of the data to equation 2.7 in the text.

We also examined the membrane-catalyzed reductions of 4-nitrophenol, 4-nitrotoluene, and 1,4-chloronitrobenzene at three different temperatures with the solution flux kept constant at 0.07 mL/cm^2-sec. As Table 2.5 shows, reduction of 4-nitrophenol proceeded to >99% conversion to the amine even at 4 °C, so the effect of temperature on the membrane-catalyzed reduction of this compound could not be determined. For 4-nitrotoluene and 1,4-chloronitrobenzene, temperature does not affect the fraction of nitro groups reduced, but the ratio of amino to nitroso products increases with increasing temperature. This again suggests that the nitroso compounds are converted to the amine as the reaction proceeds.

Table 2.5 Product distributions in the membrane-catalyzed reduction of selected nitroaromatic compounds at different temperatures. The catalytic membranes consisted of alumina modified with a PAA/PAH/AuNP film, and the flux was 0.07 mL/cm^2-sec.

Compound	T(°C)	% NO_2	% NO	% NH_2
4-Nitrophenol	4	<1	0	>99
	24	<1	0	>99
	44	<1	0	>99
4-Nitrotoluene	4	1	39	60
	24	1	31	68
	44	1	23	76
1,4-Chloronitrobenzene	4	1	27	72
	24	1	23	76
	44	1	18	81

2.3.5 Catalyst Stability

In addition to high activity, stability is also vital for developing useful catalytic membranes. Dry membranes modified with AuNPs could be stored in

an ambient environment for several months without negative effects on their activity. Figure 2.27 demonstrates that membranes are also reasonably stable under flow of a solution containing 4-nitrophenol and $NaBH_4$. The percent reduction remains essentially constant, even though over 140,000 membrane volumes have passed through the system.

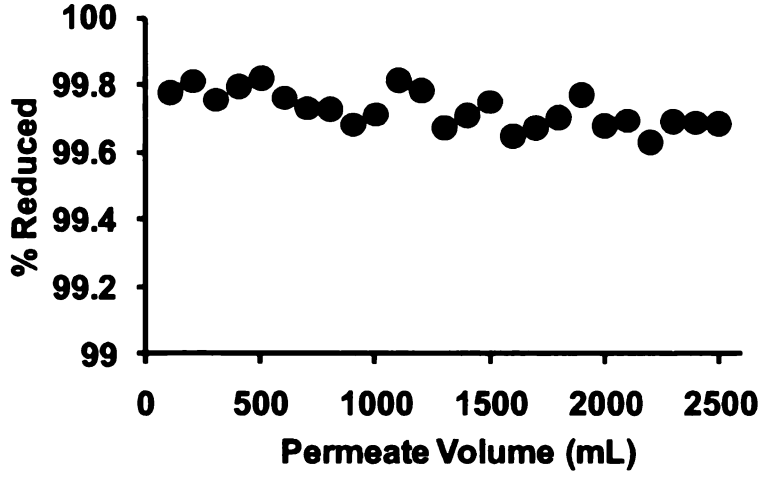

Figure 2.27 Plot of percent reduction of 4-nitrophenol vs. volume eluted through an alumina membrane modified with a PAA/PAH/AuNP film. Conditions: [4-nitrophenol] = 2.0 mM, [$NaBH_4$] = 100 mM, flux = 0.17 mL/cm^2-sec. The plot contains a compilation of 5 sequential passages of 500 mL of the reaction solution.

The data in Figure 2.27 show a turnover number >1000 moles of 4-nitrophenol reduced per mole of Au contained within the membrane. After attainment of this high turnover number, 4-nitrophenol conversion at a flux of 0.17 mL/cm^2-sec decreased only marginally, from 99.8% to 99.7%. These results indicate that with > 50-fold excess of $NaBH_4$, minimal fouling occurred on the surface of the AuNPs, and little or no Au was leached from the membrane. Larger turnover numbers may be more easily achieved with higher

concentrations of 4-nitrophenol and $NaBH_4$, but the high pH (>10) of such solutions results in slow dissolution of the alumina support and may also remove the polyelectrolyte film.[70-72] Additionally, some studies suggest that the catalytic activity of AuNPs in $NaBH_4$ reductions decreases slightly over time, perhaps because of catalyst poisoning.[73]

Analysis of the amount of Au contained in membranes before and after using them in the reduction of 4-nitrophenol for several hours at high flow rates, showed no significant decrease (<5%) in gold content. Furthermore, FESEM images of membranes that were used for 2 hours in the reduction of 4-nitrophenol at a flux of 0.030 mL/cm^2-sec show that the nanoparticles were still well separated from one another and did not leach from the membrane during the reaction (Figure 2.28). However, we do have some preliminary evidence that at higher fluxes, catalytic activity decreases over time and a cake layer can form on the surface of the membrane. Investigations into gentler reducing agents will be beneficial for future work with these catalytic membranes.

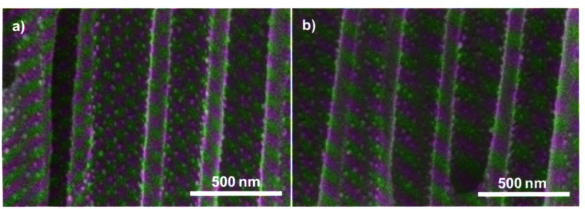

Figure 2.28 Cross-sectional FESEM images of membranes modified with PAA/PAH/AuNP films a) before and b) after flowing a solution of 1 mM 4-nitrophenol and 100 mM $NaBH_4$ through the membrane for 2 hours at 0.030 mL/cm^2-sec.

2.4 Conclusions

Overall, membranes modified with Au nanoparticles in multilayer polyelectrolyte films present a stable system that has great potential for catalyzing fast reactions. The polyelectrolyte multilayer provides a convenient platform for immobilizing active, accessible catalytic nanoparticles in a variety of porous supports including anodized alumina, track-etched polycarbonate, and nylon. The ability to vary the type and amount of polyelectrolyte and/or catalytic material makes this method even more versatile. Membranes modified by LbL deposition of polyelectrolyte/AuNP films show high catalytic activity in the reduction of nitroaromatic compounds with sodium borohydride. A comparison of the three membrane types as well as alumina powder modified with polyelectrolyte/AuNP films shows that the catalytic activity is independent of the substrate. The membranes also catalyze selective reduction of the nitro group in the presence of other reducible functional groups, and the extent of formation of nitroso products depends on ring substituents. An important asset of the membrane catalysts is the possibility of varying flux to control product distribution, as demonstrated by the formation of increased levels of nitroso intermediates at high flux. The following chapters will discuss the use of LbL formation of polyelectrolyte/nanoparticle films with other noble metal nanoparticles, additional support materials, and catalytic reactions with milder oxidizing or reducing agents.

2.5 References

(1) Ono, N. *The Nitro Group in Organic Synthesis*; Wiley-VCH: New York, 2001.

(2) Downing, R. S.; Kunkeler, P. J.; Bekkum, H. V. *Catal. Today* **1997**, *37*, 121-136.

(3) Adams, J. P. *J. Chem. Soc., Perkin Trans. 1* **2002**, 2586-2597.

(4) Jacobsen, M. F.; Moses, J. E.; Adlington, R. M.; Baldwin, J. E. *Org. Lett.* **2005**, *7*, 641-644.

(5) Tafesh, A. M.; Weiguny, J. *Chem. Rev.* **1996**, *96*, 2035-2052.

(6) Brickner, S. J.; Hutchinson, D. K.; Barbachyn, M. R.; Manninen, P. R.; Ulanowicz, D. A.; Garmon, S. A.; Grega, K. C.; Hendges, S. K.; Toops, D. S. *J. Med. Chem.* **1996**, *39*, 673-9.

(7) Figueras, F.; Coq, B. *J. Mol. Catal. A: Chem.* **2001**, *173*, 223-230.

(8) Pietrowski, M.; Zielinski, M.; Wojciechowska, M. *Catal. Lett.* **2009**, *128*, 31-35.

(9) Motoyama, Y.; Kamo, K.; Nagashima, H. *Org. Lett.* **2009**, *11*, 1345-1348.

(10) Zheng, Y.; Ma, K.; Wang, H.; Sun, X.; Jiang, J.; Wang, C.; Li, R.; Ma, J. *Catal. Lett.* **2008**, *124*, 268-276.

(11) Maity, P.; Basu, S.; Bhaduri, S.; Lahiri, G. K. *Adv. Synth. Catal.* **2007**, *349*, 1955-1962.

(12) Du, Y.; Chen, H.; Chen, R.; Xu, N. *Appl. Catal., A* **2004**, *277*, 259-264.

(13) Wen, H.; Yao, K.; Zhang, Y.; Zhou, Z.; Kirschning, A. *Catal. Commun.* **2009**, *10*, 1207-1211.

(14) Saha, A.; Ranu, B. *J. Org. Chem.* **2008**, *73*, 6867-6870.

(15) Adger, B. M.; Young, R. G. *Tetrahedron Lett.* **1984**, *25*, 5219-22.

(16) Wang, H.; Yan, J.; Chang, W.; Zhang, Z. *Catal. Commun.* **2009**, *10*, 989-994.

(17) Haber, F. *Z. Elektrochem. Angew. Phys. Chem.* **1898**, *4*, 506-13.

(18) Noel, M.; Ravichandran, C.; Anantharaman, P. N. *J. Appl. Electrochem.* **1995**, *25*, 690-8.

(19) Li, F.; Cui, J.; Qian, X.; Zhang, R.; Xiao, Y. *Chem. Commun.* **2005**, 1901-1903.

(20) Li, F.; Cui, J.; Qian, X.; Zhang, R. *Chem. Commun.* **2004**, 2338-2339.

(21) Blackie, J. A.; Turner, N.; Wells, A. *Tetrahedron Lett.* **1997**, *38*, 3043-3046.

(22) Rahaim, R. J., Jr.; Maleczka, R. E., Jr. *Org. Lett.* **2005**, *7*, 5087-5090.

(23) Blaser, H.-U. *Science* **2006**, *313*, 312-313.

(24) Blaser, H. U.; Siegrist, U.; Steiner, H.; Studer, M. In *Fine Chemicals Through Heterogeneous Catalysis*; Sheldon, R. A., Bekkum, H. v., Eds.; Wiley-VCH: Weinheim, Germany, 2001, p 389-406.

(25) Baumeister, P.; Studer, M.; Roessler, F. In *Handbook of Heterogeneous Catalysis*; Ertl, G., Knözinger, H., Wieitkamp, J., Eds.; Wiley-VCH: Weinheim, Germany, 1997, p 2186-2209.

(26) Siegrist, U.; Baumeister, P.; Blaser, H.-U.; Studer, M. *Chem. Ind. (Dekker)* **1998**, *75*, 207-219.

(27) Corma, A.; Serna, P. *Science* **2006**, *313*, 332-334.

(28) Boronat, M.; Concepcion, P.; Corma, A.; Gonzalez, S.; Illas, F.; Serna, P. *J. Am. Chem. Soc.* **2007**, *129*, 16230-16237.

(29) Corma, A.; Serna, P. *Nature Protocols* **2006**, *1*, 2590-2595.

(30) Chen, Y.; Qiu, J.; Wang, X.; Xiu, J. *J. Catal.* **2006**, *242*, 227-230.

(31) Rylander, P. *Catalytic Hydrogenation in Organic Syntheses*; Academic Press: New York, 1979.

(32) Lu, X.; Xu, X.; Wang, N.; Zhang, Q. *J. Phys. Chem. A* **1999**, *103*, 10969-10974.

(33) Takasaki, M.; Motoyama, Y.; Higashi, K.; Yoon, S.-H.; Mochida, I.; Nagashima, H. *Org. Lett.* **2008**, *10*, 1601-1604.

(34) Pradhan, N.; Pal, A.; Pal, T. *Langmuir* **2001**, *17*, 1800-1802.

(35) Pradhan, N.; Pal, A.; Pal, T. *Colloids Surf., A* **2002**, *196*, 247-257.

(36) Ghosh, S. K.; Mandal, M.; Kundu, S.; Nath, S.; Pal, T. *Appl. Catal., A* **2004**, *268*, 61-66.

(37) Hwang, C.-G.; Kim, S.-H.; Hoon, O. J.; Kim, M.-R.; Choi, S.-H. *J. Ind. Eng. Chem.* **2008**, *14*, 864-868.

(38) Jana, S.; Ghosh, S. K.; Nath, S.; Pande, S.; Praharaj, S.; Panigrahi, S.; Basu, S.; Endo, T.; Pal, T. *Appl. Catal., A* **2006**, *313*, 41-48.

(39) Liu, W.; Yang, X.; Huang, W. *J. Colloid Interface Sci.* **2006**, *304*, 160-165.

(40) Lu, Y.; Spyra, P.; Mei, Y.; Ballauff, M.; Pich, A. *Macromol. Chem. Phys.* **2007**, *208*, 254-261.

(41) Esumi, K.; Isono, R.; Yoshimura, T. *Langmuir* **2004**, *20*, 237-243.

(42) Hayakawa, K.; Yoshimura, T.; Esumi, K. *Langmuir* **2003**, *19*, 5517-5521.

(43) Mei, Y.; Sharma, G.; Lu, Y.; Ballauff, M.; Drechsler, M.; Irrgang, T.; Kempe, R. *Langmuir* **2005**, *21*, 12229-12234.

(44) Mei, Y.; Lu, Y.; Polzer, F.; Ballauff, M.; Drechsler, M. *Chem. Mater.* **2007**, *19*, 1062-1069.

(45) Kundu, S.; Lau, S.; Liang, H. *J. Phys. Chem. C* **2009**, *113*, 5150-5156.

(46) Pogorelić, I.; Filipan-Litvić, M.; Merkaš, S.; Ljubić, G.; Cepanec, I.; Litvić, M. *J. Mol. Catal. A: Chem.* **2007**, *274*, 202-207.

(47) Grabar, K. C.; Freeman, R. G.; Hommer, M. B.; Natan, M. J. *Anal. Chem.* **1995**, *67*, 735-43.

(48) Turkevich, J.; Stevenson, P. C.; Hillier, J. *Discussions of the Faraday Society* **1951**, *No. 11*, 55-75.

(49) Kidambi, S.; Bruening, M. L. *Chem. Mater.* **2005**, *17*, 301-307.

(50) Kidambi, S.; Dai, J.; Li, J.; Bruening, M. L. *J. Am. Chem. Soc.* **2004**, *126*, 2658-2659.

(51) Malaisamy, R.; Bruening, M. L. *Langmuir* **2005**, *21*, 10587-10592.

(52) Corma, A.; Concepcion, P.; Serna, P. *Angew. Chem. Int. Ed.* **2007**, *46*, 7266-7269.

(53) Gelder, E. A.; Jackson, S. D.; Lok, C. M. *Chem. Commun.* **2005**, 522-524.

(54) Akamatsu, K.; Deki, S. *J. Mater. Chem.* **1997**, *7*, 1773-1777.

(55) Link, S.; El-Sayed, M. A. *J. Phys. Chem. B* **1999**, *103*, 4212-4217.

(56) He, Y. Q.; Liu, S. P.; Kong, L.; Liu, Z. F. *Spectrochim. Acta, Part A* **2005**, *61*, 2861-2866.

(57) Shiratori, S. S.; Rubner, M. F. *Macromolecules* **2000**, *33*, 4213-4219.

(58) Hong, S. U.; Miller, M. D.; Bruening, M. L. *Ind. Eng. Chem. Res.* **2006**, *45*, 6284-6288.

(59) Miller, M. D.; Bruening, M. L. *Chem. Mater.* **2005**, *17*, 5375-5381.

(60) Stanton, B. W.; Harris, J. J.; Miller, M. D.; Bruening, M. L. *Langmuir* **2003**, *19*, 7038-7042.

(61) Dai, J.; Bruening, M. L. *Nano Lett.* **2002**, *2*, 497-501.

(62) Robinson, M.; Pask, J. A.; Fuerstenau, D. W. *J. Am. Ceram. Soc.* **1964**, *47*, 516-520.

(63) Harris, J. J.; Bruening, M. L. *Langmuir* **2000**, *16*, 2006-2013.

(64) Jani, A. M. M.; Anglin, E. J.; Mcinnes, S. J. P.; Losic, D.; Shapter, J. G.; Voelcker, N. H. *Chem. Commun.* **2009**, 3062 - 3064.

(65) Braunstein, P.; Kormann, H.-P.; Meyer-Zaika, W.; Pugin, R.; Schmid, G. *Chem. Eur. J.* **2000**, *6*, 4637-4646.

(66) Lahav, M.; Sehayek, T.; Vaskevich, A.; Rubinstein, I. *Angew. Chem. Int. Ed.* **2003**, *42*, 5576-5579.

(67) Panigrahi, S.; Basu, S.; Praharaj, S.; Pande, S.; Jana, S.; Pal, A.; Ghosh, S. K.; Pal, T. *J. Phys. Chem. C* **2007**, *111*, 4596-4605.

(68) List, B.; Pojarliev, P.; Martin, H. J. *Org. Lett.* **2001**, *3*, 2423-2425.

(69) Sasai, H.; Tokunaga, T.; Watanabe, S.; Suzuki, T.; Itoh, N.; Shibasaki, M. *J. Org. Chem.* **1995**, *60*, 7388-9.

(70) Dubas, S. T.; Schlenoff, J. B. *Macromolecules* **2001**, *34*, 3736-3740.

(71) Kharlampieva, E.; Sukhishvili, S. A. *Langmuir* **2003**, *19*, 1235-1243.

(72) Kohli, P.; Wharton John, E.; Braide, O.; Martin Charles, R. *Journal of Nanoscience and Nanotechnology* **2004**, *4*, 605-10.

(73) Wee, J.-H.; Lee, K.-Y.; Kim, S. H. *Fuel Process. Technol.* **2006**, *87*, 811-819.

Some of the results and figures contained in chapter three appeared in the following publication.
Bhattacharjee, S.; Dotzauer, D. M.; Bruening, M. L. *J. Am. Chem. Soc.* **2009**, *131*, 3601-3610

Chapter Three: Hydrogenation Reactions with Pd-Containing Catalysts

3.1 Introduction

The previous chapter showed that catalytic membranes effectively catalyze reactions in which all reactants are in the liquid phase; however, many industrial applications involve gas/liquid reactions such as hydrogenations or oxidations of substrates in the liquid phase. The preference to use heterogeneous catalysts in industry leads to the difficult task of maintaining close contact between three phases (solid catalyst/liquid/gas) within the catalytic reactor. This multiphase catalysis poses many challenges in designing the proper reactor system. Important factors to consider in designing an appropriate reactor include the rate of the reaction, mass transfer of reactants, ease of scale-up, and cost of materials. This chapter describes hydrogenation reactions with slurry reactors in which the catalyst is immobilized on an alumina powder support and flow-through membrane reactors where the catalyst is immobilized in the pores of flat disk-shaped alumina membranes. These initial studies examine reactions where the gas is simply bubbled into the solvent. Chapter four discusses gas/liquid interfacial contactors.

In this research area, we are particularly interested in hydrogenation reactions because they occur on short time scales and are widely used in the reduction of olefins and a number of other functional groups.[1] Previous studies in the Bruening group focused on the hydrogenation of allyl alcohols containing several different alkyl substituents in the position α to the double bond.[2-4] These studies showed that Pd nanoparticles embedded in polyelectrolyte multilayer

films catalyze hydrogenation of smaller molecules at a faster rate than molecules containing bulkier alkyl substituents, presumably because of faster transport of the smaller molecules to the catalyst surface. As an extension of this work, we were interested in looking at the effect of nanoparticle size on activity and selectivity in these reactions. Control over particle size is often necessary for creating highly active nanoparticle catalysts for hydrogenation of alkenes[5-9] or partial hydrogenation of alkynes[10,11] and conjugated alkenes.[12] Moreover, nanoparticle catalysts showed high intermolecular selectivities in the hydrogenation of alkenes[13] and allylic alcohols,[14,15] but these studies did not look at selectivity as a function of particle size. Investigations of catalyst selectivity as a function of particle size should provide insight into whether the enhanced catalyst activity for certain compounds occurs due to steric effects, increased catalyst surface area, or changes in the nanoparticle electronic properties. The initial studies in this chapter use catalysts comprised of alumina powder modified with polyelectrolyte/PdNP films to explore the effect of nanoparticle size on reactivity/selectivity in slurry reactions.

The second part of this chapter focuses on hydrogenation reactions in catalytic membranes. Slurry reactions often require fast stirring to maintain contact between gas, liquid, and catalyst in the reaction system, but diffusion of the reactants to the catalyst surface may still limit the reaction rate in the case of fast kinetics. Flow-through catalytic membrane contactors can overcome this diffusion limitation and also avoid the need to separate the catalyst from the reaction mixture. By forcing a premixed reactant stream containing the liquid and

the dissolved gas through the membrane, efficient contact occurs between the reactants and the catalyst on the pore walls. When membrane pore diameters are small, the diffusion time is negligible compared to reaction times, and the reaction rate depends on either kinetics or the rate of mass flow into the membrane. As discussed in Chapter 2, membrane contactors also allow variation of the contact time between the reactants and the catalyst, which may allow control over selectivity or product distribution. Moreover, catalytic membrane reactors could provide easier scale-up for industrial-scale reactions than conventional slurry reactors. This work uses membranes containing PdNPs for the hydrogenation of a number of substrates including allyl alcohol and several nitroaromatic compounds.

3.2 Experimental Methods

3.2.1 Materials

PEI (M_w = 25,000 Da), PAA (M_w = 90,000 Da), PAH (M_w = 15,000 Da), α-alumina (100 mesh, ~100 μm particle size), 5% Pd on alumina, allyl alcohol, 2-buten-1-ol (mixture of isomers), 2-methyl-2-propen-1-ol, isobutyraldehyde, nitrobenzene, 4-nitrophenol, 4-nitrotoluene, potassium tetrachloropalladate(II), potassium hexachloropalladate(IV), and sodium borohydride were purchased from Aldrich. PAA (M_w = 5,000 Da) was obtained from Polysciences, and butyraldehyde and propionaldehyde were purchased from Fluka. 1-Butanol (J.T. Baker), n-propyl alcohol (Columbus Chemical), and isobutyl alcohol (Spectrum) were used as received. Anodisc aluminum oxide membranes (25 mm disks with

0.2 μm diameter pore sizes) were acquired from Whatman. Aqueous solutions were prepared with deionized water (18.2 MΩ cm, Milli-Q purification system), and hydrogen (99.9%) was obtained from AGA gases.

3.2.2 Modification of Alumina Powder with Polyelectrolyte/PdNP Films

Previous studies in the Bruening group involved the preparation of $[PAA/PEI\text{-}Pd(0)]_x$ films on alumina powder.[2-4] Variation of the concentration of Pd in the polyelectrolyte deposition solution afforded control over the size of the Pd nanoparticles. However, the presence of Pd precursors at concentrations >10 mM in PEI solutions results in flocculation of the polyelectrolyte. Thus, this research incorporated the Pd precursor into the PAA solution to form $[PAA\text{-}Pd(0)/PEI]_3$ films on alumina (Figure 3.1). In this modified procedure, 15 g of alumina was alternately suspended for 10 min in a 100 mL solution that contained 0.02 M PAA (M_w = 90,000, pH adjusted to 4.0 with 0.1 M NaOH) and 1, 4, or 8 mM K_2PdCl_4, and for 10 min in a 100 mL solution that contained PEI (1 mg/mL, pH adjusted to 9.0 with 0.1 M HCl). After the deposition of each polyelectrolyte layer, the alumina was rinsed four times by suspension in 100 mL of deionized water, stirring for 5 min, allowing the alumina to settle, and decanting the supernatant. After deposition of three PAA-Pd(II)/PEI bilayers, reduction to Pd(0) occurred by stirring the modified alumina powder in 100 mL of freshly prepared 0.1 M $NaBH_4$ for 30 min, followed by washing with four 100-mL aliquots of deionized water as described above. After decanting the final water

rinse, the resulting powder was dried under vacuum for 8 hours to remove residual water.

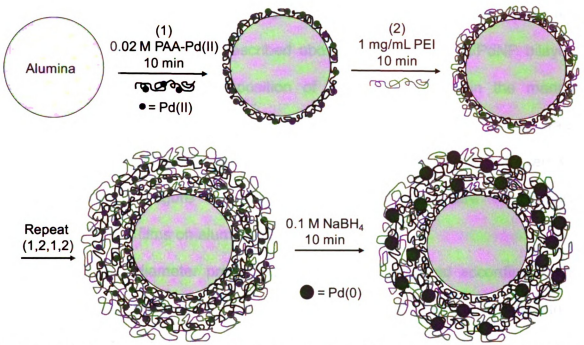

Figure 3.1 Schematic diagram showing the formation of $[PAA\text{-}Pd(0)/PEI]_3$ films on alumina powder. Rinses are not shown.

Alternatively, alumina powder was also modified with preformed Pd nanoparticles using the same procedure described in chapter 2 for formation of polyelectrolyte/AuNP films on alumina. In a 100-mL flask, 7.5 g of 100 mesh alumina was added to 50 mL of a pH 4.5 solution containing 0.02 M PAA (M_w = 5,000) and 0.5 M NaCl, and then stirred vigorously for 10 min. The alumina was allowed to settle and the supernatant was decanted. To remove excess polyelectrolyte, the alumina particles were washed 4 times by adding 50 mL of deionized water, stirring, letting the alumina settle, and decanting the water. Next, 50 mL of a pH 4.5 solution containing 0.02 M PAH and 0.5 M NaCl was added to the alumina, and this mixture was stirred for 10 min, after which the

particles were washed as described above. To deposit the Pd nanoparticles, 50 mL of as-prepared Pd nanoparticle solution was added to the PAA/PAH-modified alumina and stirred for 10 min. The alumina was then allowed to settle and rinsed 4 times with water as described above. Additional PAH/PdNP bilayers were added by alternating deposition of PAH and PdNPs in the manner described above with rinsing between each layer. After decanting the final water rinse, the resulting powder was dried under vacuum for 8 hours to remove residual water. Figure 3.2 shows the overall procedure for forming PAA/[PAH/PdNP]$_x$ films on alumina powder.

The ~7nm diameter preformed PdNPs were prepared according to the citrate reduction method.[16] In a 250 mL volumetric flask equipped with a condenser, 100 mL of aqueous K_2PdCl_6 (0.393 mM) was heated to boiling under vigorous stirring, and 12 mL of a heated 1% sodium citrate solution was added to the Pd solution under continued stirring. After adding the sodium citrate, the

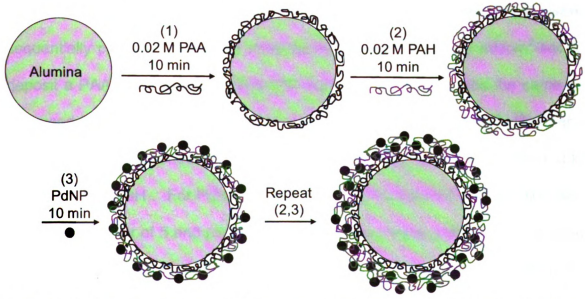

Figure 3.2 Schematic diagram showing the formation of PAA/[PAH/PdNP]$_x$ films on alumina powder. Rinses are not shown.

solution turned from yellow to brown. The mixture was boiled while stirring for 4 hours, during which the solution gradually changed from light brown to dark brown in color. The solution was then removed from the heat and cooled to room temperature. The resulting Pd nanoparticle solution was stored in an amber bottle at 5 °C until use.

3.2.3 Modification of Alumina Membranes with Polyelectrolyte/PdNP Films

Alumina membranes were pretreated in a UV/ozone cleaner for 15 min and then modified with polyelectrolyte/PdNP films by the same method described in chapter 2 for formation of polyelectrolyte/AuNP films in alumina membranes. During film formation, the membranes were placed in an Amicon 8010 ultrafiltration cell, and all solutions were passed through the membranes using a peristaltic pump (Cole Parmer Masterflex C/L) attached to the permeate side of the Amicon cell. Briefly, solutions of PAA (10-15 mL), water (40 mL), PEI (10-15 mL), water (40 mL), citrate-stabilized Pd-nanoparticles, and water (40 mL) were sequentially passed through the membranes at a flux of ~ 0.02 mL/cm^2-sec to deposit a PAA/PEI/PdNP film. The PAA solution composition was the same as that used for modification of alumina powder with PAA/[PAH-PdNP]$_x$ films, and the PEI solution concentration was 0.02 M in 0.5 M NaCl with the pH adjusted to 9.0 with 1 M NaOH . For PdNP deposition, the as-prepared PdNP solution was diluted by a factor of 5 and passed through the membrane until the PdNPs were no longer adhering to the polyelectrolyte layer, i.e., the solution exiting the

membrane exhibited the same brown color as the solution entering the membrane.

3.2.4 Characterization

Preformed citrate-stabilized PdNPs were characterized by transmission electron microscopy (TEM, JEM-2200FS microscope) to determine their approximate size and shape. TEM Samples were prepared by diluting the as-prepared PdNP solution by a factor of 5 with water and placing a 2 µL drop of this mixture on a carbon-coated copper grid. Pd-containing alumina membrane samples were imaged using field-emission scanning electron microscopy (FESEM) with a Hitachi S-4700 II microscope. Prior to imaging, membrane samples were fractured to reveal a cross-section and coated with 5 to 10 nm of Au with a Pelco SC-7 sputter coater.

The amounts of palladium in modified alumina powder catalysts were determined by flame atomic emission spectroscopy (FAES) or inductively coupled plasma optical emission spectroscopy (ICP-OES, Varian 710-ES). Standard solutions were prepared by dissolving K_2PdCl_4 in 2% HNO_3, and sample solutions were prepared by adding the desired amount of alumina powder catalyst to 2 mL of aqua regia, agitating the mixture by sonication, removing the supernatant (the α-alumina support does not dissolve in aqua regia), and diluting the supernatant with deionized water prior to elemental analysis. Determination of Pd content in alumina membranes occurred similarly by dissolving the Pd from the alumina membranes with 2 mL aliquots of aqua

regia and diluting those solutions with deionized water prior to elemental analysis.

3.2.5 Hydrogenation Reactions with Pd-Containing Alumina Powder

Catalytic hydrogenation reactions were carried out in a 100-mL, three-neck, round-bottomed flask (Figure 3.3). A desired amount of alumina-supported catalyst was suspended in 25 mL of deionized water and bubbled with H_2 for 30 min prior to adding 25 mL of a 50 mM aqueous solution of the allylic substrate. Hydrogen was constantly bubbled into the solution, which was stirred vigorously during the reaction. Different amounts of catalyst were used for hydrogenation reactions because each powder has a different wt% of Pd. The values are shown in Table 3.1. Sample aliquots were removed from the reaction flask at specific time intervals, filtered through cotton, and then diluted by a factor of 3 prior to GC analysis (Shimadzu GC-17A equipped with an RTx-BAC1column).

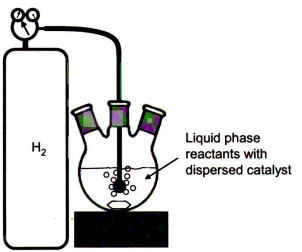

Figure 3.3 Schematic diagram of the apparatus used for slurry hydrogenation reactions with Pd-containing alumina powder catalysts at room temperature and atmospheric pressure.

In hydrogenation of allyl alcohol, β-methallyl alcohol, and crotyl alcohol, we observed mixtures of the isomerization product and the reduced product (Scheme 3.1, page 119). Response factors were determined from the peak areas obtained in the analysis of a 1:1:1 mixture of the starting material, isomerization product, and hydrogenation product and were used to calculate the turnover frequency (TOF) of the catalyst. TOF's were calculated by plotting percent hydrogenation vs. time and determining the slope at conversions less than 50 percent. Each experiment was repeated twice and the ± values represent the difference between the average and the data points

3.2.6 Hydrogenation Reactions with Pd-Containing Membranes

Hydrogenation reactions performed with alumina membranes were carried out by bubbling H_2 into a substrate solution for a set time and then (while still bubbling the solution above the membrane) passing the solution through a Pd nanoparticle-modified membrane at a given flux (Figure 3.4). For hydrogenation of allylic compounds, samples of the membrane permeate were analyzed by GC (Shimadzu GC-17A) without any sample pretreatment. For hydrogenation of nitroaromatic compounds, samples of the permeate were analyzed by UV-Vis spectrophotometry or GC-MS (Hewlett-Packard G1800B GCD system with a HP-5MS column) to determine the amount of starting material that was hydrogenated. Prior to GC-MS analysis, 3 mL of sample was extracted three times into 1 mL portions of diethyl ether, which were then combined. For some experiments, the permeate solution was collected, resaturated with H_2, and

passed through the Pd nanoparticle-containing membrane multiple times to achieve higher conversion.

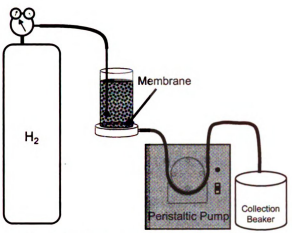

Figure 3.4 Schematic diagram of the apparatus used for flow-through membrane hydrogenation reactions with Pd-containing alumina membranes.

3.3 Results and Discussion

3.3.1 Characterization of Polyelectrolyte/PdNP Films

Examination of the effect of nanoparticle size on catalytic selectivity required the ability to prepare a series of catalysts with different, well-defined particle sizes. Kidambi et al. prepared $[PAA/PEI\text{-}Pd(II)]_3PAA$ films using 2 mM Pd(II) in the PEI-Pd(II) deposition solution, and subsequently reduced the Pd(II) in the film to obtain $[PAA/PEI\text{-}Pd(0)]_3PAA$ coatings containing Pd nanoparticles with diameters of 1-3 nm.[3] To vary the nanoparticle size, we increased the concentration of Pd(II) in the PEI deposition solution, but with Pd(II) concentrations >10 mM, the PEI solution became cloudy, perhaps because the Pd(II) cross-linked PEI chains. Thus we chose to add Pd(II) to the PAA, rather than the PEI, deposition solution. The 20 mM PAA deposition solution remained clear at Pd(II) concentrations as high as 15 mM. Previous studies by Rubner and

coworkers demonstrated adsorption of metal ions into preformed PAA/PAH films and subsequent formation of nanoparticles,[17,18] but in our work, we incorporated the metal ions during the polyelectrolyte LbL assembly.

The sizes of Pd nanoparticles in $[PAA\text{-}Pd(0)/PEI]_3$ films increased with increasing concentrations of Pd(II) in PAA deposition solutions. Previous work by Bhattacharjee showed that with Pd(II) concentrations of 1, 4, or 8 mM in the PAA deposition solutions, the average particle diameters in $[PAA\text{-}Pd(0)/PEI]_3$ films on carbon-coated copper TEM grids were 2.2 ± 0.6, 2.9 ± 0.5, and 3.2 ± 0.6 nm, respectively.[19] Due to the difficulty of imaging Pd nanoparticles on alumina powder, the diameters obtained from films on TEM grids were used as estimates of the diameters of Pd nanoparticles in films on alumina powder.

Alumina powder catalysts containing films with preformed Pd nanoparticles were also studied to provide a slightly larger particle size for additional comparison. To investigate the effect of diffusion through the polyelectrolyte multilayer film on activity/selectivity, we modified alumina powder with $PAA/[PAH/PdNP]_x$ films containing 1, 2, or 3 PAH/PdNP bilayers. The citrate-stabilized Pd nanoparticles exhibited a brown color with a peak absorbance at ~250 nm (Figure 3.5), which is consistent with the literature for particles with diameters of ~7 nm.[20] Further analysis by TEM showed a monodisperse size distribution with an average nanoparticle diameter of 7.2 ± 1.2 nm (Figure 3.6).

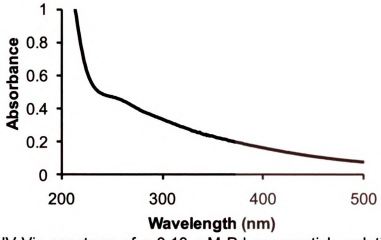

Figure 3.5 UV-Vis spectrum of a 0.10 mM Pd nanoparticle solution showing a peak absorbance at 250 nm. Molarity is given with respect to Pd atoms.

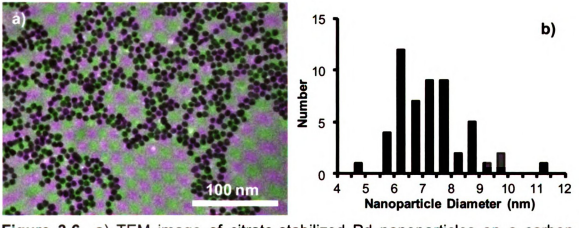

Figure 3.6 a) TEM image of citrate-stabilized Pd nanoparticles on a carbon-coated copper grid. b) Histogram of Pd nanoparticle diameters taken from several TEM images. The average particle diameter was 7.2 ± 1.2 nm.

The Pd content of each catalyst was determined by FAES or ICP-OES, and Table 3.1 presents these results. Catalysts modified with $[PAA\text{-}Pd(0)/PEI]_3$ films exhibited increased Pd loading with increased Pd(II) concentration during deposition. The catalyst prepared with a Pd(II) concentration of 8 mM exhibited unusually high loading, presumably due to enhanced adsorption of the Pd(II) ions to the amine groups in the already-deposited polyelectrolytes. The Pd loading in

catalysts modified by PAA/[PAH/PdNP]$_x$ films increased linearly with increasing the number of PAH/PdNP bilayers (Figure 3.7).

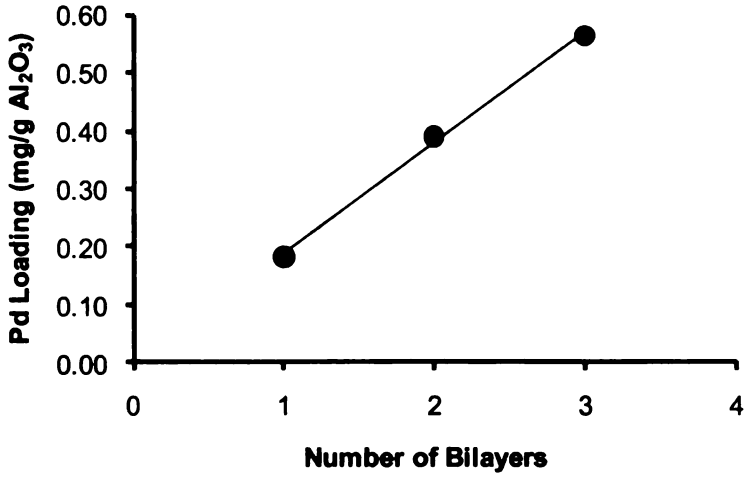

Figure 3.7 Plot of Pd loading vs. number of PAH/PdNP bilayers in catalysts containing PAA/[PAH/PdNP]$_x$ films.

Table 3.1 Pd content of several different Pd catalysts used for hydrogenation reactions.

Catalyst	Pd loading (mg Pd / g Al_2O_3)	Mass of catalyst used in hydrogenation (mg)
[PAA-Pd(0)/PEI]$_3$ on Al_2O_3, Pd(II) = 1 mM[a]	0.28	500
[PAA-Pd(0)/PEI]$_3$ on Al_2O_3, Pd(II) = 4 mM[a]	0.97	250
[PAA-Pd(0)/PEI]$_3$ on Al_2O_3, Pd(II) = 8 mM[a]	6.29	125
PAA/[PAH/PdNP]$_1$ on Al_2O_3	0.18	250
PAA/[PAH/PdNP]$_2$ on Al_2O_3	0.39	125
PAA/[PAH/PdNP]$_3$ on Al_2O_3	0.56	100

[a]The initial concentration of K_2PdCl_4 in the PAA deposition solutions.

3.3.2 Hydrogenation of Allylic Compounds with Pd-Containing Alumina Powder Catalysts

To investigate catalytic selectivity as a function of nanoparticle diameter, we determined TOFs (moles hydrogenated/mol Pd/h) for hydrogenation of allyl alcohol, β-methallyl alcohol, and crotyl alcohol over several different catalysts. Unfortunately, isomerization of the unsaturated alcohols to the corresponding aldehydes (Scheme 3.1) complicated the interpretation of the TOFs because the isomerization product does not readily undergo hydrogenation. Thus, TOFs were calculated both for the initial hydrogenation rate and the sum of the initial hydrogenation and isomerization rates.

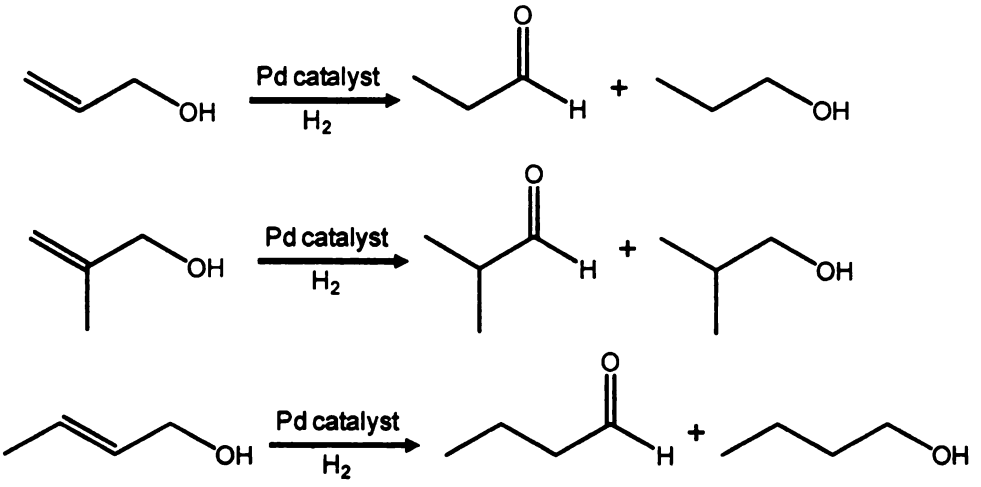

Scheme 3.1 Pd-catalyzed hydrogenation of allyl alcohol, β-methallyl alcohol, and crotyl alcohol.

Table 3.2 shows the hydrogenation TOF's and corresponding selectivities (TOF ratios) for the three $[PAA\text{-}Pd(0)/PEI]_3$ catalysts as well as a commercially available 5% Pd on alumina catalyst. Although the commercially available catalyst showed approximately the same hydrogenation TOF for all three compounds, the $[PAA\text{-}Pd(0)/PEI]_3$ catalysts had significantly different TOF's for

Table 3.2. TOFs and TOF ratios (selectivities) for unsaturated-alcohol hydrogenation catalyzed by Pd catalysts that contained Pd nanoparticles with different diameters. Values in parentheses are the sum of TOFs for hydrogenation and isomerization.

Catalyst	Average nanoparticle diameter (nm)[d]	TOF (moles hydrogenated/mol Pd/h)[a,b]			Ratio of TOFs	
		Allyl alcohol	β-methallyl alcohol	Crotyl alcohol	Allyl / β-methallyl	Allyl / Crotyl
$[PAA\text{-}Pd(0)/PEI]_3$ $[Pd(II)]$=1 mM[c]	2.2	2100 ± 280 (2300 ± 300)	5 ± 1 (5 ± 1)	56 ± 8 (65 ± 9)	420 (460)	38 (35)
$[PAA\text{-}Pd(0)/PEI]_3$ $[Pd(II)]$=4 mM[c]	2.9	1500 ± 80 (1800 ± 80)	18 ± 3 (18 ± 3)	74 ± 8 (90 ± 8)	83 (100)	20 (20)
$[PAA\text{-}Pd(0)/PEI]_3$ $[Pd(II)]$=8 mM[c]	3.2	1700 ± 300 (2000 ± 400)	29 ± 9 (46 ± 10)	300 ± 60 (370 ± 100)	59 (43)	5.7 (5.4)
Commercial 5% Pd on Al_2O_3	-	1200 ± 300 (1600 ± 300)	1100 ± 50 (1700 ± 100)	1400 ± 50 (1600 ± 50)	1.1 (0.9)	0.9 (1.0)

[a]50 mL of 25 mM substrate was hydrogenated in water. TOFs were initial values determined at conversions less than 50%.
[b]The catalysts used in this study came from different batches than the catalysts used in reference 21 and have somewhat different TOFs and selectivities than previously published data. Trends are similar in the two cases.[21]
[c]The initial concentration of K_2PdCl_4 in the PAA deposition solutions.
[d]Average Pd nanoparticle diameter determined by Bhattacharjee.[19]

each compound. In general, the TOF was higher for allyl alcohol than for β-methallyl alcohol and crotyl alcohol for each $[PAA\text{-}Pd(0)/PEI]_3$ catalyst. More importantly, the selectivity (ratio of TOF's) changed dramatically with the particle size. The trend in Table 3.2 is that the TOF for hydrogenation of allyl alcohol decreases or remains the same with increasing nanoparticle size, while the corresponding TOFs for β-methallyl alcohol and crotyl alcohol increase with increasing nanoparticle size. This occurs even though the surface area to volume ratio for the catalyst is smaller for larger particles. As a result of this trend, selectivities decreased by a factor of ~7 upon going from nanoparticle

sizes of 2.2 nm to 3.2 nm. Similar trends occurred when analyzing the sum of hydrogenation and isomerization.

The high selectivities of nanoparticles in polyelectrolyte films may occur in part because the surrounding polyelectrolyte decreases the rate at which bulkier molecules reach catalytic sites. Several studies showed that polyelectrolyte multilayers provide a significant barrier to the diffusion of small compounds, and even molecules as small as glycerol and methanol show much slower transport than water in polyelectrolyte films.[22] To examine whether simple diffusion through polyelectrolyte films enhances selectivity, we prepared catalysts with PAA/[PAH/PdNP]$_x$ films containing 1, 2, and 3 PAH/PdNP bilayers. By using preformed PdNPs in the deposition process, we were able to ensure that the size of the PdNPs was the same for each catalyst. Thus any differences in reactivity or selectivity should be due strictly to diffusion through the polyelectrolyte and not due to differences in particle size.

Table 3.3 shows that catalysts prepared by LbL deposition with preformed Pd nanoparticles exhibit substantially higher TOFs (at least 5 times greater for each substrate) than catalysts containing in-situ prepared Pd nanoparticles, even though the preformed nanoparticles have a larger diameter and thus a smaller surface area to volume ratio. This enhanced activity is most likely due to the high accessibility of the reactants to the catalytic nanoparticles contained in the exterior nanoparticle layer of the PAA/[PAH/PdNP]$_x$ films. Conversely, in-situ prepared nanoparticles may be completely embedded within the polyelectrolyte film leading to much less accessible catalyst sites.

Table 3.3. TOFs and TOF ratios (selectivities) for unsaturated-alcohol hydrogenation catalyzed by Pd catalysts that contained PAA/[PAH/PdNP]$_x$ films with 1, 2, and 3 PAH/PdNP bilayers. Values in parentheses are the sum of TOFs for hydrogenation and isomerization.

Catalyst	TOFs (moles hydrogenated/ mol Pd/ h)[a]			Ratio of TOFs	
	Allyl alcohol	β-methallyl alcohol	Crotyl alcohol	Allyl / β-methallyl	Allyl / Crotyl
PAA/[PAH/PdNP]$_1$	11400 ± 700 (13100 ± 1100)	270 ± 50 (350 ± 80)	1500 ± 150 (1800 ± 150)	42 (37)	7.6 (7.3)
PAA/[PAH/PdNP]$_2$	5600 ± 100 (6400 ± 80)	90 ± 50 (110 ± 50)	600 ± 50 (760 ± 100)	62 (58)	9.3 (8.4)
PAA/[PAH/PdNP]$_3$	5100 ± 50 (5600 ± 90)	170 ± 60 (220 ± 80)	640 ± 60 (780 ± 120)	30 (25)	8.0 (7.2)

[a]50 mL of 25 mM substrate was hydrogenated in water. TOFs were initial values determined at conversions less than 50%.

More importantly, we see that while the number of layers does affect catalytic activity, it has little effect on selectivity in the hydrogenation of allyl alcohol, β-methallyl alcohol, and crotyl alcohol. When going from one bilayer to two bilayers, the TOF decreases significantly for each substrate. This decrease in activity suggests that the addition of a second polyelectrolyte/PdNP bilayer over the top of the initial nanoparticle layer inhibits diffusion of the reactants to the interior nanoparticles. However, the extent of decreased activity is similar for each substrate, as seen in the similar selectivities for each catalyst. Furthermore, the TOFs for the three-layer catalyst remained approximately the same as the two layer catalyst. The 7.2 nm diameter nanoparticles exhibited a much higher selectivity than expected based on the trend of decreased selectivity with increased nanoparticle size shown in Table 3.2. However, the preformed Pd nanoparticles had citrate stabilizers and thus a different composition than in-situ

prepared nanoparticles. Hence, direct comparison between the two nanoparticle systems should be viewed with caution. Further studies with different sizes of citrate-stabilized Pd nanoparticles could provide additional insight into selectivity as a function of nanoparticle size.

Previous studies of nanoparticle reactivity suggest that the size-based selectivity trends we observed may arise from geometrical effects.[23] Doyle, et al. proposed that the sensitivity of catalytic hydrogenation rates to nanoparticle size occurs because the reaction takes place on specific types of atoms that are more (or less) prevalent on small particles.[5] Nanoparticles with large diameters mainly contain terraces with atoms having high coordination numbers, whereas smaller nanoparticles have more edge and corner atoms with low coordination numbers. A recent study based on STM images showed that Pd nanoparticles with diameters < 4 nm contain many defects, while nanoparticles with diameters > 4 nm have more large and well-defined facets.[12,24] Additionally, some studies have shown that the dependence of TOF on particle size disappears when TOF is calculated with respect to a defined type of atom (edge atoms, for example), which would make the reaction depend on nanoparticle structure rather than size.[12,25,26]

In general, we see that the TOFs for hydrogenation of allyl alcohol decrease slightly with increasing nanoparticle diameter, while the TOFs for β-methallyl alcohol and crotyl alcohol increase as nanoparticle size increases. One explanation for this observation is that in the hydrogenation of monosubstituted double bonds suchas allyl alcohol, defect atoms are the primary active centers

for catalysis, whereas hydrogenation of multisubstituted double bonds occurs more readily on terraces. Hence, TOFs for the monosubstituted compounds increase as nanoparticle size decreases because of a larger fraction of defect atoms in the small nanoparticles. The higher TOF of allyl alcohol with the smallest nanoparticle size could be attributed to the increased surface area of the smaller particles. It is also possible that hydrogenation of multisubstituted double bonds is more restricted on the terraces of the smallest nanoparticles because the active site is smaller. Conversely, the terraces of larger particles have a larger binding area that may allow hydrogenation of multisubstituted double bonds to take place more readily.

Hydrogenation of mixtures of the different alcohols was performed to determine if monosubstituted and multisubstituted compounds are hydrogenated on the same sites or different sites. In these experiments, mixtures of allyl alcohol with either β-methallyl alcohol or crotyl alcohol were hydrogenated with the $[PAA\text{-}Pd(0)/PEI]_3$ catalysts under the same conditions as in the single substrate hydrogenations. These experiments were carried out with the catalysts prepared with 1 mM K_2PdCl_4 and 8 mM K_2PdCl_4. The TOFs and selectivities obtained with the 1 mM catalyst were similar to those determined from single component systems. However, the large difference in hydrogenation rates among the three substrates makes it difficult to see if they were reacting at different active sites. Conversely, the initial TOFs of β-methallyl alcohol and crotyl alcohol were much lower in the mixed component systems using the 8 mM catalyst, which resulted in much higher selectivities than those determined from

the single component systems. Furthermore, once the majority of allyl alcohol reacted, the rate of hydrogenation of β-methallyl alcohol or crotyl alcohol increased to values similar to those in the single component systems (Figures 3.8 and 3.9). Mixed component experiments were also performed with a commercial 5% Pd on alumina catalyst, and again the activities of β-methallyl alcohol and crotyl alcohol were lower than single component experiments until most of the allyl alcohol reacted. This suggests that all 3 compounds react at the same active sites, and apparently monosubstituted double bonds are able to bind

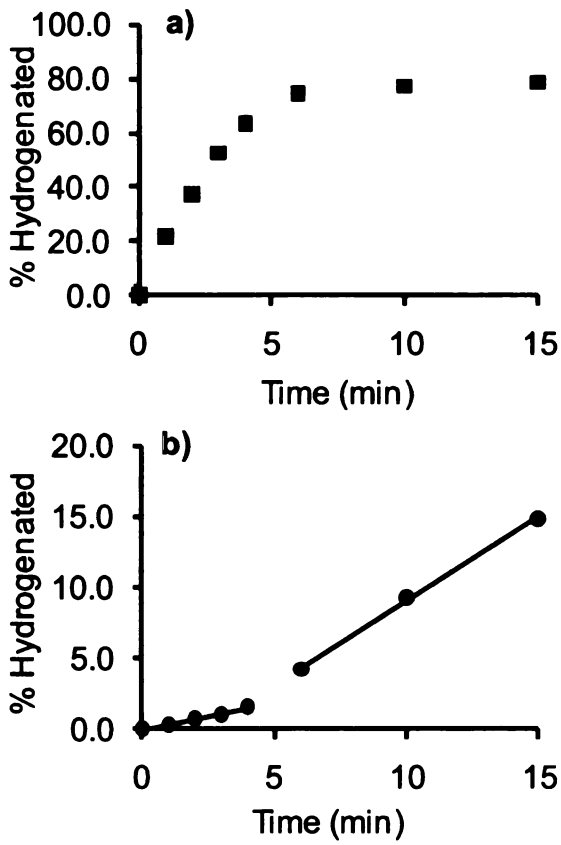

Figure 3.8 Percent hydrogenation of a) allyl alcohol and b) β-methallyl alcohol during competitive hydrogenation of these substrates using a $[PAA\text{-}Pd(0)/PEI]_3$ catalyst prepared with 8 mM Pd(II). The initial concentration of each substrate was 25 mM. After 6 min, allyl alcohol was consumed due to hydrogenation and formation of ~20% propionaldehyde. In (b), lines represent slopes before and after reaction of allyl alcohol.

more easily to the surface than multisubstituted double bonds. Therefore, the enhanced selectivity observed with smaller particles is most likely due to the ability of allyl alcohol to bind more easily to the active sites of smaller nanoparticles.

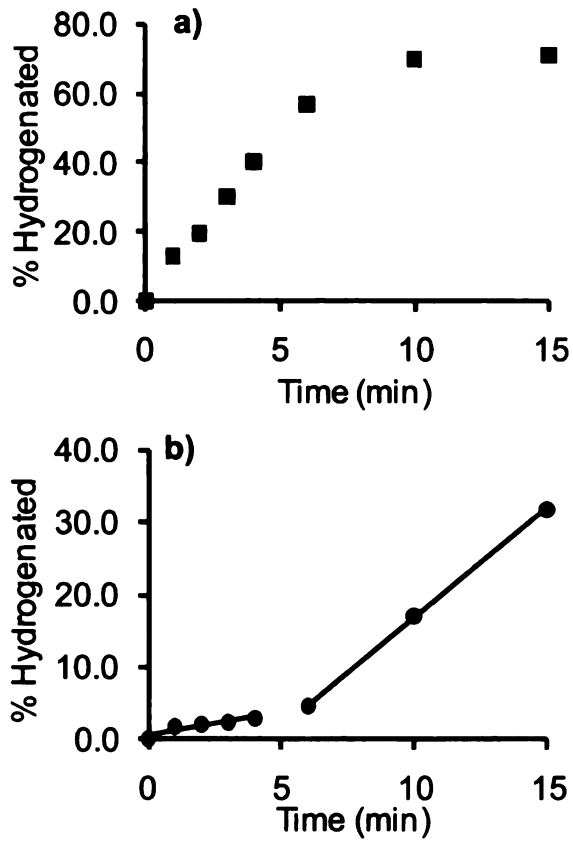

Figure 3.9 Percent hydrogenation of a) allyl alcohol and b) crotyl alcohol during competitive hydrogenation of these substrates using a [PAA-Pd(0)/PEI]$_3$ catalyst prepared with 8 mM Pd(II). The initial concentration of each substrate was 25 mM. After 6 min, most of the allyl alcohol was consumed due to hydrogenation and formation of ~20% propionaldehyde. In (b), lines represent slopes before and after reaction of allyl alcohol.

3.3.3 Hydrogenation of Allylic Compounds with Pd-Containing Membranes

The results in Table 3.3 demonstrate that catalysts containing citrate-stabilized Pd nanoparticles are especially active in the hydrogenation of allylic alcohols. While powder-supported catalysts are beneficial for understanding reaction kinetics, membrane-supported catalysts may offer additional advantages by providing enhanced contact between the reactants and the catalyst, separating the catalyst from the reactant mixture, and allowing reactions to run continuously. We modified alumina membranes with a single PAA/PEI/PdNP layer and performed initial flow-through hydrogenation studies with allyl alcohol.

In the hydrogenation experiments with membranes, solutions were sparged with H_2 before passing them through an alumina membrane coated with a PAA/PEI/PdNP film. To determine whether the sparging time was sufficient to saturate the solution with H_2, we performed allyl alcohol hydrogenation experiments with all conditions remaining constant except for the initial H_2 bubbling time (Figure 3.10). Upon increasing the initial H_2 bubbling time from 2 minutes to 15 minutes, the concentration of allyl alcohol hydrogenated to 1-propanol after passage through the membrane increased from 1.0 to 1.4 mM. However, samples collected from the feed solution after bubbling with H_2 for the given amount of time showed similar increases in the concentration of 1-propanol from 0 to 0.4 mM. Though the feed solution did not pass through the PdNP-containing membrane, it was still in contact with the upper membrane surface during the initial bubbling time, and some of the allyl alcohol was hydrogenated to 1-propanol via catalysis at the upper membrane surface. The plot in Figure

3.10b shows that the difference between the concentration of 1-propanol in the permeate solution and in the feed solution is nearly the same for all initial bubbling times. Thus, H_2 saturation occurs fairly quickly, so subsequent experiments utilized a 2 minute bubbling time before passing the feed solution through a modified membrane.

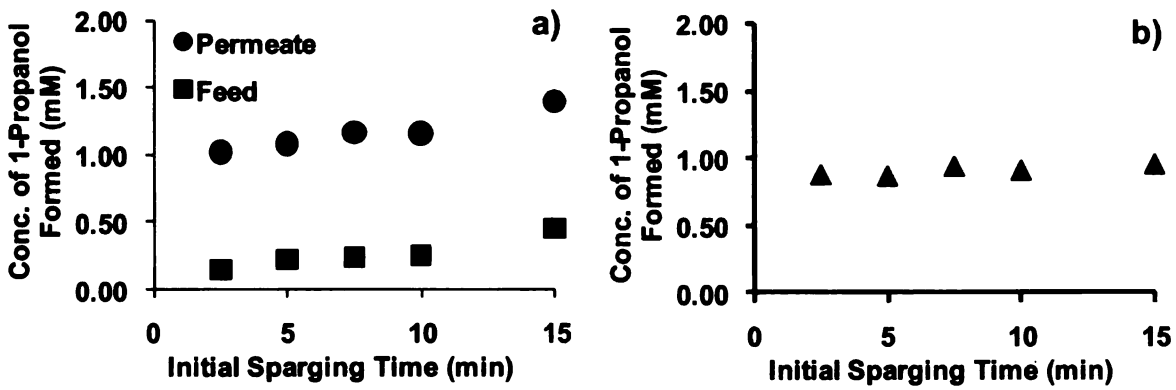

Figure 3.10 a) Conc. of 1-propanol formed vs. initial H_2 sparging time in membrane-catalyzed hydrogenation of 5 mM allyl alcohol. The flux through the Pd nanoparticle-modified alumina membrane was 0.023 mL/cm^2-sec. Circles represent the concentration of 1-propanol in the permeate solution and squares represent the concentration of 1-propanol in the feed solution. The plot in b) represents the difference in the 1-propanol concentration in the permeate and the feed.

The results in Figure 3.10 show that nearly 20% of a 5 mM allyl alcohol solution is hydrogenated to 1-propanol upon passing through a Pd-containing alumina membrane. To determine if the amount hydrogenated is limited by reaction kinetics or hydrogen solubility in water, we performed reactions with a series of initial allyl alcohol concentrations. At initial concentrations < 1 mM, nearly all of the allyl alcohol is hydrogenated to 1-propanol during passage through the membrane because at these concentrations, allyl alcohol is the limiting reactant. However, at allyl alcohol concentrations > 5 mM the amount

hydrogenated remains essentially constant because H_2 is the limiting reagent. The solubility of H_2 in water at 1 atm of H_2 is roughly 0.8 to 1.0 mM,[27,28] and this corresponds to the maximum concentration of allyl alcohol that could undergo hydrogenation (Figure 3.11).

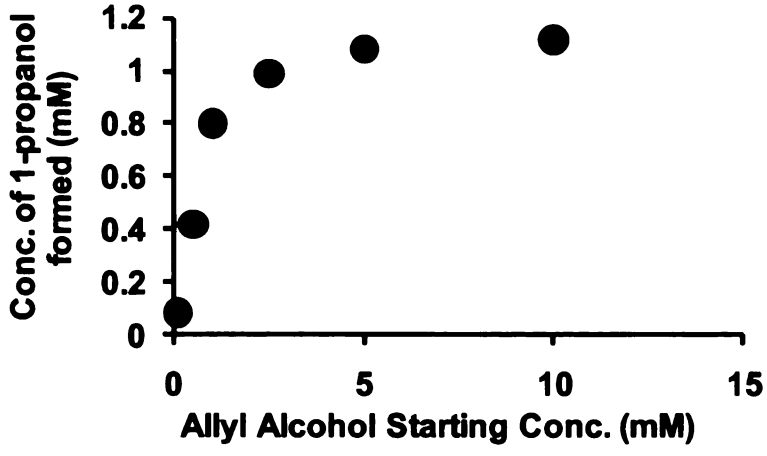

Figure 3.11 Concentration of 1-propanol formed in membrane-catalyzed hydrogenation with several initial allyl alcohol concentrations. Solutions were sparged with H_2, and the flux through the Pd nanoparticle-modified alumina membrane was 0.023 mL/cm^2-sec.

We performed allyl alcohol hydrogenation with multiple passes through the membrane to see if additional conversion of allyl alcohol to 1-propanol could be obtained. When collecting the permeate and simply passing it through the membrane again, no additional conversion was achieved. As expected, to obtain higher conversions, the solution needed to be resaturated with H_2 before again passing it through the membrane. In subsequent multiple pass experiments, permeate solutions were collected, resparged with H_2 for 2 min, and then passed through the membrane again. The plot in Figure 3.12 shows the concentration of 1-propanol after 5 passes of an allyl alcohol solution (initial concentration = 20

mM) through a PdNP-modified membrane. The concentration of 1-propanol that formed in each pass through the PdNP-modified membrane remained essentially constant at ~1.1 mM. Thus, essentially all of the H_2 was consumed each time the solution passed through the membrane.

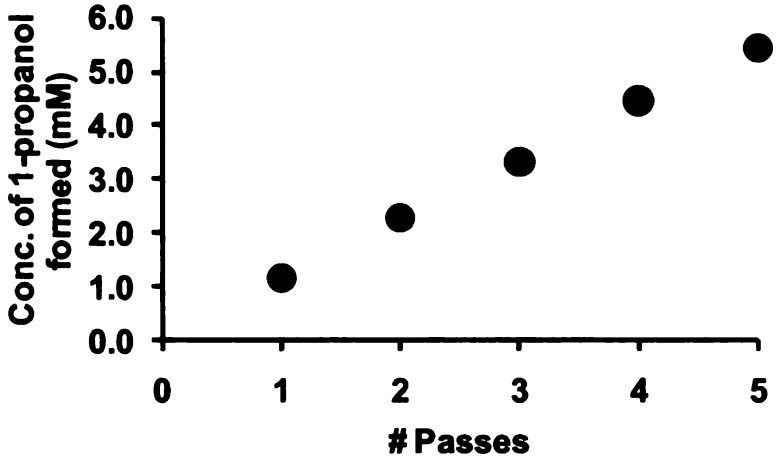

Figure 3.12 Cumulative concentration of 1-propanol formed in membrane-catalyzed hydrogenation of a 20 mM allyl alcohol solution after multiple passes through an alumina membrane modified with a PAA/PEI/PdNP film. Solutions were sparged with H_2 for 2 min before each pass, and the flux through the membrane was 0.023 mL/cm^2-sec.

For hydrogen-sparged solutions containing 10 mM allyl alcohol, increasing the flux through the PdNP-modified membrane from 0.023 to 0.13 mL/cm^{2}sec did not significantly alter the amount of 1-propanol that was formed upon passage through the membrane (Figure 3.13). This suggests that the reaction conversion was still limited by the amount of H_2 in the solution even at higher flow rates.

The use of solvents with higher hydrogen solubility leads to increased conversion of allyl alcohol to 1-propanol. For example, the solubility of H_2 in ethanol is ~3 mM under atmospheric conditions.[29] When performing reactions with a variety of initial allyl alcohol concentrations in ethanol, nearly all of the allyl alcohol was

converted to 1-propanol or the isomer product at allyl alcohol concentrations < 2 mM (Figure 3.14). At allyl alcohol concentrations > 5 mM, the reaction again began to be limited by hydrogen solubility as the concentration of 1-propanol in the permeate was ~3.1 mM.

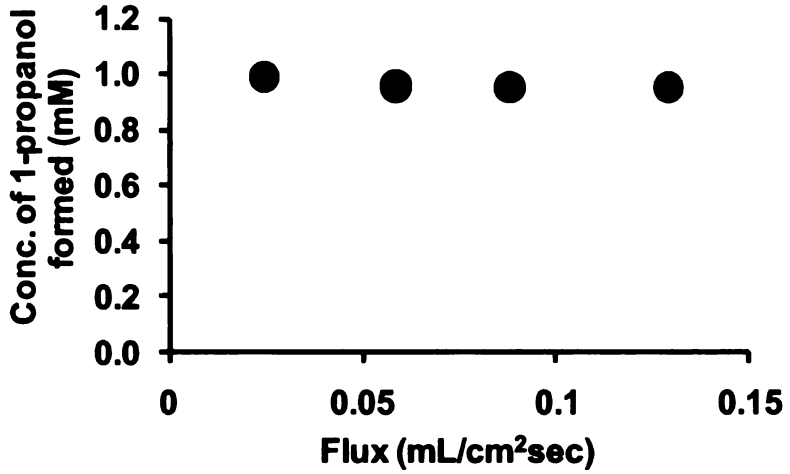

Figure 3.13 Concentration of 1-propanol formed during membrane-catalyzed hydrogenation as a function of flux through an alumina membrane modified with a PAA/PEI/PdNP film. The initial allyl alcohol concentration was 10 mM, and solutions were sparged with H_2 for 2 min before a single pass through the membrane.

Figure 3.14 Concentration of 1-propanol formed in membrane-catalyzed hydrogenation with several initial allyl alcohol concentrations in ethanol. Solutions were sparged with H_2, and the flux through the PAA/PEI/PdNP-modified alumina membrane was 0.023 mL/cm^2-sec.

3.3.4 Hydrogenation of Nitroaromatic Compounds with Pd-Containing Membranes

To further demonstrate the use of Pd-modified membranes for hydrogenation reactions, we utilized alumina membranes modified with a PAA/PEI/PdNP film for the hydrogenation of 4-nitrophenol to 4-aminophenol (Scheme 3.2). As we discussed in chapter 2, the reduction of aromatic nitro groups is important in synthetic chemistry, and the formation of aromatic amines via hydrogenation is especially attractive because the reducing agent is readily removed from the reaction mixture during the reaction. In initial studies of membrane-based 4-nitrophenol hydrogenation, aqueous solutions of 4-nitrophenol were sparged with H_2 and passed through an alumina membrane coated with a PAA/PEI/PdNP film. Similar to the previous experiments with allyl alcohol, reactions were primarily limited by the amount of 4-nitrophenol when its initial concentration was < 0.1 mM (Figure 3.15). At higher concentrations, the conversion reached a plateau, presumably because of the limited amount of H_2 in the solution. Roughly 7% of a 4 mM 4-nitrophenol solution was reduced upon passing through a PAA/PEI/PdNP-modified alumina membrane. This corresponds to a change in 4-nitrophenol concentration of ~ 0.3 mM, which requires a H_2 concentration of 0.9 mM in the solution.

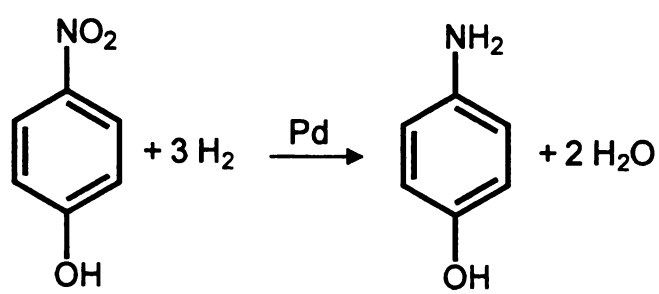

Scheme 3.2 Pd-catalyzed hydrogenation of 4-nitrophenol to 4-aminophenol.

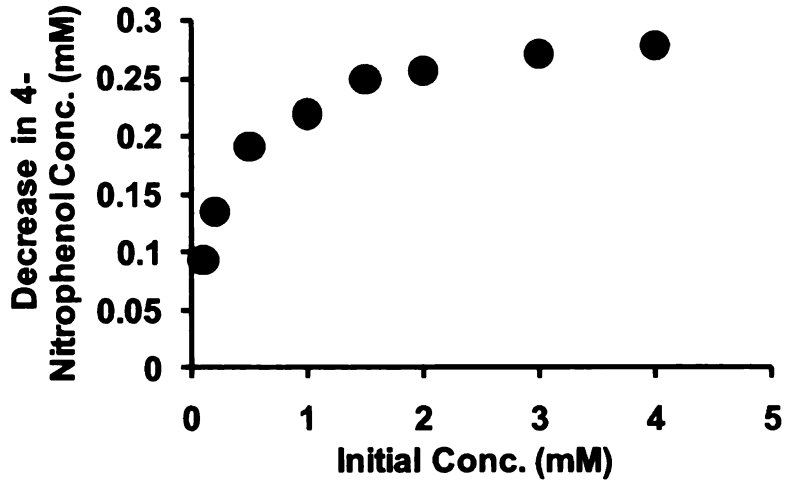

Figure 3.15 Decrease in 4-nitrophenol concentration in membrane-catalyzed hydrogenation with several initial 4-nitrophenol concentrations. Solutions were sparged with H_2, and the flux through the Pd nanoparticle-modified alumina membrane was 0.023 mL/cm^2-sec.

We performed additional hydrogenation reactions with nitrobenzene and 4-nitrotoluene. For both compounds, ~7% reduction of the nitro compound occurred upon passing a 4 mM aqueous solution through a Pd nanoparticle-modified membrane at a flux of 0.023 mL/cm^2-sec. The fact that the reaction is limited by H_2 concentration should be especially useful for minimizing side reactions. Since the hydrogen is used up in the reaction with the starting material, there is less hydrogen available to react with the initial hydrogenation products in further reactions. Thus, future studies of membrane-based nitroaromatic compound hydrogenation could examine the chemoselective hydrogenation of nitro groups in the presence of other reducible functional groups.

3.4 Conclusions

This chapter showed that Pd nanoparticle size greatly affects selectivity in the hydrogenation of monosubstituted over disubstituted double bonds with polyelectrolyte/PdNP films deposited on alumina powder. While a commercial 5% Pd on alumina catalyst showed no selectivity for the hydrogenation of allyl alcohol over β-methallyl alcohol or crotyl alcohol, catalysts containing [PAA-Pd(0)/PEI]$_3$ films showed selectivities as high as 420 for allyl alcohol over β-methallyl alcohol and 38 for allyl alcohol over crotyl alcohol. Moreover, as the nanoparticle size increases, selectivities decrease by a factor of 7. In studies utilizing PAA/[PEI/PdNP]$_x$ films with 1, 2, and 3 PEI/PdNP bilayers, the selectivity was not significantly affected by the number of layers in the film. This suggests that the changes in selectivity observed with the [PAA-Pd(0)/PEI]$_3$ catalysts are due primarily to differences in particle size and not to diffusion through the polyelectrolyte multilayer films. Differences in selectivities might occur because monosubstituted double bonds bind more easily to the active sites of smaller nanoparticles than multisubstituted double bonds do. Thus, the selectivities are lower with larger particles because it is easier for the multisubstituted double bonds to adsorb and react at the less hindered active sites.

Additionally, we demonstrated that alumina membranes modified with Pd-nanoparticle-containing films effectively reduce allyl alcohol to 1-propanol in flow-through hydrogenation reactions. However, these reactions gave relatively low conversions due to the low solubility of H_2 in water. When using ethanol as the solvent, conversion increased by a factor of three as a result of the increased

hydrogen solubility. In each case, the reaction conversion was primarily limited by H_2 solubility once the initial allyl alcohol concentration singificantly exceeded the concentration of H_2 in the solution. Similar results were obtained in the hydrogenation of several nitroaromatic compounds. Future hydrogenation studies with Pd-containing membranes should focus on methods to overcome the H_2 solubility limitations.

3.5 References

(1) Nishimura, S. *Handbook of Heterogeneous Catalytic Hydrogenation for Organic Synthesis*; John Wiley & Sons, Inc., 2001.

(2) Kidambi, S.; Bruening, M. L. *Chem. Mater.* **2005**, *17*, 301-307.

(3) Kidambi, S.; Dai, J.; Li, J.; Bruening, M. L. *J. Am. Chem. Soc.* **2004**, *126*, 2658-2659.

(4) Bhattacharjee, S.; Bruening, M. L. *Langmuir* **2008**, *24*, 2916-2920.

(5) Doyle, A. M.; Shaikhutdinov, S. K.; Freund, H.-J. *Angew. Chem. Int. Ed.* **2005**, *44*, 629-631.

(6) Doyle, A. M.; Shaikhutdinov, S. K.; Jackson, S. D.; Freund, H.-J. *Angew. Chem. Int. Ed.* **2003**, *42*, 5240-5243.

(7) Wilson, O. M.; Knecht, M. R.; Garcia-Martinez, J. C.; Crooks, R. M. *J. Am. Chem. Soc.* **2006**, *128*, 4510-4511.

(8) Shaikhutdinov, S.; Heemeier, M.; Baumer, M.; Lear, T.; Lennon, D.; Oldman, R. J.; Jackson, S. D.; Freund, H. J. *J. Catal.* **2001**, *200*, 330-339.

(9) Xu, B.; Liew, K. Y.; Li, J. *J. Am. Oil Chem. Soc.* **2007**, *84*, 117-122.

(10) Ruta, M.; Semagina, N.; Kiwi-Minsker, L. *J. Phys. Chem. C* **2008**, *112*, 13635-13641.

(11) Semagina, N.; Renken, A.; Kiwi-Minsker, L. *J. Phys. Chem. C* **2007**, *111*, 13933-13937.

(12) Silvestre-Albero, J.; Rupprechter, G.; Freund, H.-J. *J. Catal.* **2006**, *240*, 58-65.

(13) Vasylyev, M. V.; Maayan, G.; Hovav, Y.; Haimov, A.; Neumann, R. *Org. Lett.* **2006**, *8*, 5445-5448.

(14) Niu, Y.; Yeung, L. K.; Crooks, R. M. *J. Am. Chem. Soc.* **2001**, *123*, 6840-6846.

(15) Oh, S.-K.; Niu, Y.; Crooks, R. M. *Langmuir* **2005**, *21*, 10209-10213.

(16) Dokoutchaev, A.; James, J. T.; Koene, S. C.; Pathak, S.; Prakash, G. K. S.; Thompson, M. E. *Chem. Mater.* **1999**, *11*, 2389-2399.

(17) Joly, S.; Kane, R.; Radzilowski, L.; Wang, T.; Wu, A.; Cohen, R. E.; Thomas, E. L.; Rubner, M. F. *Langmuir* **2000**, *16*, 1354-1359.

(18) Wang, T. C.; Rubner, M. F.; Cohen, R. E. *Langmuir* **2002**, *18*, 3370-3375.

(19) Bhattacharjee, S. PhD Dissertation, Michigan State University, 2008.

(20) Teranishi, T.; Miyake, M. *Chem. Mater.* **1998**, *10*, 594-600.

(21) Bhattacharjee, S.; Dotzauer, D. M.; Bruening, M. L. *J. Am. Chem. Soc.* **2009**, *131*, 3601-3610.

(22) Liu, X.; Bruening, M. L. *Chem. Mater.* **2003**, *16*, 351-357.

(23) Bond, G. C. *Surf. Sci.* **1985**, *156*, 966-981.

(24) Freund, H. J.; Baumer, M.; Libuda, J.; Risse, T.; Rupprechter, G.; Shaikhutdinov, S. *J. Catal.* **2003**, *216*, 223-235.

(25) Li, Y.; Boone, E.; El-Sayed, M. A. *Langmuir* **2002**, *18*, 4921-4925.

(26) Semagina, N.; Renken, A.; Laub, D.; Kiwi-Minsker, L. *J. Catal.* **2007**, *246*, 308-314.

(27) Jauregui-Haza, U. J.; Pardillo-Fontdevila, E. J.; Wilhelm, A. M.; Delmas, H. *Lat. Am. Appl. Res.* **2004**, *34*, 71-74.

(28) Baranenko, V. I.; Kirov, V. S. *At. Energ.* **1989**, *66*, 24-8.

(29) Purwanto, P.; Deshpande, R. M.; Chaudhari, R. V.; Delmas, H. *J. Chem. Eng. Data* **1996**, *41*, 1414-1417.

Some of the text and figures contained in chapter four appeared in the following publication.
Dotzauer, D. M.; Abusaloua, A.; Miachon, S.; Dalmon, J.-A.; Bruening, M. L. *Appl. Catal., B, In Press, Corrected Proof.*

Chapter Four: Catalytic Wet Air Oxidation with Pt-Containing Membranes

4.1. Introduction

The previous two chapters described the benefits of using catalytic membranes for chemical synthesis reactions and reactions in which the control over product formation is important. However, the membranes described in those chapters suffer from difficulty in scaling up the system for higher throughput. This chapter focuses on the use of catalytic membranes for the environmental application of catalytic wet air oxidation. Wet air oxidation is an important wastewater treatment process in which hazardous organic pollutants react with oxygen to give more benign compounds, ideally H_2O and CO_2.[1-3] This technique is attractive for processing wastewater that is too dilute to be treated by incineration[4,5] and too concentrated to be treated by biological methods.[6-9] Traditional wet air oxidation of organic and inorganic substrates often requires high temperature and pressure (150-350 °C, 20-200 bar air),[10,11] but the use of catalysts such as Pt, Ru, or other precious metals immobilized on inorganic powders allows much milder reaction conditions (room temperature, 1 to 5 bar air).[12-14] However, implementation of catalytic wet air oxidation in conventional stirred tank reactors requires a catalyst recovery step, and reaction rates are often limited by diffusion of oxygen and/or the liquid phase compounds to the catalyst surface.

Porous membranes are an attractive alternative to powders as catalyst supports because the high internal surface area of the membrane affords a high loading of the active catalyst material and there is no need to separate the

catalyst from the reaction mixture. Thus, reactions can be run continuously. Furthermore, catalytic membranes operated as gas/liquid contactors enhance the accessibility of the reactants to the metal catalyst.[15,16] As we showed in chapter one, the two most common membrane configurations for gas/liquid reactions are flow-through and interfacial contactors. We discussed the use of flow-through contactors for hydrogenation reactions with Pd-containing membranes in chapter three. Flow-through contactors, where all reactants flow through the membrane in a single solution, are advantageous because when the membrane pores are sufficiently small, reactions will not be limited by the rate of mass transport to the catalyst.[17] Also, by controlling the flow rate and, hence, the residence time of a substrate within the membrane, side reactions may be minimized to give high selectivity for a particular product.[18-22] Unfortunately, as we demonstrated in chapter three, the low solubility of the gaseous reactant in the liquid phase often limits the extent of reaction in gas/liquid reactions with flow-through contactors.[17] A similar problem occurs in fixed-bed reactors.

In interfacial contactors, the walls of a catalytic membrane serve as the interface between the gas and liquid phases (Figure 4.1) to allow rapid transport of gas to the solid-liquid-catalyst interface and provide a high catalytic activity.[23] Recent work by Pera-Titus et al. also suggests that the enhanced catalytic activity in interfacial contactors may be due to increased gas solubility in the confined pores of the membrane.[24] However, if pore sizes are larger than 10 nm, this effect is usually not observed.

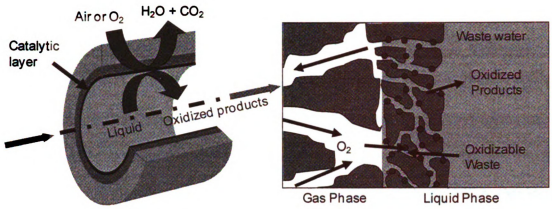

Figure 4.1. Schematic diagram showing the interfacial contactor configuration in a tubular membrane and its application to wet air oxidation.

Recently, the "Watercatox" process was developed as a method to oxidize organic content in industrial wastewater using catalytic membrane reactors while allowing much lower temperatures and pressures than traditional wet air oxidation or incineration. This is a joint project between groups in Lyon, France and Oslo, Norway in which catalytically active tubular ceramic membranes are used for wet air oxidation of model effluents in the laboratory and then scaled-up to pilot-size for oxidation of industrial effluents.[25-30] They showed that the interfacial contactor configuration leads to increased activity when compared to a conventional stirred tank reactor,[29] and that the high activity stems from the ability to control the location of the gas/liquid interface within the membrane (Figure 4.1).

The location of the gas/liquid interface is a crucial factor because mass transfer of pollutants and O_2 to the reaction zone can greatly affect the reaction rate. Several studies by Vospernik et al. specifically examined the effect of pressure difference on catalytic activity in wet air oxidation of formic acid.[31-33]

These studies showed that the concentration of formic acid is depleted as a function of distance travelled radially into the membrane. Likewise, the concentration of O_2 in the liquid phase decreases rapidly to zero as a function of radial distance from the gas/liquid interface. As a result, the thickness of the reaction zone is only on the order of 5 to 20 μm depending on reaction conditions.[33] They also found that as the transmembrane pressure increases, the location of the gas/liquid interface moves from the support layer with large pore sizes to the intermediate and skin layers with smaller pore sizes, and the activity of the membrane for formic acid oxidation increases. This increased activity is likely due to both the higher catalyst loading in the intermediate and skin layers (higher surface area for catalyst deposition) and the shorter diffusion distance of formic acid to the reaction zone.[32]

In the interfacial contactors thus far employed for wet air oxidation, catalytic noble metal particles were formed in the membrane by evaporation/recrystallization/reduction and anionic impregnation/reduction methods,[34,35] but other methods of catalyst deposition may have better control over catalyst deposition and provide even higher catalytic activities. Among the many methods for incorporating precious metal catalysts in porous materials,[36-41] layer-by-layer (LbL) adsorption of polyelectrolyte/metal nanoparticle films is attractive because it offers fine control over nanoparticle size and composition and can be applied to a variety of membrane materials.[42] Ideally, the catalyst should be highly concentrated in the membrane region where the gas/liquid interface occurs, and the interface should be maintained close to the inner layer

of the membrane to limit diffusion distances for the liquid phase reactants. Because LbL nanoparticle adsorption within membranes is very rapid, the depth to which deposited nanoparticles penetrate the membrane can be readily controlled by limiting the amount of nanoparticle-containing solution passed through the membrane. Hence it is a simple matter to localize catalyst deposition in the inner layer of a tubular membrane.

This chapter discusses the wet air oxidation of formic acid, acetic acid, and phenol using tubular ceramic membranes modified with Pt nanoparticles by LbL deposition. Many of the results described in this chapter were obtained in collaboration with Miachon and coworkers at the Institute of Researches on Catalysis and Environment in Lyon, France (IRCELYON). Results from these membranes are compared with results from membranes modified by conventional impregnation techniques used in the Watercatox project. The LbL modified membranes have especially high specific activities in the oxidation of these model compounds.

4.2 Experimental Methods

4.2.1 Materials

Anodisc aluminum oxide membranes (25 mm disks with 0.1 μm diameter pore sizes, Whatman), tubular ceramic membranes (Pall Exekia) and 100 mesh aluminum oxide (Aldrich) were modified with catalytic nanoparticles using the LbL technique. The tubular membranes (25 cm long, 7 mm inner diameter, 10 mm outer diameter) consisted of three layers: a TiO_2-covered alumina support layer

with 12 μm-diameter pores, a TiO_2-covered alumina intermediate layer with 0.8 μm-diameter pores, and a ZrO_2 inner layer with 50 nm-diameter pores. Hexachloroplatinic acid, sodium citrate, sodium borohydride, poly(allylamine hydrochloride) (PAH, Mw = 17,000), and poly(ethylenimine) (PEI, branched, Mw = 25,000) were obtained from Aldrich. Poly(acrylic acid) (PAA, Mw = 5,000) was obtained from Polysciences Inc.

4.2.2 Modification of Aluminum Oxide Powder

LbL modification of the alumina powder involved: 1) stirring 2.5 g of alumina powder in 20 mL of PAA solution (0.02 M PAA, 0.5 M NaCl, pH adjusted to 4.5 with 1.0 M NaOH) for 10 minutes; 2) stirring the PAA-modified powder in 20 mL of PAH solution (0.02 M PAH, 0.5 M NaCl, pH adjusted to 5.0 with 0.1 M HCl) for 10 minutes; and 3) stirring the PAA/PAH-coated powder in 20 mL of a Pt nanoparticle solution for 10 minutes. (Polymer concentrations are given with respect to the repeating unit.) After each of the above steps, the liquid was decanted, and the alumina powder was washed three times with 20 mL of deionized water. Pt nanoparticles were prepared with thiol or citrate stabilizing agents. To synthesize the thiol-stabilized particles, under vigorous stirring 5 mL of 0.0676 M $NaBH_4$ was added to an aqueous solution containing 10 mL of 3.38 mM $H_2PtCl_6 \cdot 6H_2O$ and 1 mL of 0.0237 M mercaptosuccinic acid (MSA).[43] The resulting MSA-stabilized Pt nanoparticle solution was diluted by a factor of 4 prior to use in LbL adsorption on alumina powder. To prepare the citrate-stabilized particles, 30 mL of a heated 1 wt% aqueous sodium citrate solution was added to

255 mL of a refluxing solution of 0.3 mM $H_2PtCl_6 \cdot 6H_2O$ under vigorous stirring. The solution was refluxed for 4 hours to allow completion of the reaction.[44] The resulting Pt nanoparticle solution was used directly for deposition on alumina powder. Alumina powder was also modified by the anionic impregnation/ reduction technique by stirring 2.5 g of the powder in a 0.1 g/L solution of $H_2PtCl_6 \cdot 6H_2O$ for 2 hours, washing three times with 20 mL of deionized water, and reducing the Pt ions to nanoparticles by adding 20 mL of 0.1 M $NaBH_4$ and stirring for 10 minutes.

4.2.3 Modification of Disk-Shaped Alumina Membranes

LbL modification of disk-shaped alumina membranes was described in chapter two for membranes containing polyelectrolyte/AuNP films. Briefly, deposition of each layer involved passing the polyelectrolyte or nanoparticle solution through the membrane using a peristaltic pump located at the permeate side of the membrane. During membrane modification, the films were formed by flowing a PAA solution (0.02 M PAA, 0.5 M NaCl, pH adjusted to 4.5 with 1.0 M NaOH), water, PAH solution (0.02 M PAH, 0.5 M NaCl, pH adjusted to 5.0 with 0.1 M HCl), water, citrate- or thiol-stabilized Pt-nanoparticle solution (as-prepared nanoparticles diluted by a factor of 10), and water through the membranes.

Several alumina membranes were also modified by the LbL method with Au, Pd, and Ru nanoparticles to compare with the activity of Pt nanoparticles. The Au nanoparticles were citrate-stabilized with an expected diameter of ~2.6 nm and prepared according to a literature procedure[45] in which 1 mL of 1%

$HAuCl_4$ was added to 90 mL of H_2O at room temperature and stirred for 1 min, followed by addition of 2 mL of 38.8 mM sodium citrate and stirring for 1 min. Reduction occurred by adding 1 mL of 0.075% $NaBH_4$ in 38.8 mM sodium citrate and stirring the colloidal solution for an additional 5 min. The Pd nanoparticles were also citrate-stabilized and had an expected diameter of ~7 nm.[46] In the synthesis of these particles, 50 mL of an aqueous 0.393 mM solution of K_2PdCl_6 was heated to reflux, a heated 1 % solution of sodium citrate (6mL) was added, and the refluxing was allowed to continue for 4 h. The Ru nanoparticles were prepared by adding 0.5 mL of a 0.1 M $NaBH_4$ solution dropwise to 10 mL of 2 mM $RuCl_3$ under vigorous stirring.[47] The Ru nanoparticles had an expected diameter of 1.8 nm and were positively charged due to the absence of any additional stabilizing agent.[47] Membrane modification with the Ru nanoparticles involved deposition of 1.5 PAA/PAH bilayers prior to nanoparticle deposition because of the positive charge on these particles. Citrate-stabilized Au and Pd nanoparticles were adsorbed on 1-bilayer PAA/PAH films in the same manner as the Pt nanoparticles.

Anionic impregnation of alumina membranes was carried out by flowing a 0.1 g/L solution of Pt (in the form of H_2PtCl_6) through a membrane at a flow rate of 0.0005 mL/cm^2-sec for 4 hours followed by rinsing with water at a flow rate of 0.01 mL/cm^2-sec for 1 hour. Reduction of Pt was carried out by flowing a 0.1 M solution of $NaBH_4$ through the membrane at 0.0005 mL/cm^2-sec for 30 min and again passing water at 0.01 mL/cm^2-sec for 10 min.

4.2.4 Modification of Tubular Ceramic Membranes

Tubular ceramic membranes were modified by several variations of the LbL method as well as by the evaporation/crystallization/reduction and anionic impregnation/reduction techniques. (See below.) During LbL modification, polyelectrolyte and metal nanoparticle solutions were deposited by flowing from the inside of the tubular membrane to the outside as shown in Figure 4.2.

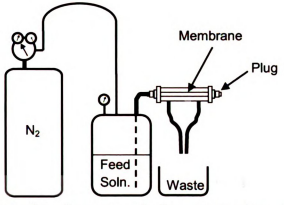

Figure 4.2 Schematic diagram of the apparatus used for depositing polyelectrolyte/metal nanoparticle films in tubular ceramic membranes. The pressurized solution flows though the membrane pores in an inside-out configuration.

4.2.4.1 Method 1 - LbL Adsorption with Ex-Situ Nanoparticle Formation $[PAA/PAH/PtNP]_1$

Modification of tubular membranes with PAA/PAH/PtNP films was similar to modification of disk-shaped membranes except the deposition solutions were diluted more to limit pore blocking that could occur due to smaller pore sizes. The modification procedure included sequential flow through the membrane (as shown in Figure 4.2) of 250 mL of PAA solution (0.002 M PAA, 0.1 M NaCl, pH adjusted to 4.5 with 1M NaOH), 500 mL of water, 250 mL of PAH solution (0.002

M PAH, 0.1 M NaCl, pH adjusted to 5 with 0.1 M HCl), 500 mL of water, and 1000 mL of a citrate-stabilized PtNP solution prepared by diluting 25 mL of the as-prepared nanoparticle solution with 975 mL of water. The flow rate of the solutions through a given membrane was between 20 and 25 mL/min and was maintained by applying a pressure between 0.2 and 0.5 bar. Figure 4.3 shows a general scheme of this procedure. Similarly, tubular membranes were also modified with PAA/PAH/AuNP films. The deposition procedure was the same as that described for Pt nanoparticles except 25 mL of the as-prepared Au nanoparticle solution[45] was used in place of 25 mL of the as-prepared Pt nanoparticle solution.

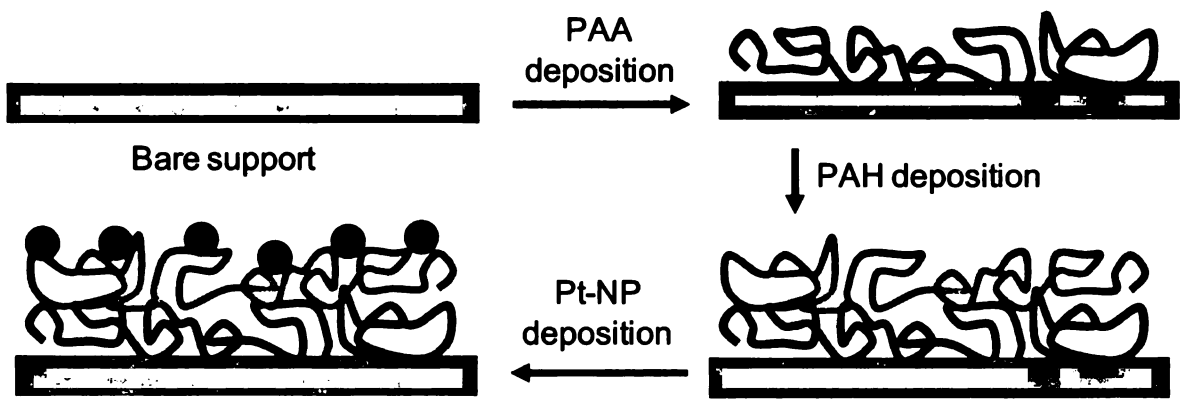

Figure 4.3 Schematic diagram of modification of membrane surfaces (including pores) using LbL deposition of PAA/PAH/PtNP films.

4.2.4.2 Method 2 - LbL with In-Situ Nanoparticle Formation $[PAA/PEI\text{-}Pt(0)]_1$

In a slight modification to previous procedures for modifying alumina powder with polyelectrolyte/PdNP films,[48,49] method 2 incorporated a PEI-Pt(II) complex in the deposition procedure rather than preformed Pt nanoparticles. Briefly modification included sequential flow through the membrane of 250 mL of

PAA solution (0.002 M PAA, 0.1 M NaCl, pH adjusted to 4.5 with 1M NaOH), 500 mL of water, and 250 mL of PEI solution that contained Pt(II) (0.002 M PEI, 0.0004 M K_2PtCl_4, pH adjusted to 9 with 1.0 M HCl), and 500 mL H_2O. To form Pt nanoparticles, 250 mL of 0.1 M $NaBH_4$ solution was passed through the membrane to reduce the Pt ions to PtNPs (Figure 4.4), and the membrane was then rinsed by the passage of 500 mL of water.

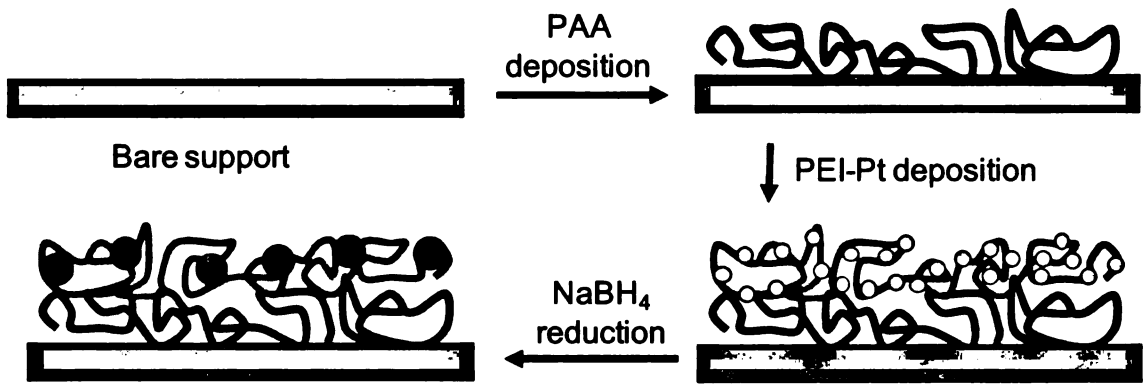

Figure 4.4 Schematic diagram of modification of membrane surfaces (including pores) using LbL deposition of PAA/PEI-Pt(II) films followed by reduction with $NaBH_4$.

4.2.4.3 Method 3 – LbL with In-Situ Nanoparticle Formation $[Pt(0)/PEI]_2$

Similar to a previous method for modifying alumina powder,[50] the membrane was first immersed in a solution of hexachloroplatinic acid (0.1 g Pt/L) for 20 hours. After mounting the membrane in the apparatus displayed in figure 4.2, 500 mL of water was passed through the membrane pores to remove excess Pt solution. PEI was deposited by flowing 250 mL of solution (0.002 M PEI, 0.1 M NaCl, pH adjusted to 9 with 1 M HCl) through the membrane, which was subsequently rinsed by passage of 500 mL of water. A second $PtCl_6^{2-}$/PEI

bilayer was deposited similarly before reducing the Pt with $NaBH_4$ in the same manner as in method 2 (Figure 4.5).

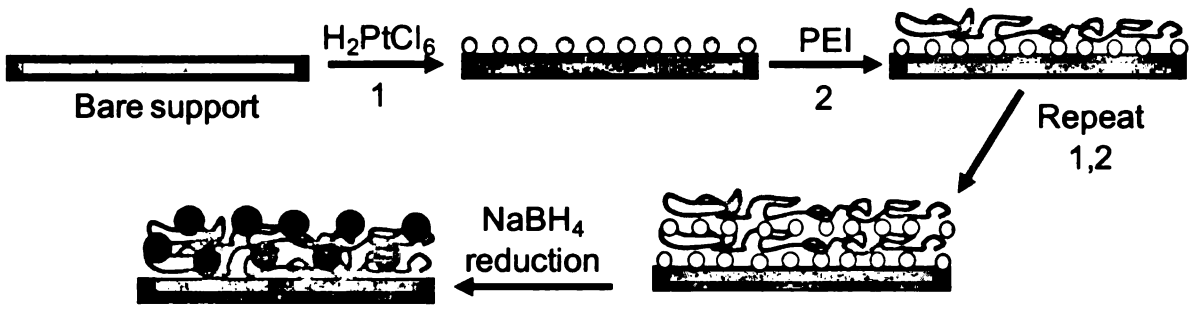

Figure 4.5 Schematic diagram of modification of membrane surfaces (including pores) using LbL deposition of $[Pt(IV)/PEI]_2$ films followed by reduction with $NaBH_4$.

4.2.4.4 Method 4 – Evaporation/Recrystallization/Reduction

The technique of evaporation/recrystallization/reduction was similar to a previously reported procedure in the Watercatox project.[35] Briefly, the membrane was immersed in a 0.1g/L chloroplatinic acid solution for 4 hours, removed from the solution, and allowed to dry at room temperature. Evaporation of the solvent led to concentration of the Pt precursor on the surface of the membrane with more of the Pt located in the inner layer. Reduction of the Pt was performed by placing the membrane under flowing H_2 at 200 °C for 12 hours (Figure 4.6).

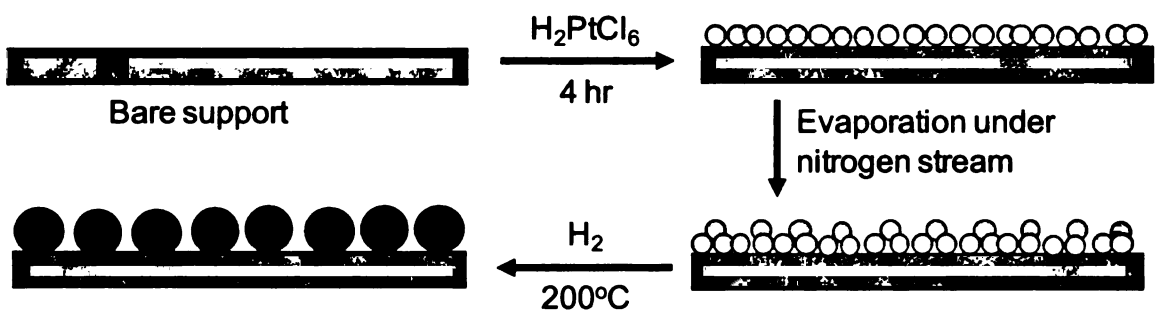

Figure 4.6 Schematic diagram of modification of membrane surfaces (including pores) using evaporation/recrystallization of H_2PtCl_6 followed by reduction with H_2 at 200 °C.

4.2.4.5 Method 5 – Anionic Impregnation/Reduction

The anionic impregnation technique was also performed in a manner similar to previous Watercatox research.[35] In this case, the support was immersed in a 0.1 g/L chloroplatinic acid solution for 4 hours and then rinsed by flowing a 0.1 N nitric acid solution through the membrane pores for 1 hour to remove any unbound Pt species from the membrane. After rinsing with water and then drying under flowing N_2 at 100 °C for 1 hour, the Pt was reduced under flowing H_2 at 200 °C for 12 hours (Figure 4.7).

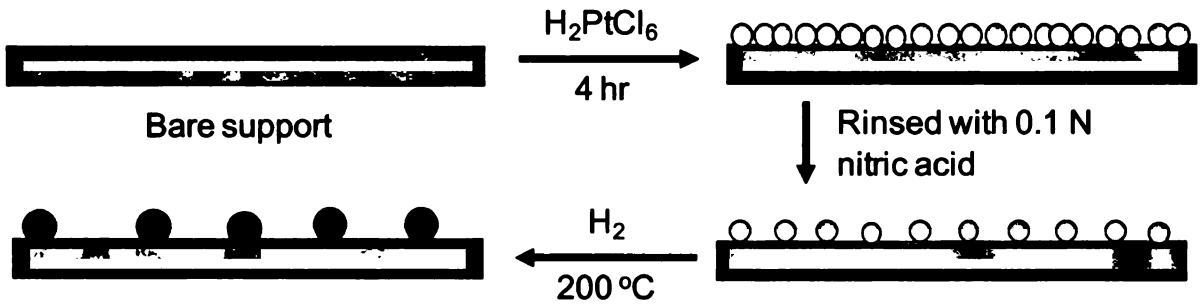

Figure 4.7 Schematic diagram of modification of membrane surfaces (including pores) using anionic impregnation with H_2PtCl_6 followed by reduction with H_2 at 200 °C.

4.2.5 Characterization

Nanoparticles were characterized by transmission electron microscopy (JEM-2200FS microscope) to determine their approximate size and shape. TEM Samples were prepared by diluting the as-prepared PtNP solutions by a factor of 5 with water and placing a 2 µL drop of this mixture on a carbon-coated copper grid. TEM was also used to demonstrate the deposition of nanoparticle-containing films in disk-shaped porous alumina membranes. Prior to imaging,

the membrane was ground into a powder with a mortar and pestle and dispersed in water using a vortex mixer. A 2 μL drop of the resulting solution was then placed onto a carbon-coated copper grid and dried before analysis.

The Pt content of the disk-shaped membranes and alumina powder was determined by completely leaching the metal with aqua regia (3 parts HCl, 1 part HNO_3) and analyzing the leachate by flame atomic absorption spectroscopy (FAAS). For tubular membranes, the amount of deposited Pt was estimated by chemical analysis of the deposition solutions before and after passing them through the membrane. These values were verified by grinding the membranes into powder with a mortar and pestle, dissolving the Pt in aqua regia, and analyzing the solution by FAAS.

4.2.4 Catalytic Reactions

Formic acid, acetic acid, and phenol were employed as substrates for oxidation reactions. Initial experiments were performed with formic acid and powder catalysts to see if the nanoparticle stabilizer or deposition technique affected the nanoparticle activity. In these reactions, oxygen was continuously bubbled into 50 mL of a vigorously stirred solution containing catalyst and 5 g/L of formic acid. Samples of the reaction mixture were collected after several time intervals, filtered to remove the catalyst, and analyzed by ion chromatography (Dionex LC20, Ionpac AS16 column) to determine the amount of formic acid that remained in solution. Similar experiments were also performed with powders prepared by grinding tubular membranes.

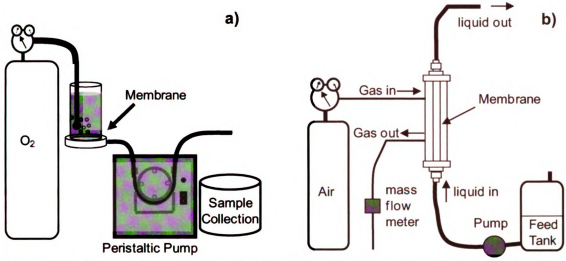

Figure 4.8 Schematic diagram of the wet air oxidation apparatuses that employ a) disk-shaped membranes as flow through contactors and b) tubular catalytic membranes as interfacial contactors.

Flow-through reactions performed with disk-shaped membranes were carried out by bubbling O_2 into a formic acid solution for 2 minutes and then passing that solution during continuous bubbling through a nanoparticle-modified membrane at a given flux (Figure 4.8a). Samples of the membrane permeate were analyzed by IC to determine the extent of formic acid oxidation. For some experiments, the permeate solution was collected, resaturated with O_2, and passed through the nanoparticle-containing membrane multiple times to achieve higher conversion.

For interfacial contactor reactions, the modified tubular membranes were mounted in a gas tight module that allows the flow of liquid through the lumen of the tube and countercurrent gas flow on the shell side of the tube (Figure 4.8b). The liquid flow rate was typically between 7 and 10 mL/min, and the gas overpressure was set to values between 0.2 and 4 bar. The gas flow rate was

maintained at 50 mL/min with a mass flow controller. The system initially operated under N_2 until the desired pressure was reached and remained constant for 10 min. Then the gas was switched from N_2 to air to begin the oxidation reactions, which were carried out at 20, 60, or 80 °C by controlling the temperature of the feed solution. The starting concentrations of formic acid, acetic acid, and phenol were 5 g/L (0.108 M), 3.25 g/L (0.054 M), and 1.7 g/L (0.018 M), respectively, which corresponded to carbon contents of approximately 1.3 g/L in each case. For these reactions, the conversion of each substrate was monitored using total organic carbon (Shimadzu TOC 5050A) and/or HPLC (Varian Prostar with UV-Vis detection) analysis. The uncertainty in the calculated specific activities was < 10% for formic acid oxidation experiments and < 20% for acetic acid and phenol oxidation experiments.

4.3 Results and Discussion

4.3.1 Characterization of Polyelectrolyte/PtNP Films

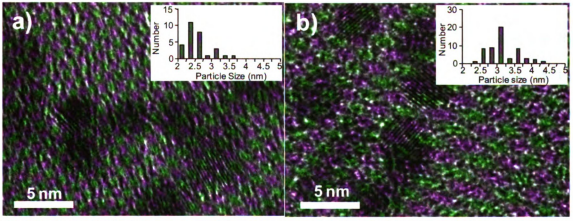

Figure 4.9 TEM images of a) mercaptosuccinic acid-stabilized Pt nanoparticles and b) citrate-stabilized Pt nanoparticles on carbon-coated copper grids. The inset in each image shows the nanoparticle size distribution determined from several high resolution TEM images.

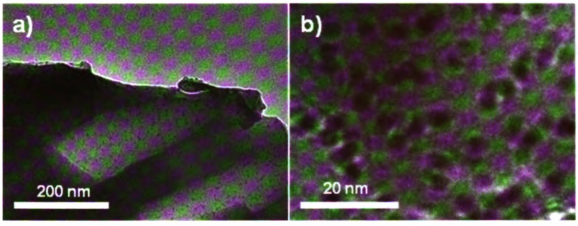

Figure 4.10 Low (a) and high (b) magnification TEM images of Pt nanoparticles immobilized in the pores of an alumina membrane modified with a PAA/PAH/PtNP film. The Pt nanoparticles contained in the film are citrate-stabilized.

TEM images of the nanoparticles and membrane samples were collected to determine the size and shape of the Pt nanoparticles and to see if these particles were effectively deposited in the membranes. Figure 4.9 shows TEM images and size distributions of MSA- and citrate-stabilized Pt nanoparticles. The average particle diameters were 2.6 ± 0.3 and 3.2 ± 0.5 nm, respectively. Figure 4.10 presents TEM images of the citrate-stabilized Pt nanoparticles immobilized in a disk-shaped alumina membrane. These images show that the LbL method yields a high density of nanoparticles within the pores of the membrane and that there is minimal nanoparticle aggregation, which should lead to accessible nanoparticles with a high catalytic surface area.

The amount of Pt in each of the types of tubular membranes was determined by FAAS of precursor Pt solutions before and after passing them through the membrane. These values were later confirmed by dissolving the Pt in aqua regia and analyzing these solutions by FAAS. The two values were in

good agreement for each membrane type except those prepared by method 5 (Table 4.1). The difference in the two values for method 5 is likely due to some Pt being washed away in the nitric acid rinsing step during the membrane modification. This Pt loss was not accounted for in the initial mass balance. The Pt content was 200-1000 mg of Pt per m^2 (1-5 mg of Pt per membrane), based on the area calculated from the inner tube diameter. The relatively similar Pt loading among the different membranes facilitates the comparison of the catalytic activities for the different deposition methods.

Table 4.1 Pt contents in tubular membranes

Modification Method	Pt loading (mg Pt / m^2)[a]	
	Mass Balance[b]	Membrane Powder[c]
1	220 ± 40	220 ± 20
2	220 ± 20	200 ± 20
3	910 ± 90	830 ± 80
4	470 ± 60	480 ± 40
5	690 ± 90	400 ± 40

[a]based on an internal membrane surface area of 0.00506 m^2 calculated from an internal tube diameter of 7 mm and an active length of 230 mm.
[b]determined by chemical analysis of precursor solutions before and after deposition.
[c]determined by chemical analysis of solutions prepared by removing Pt from ground membrane samples with aqua regia.

4.3.2 Wet Air Oxidation Catalyzed by Pt Nanoparticles on Alumina Powder

To examine the effect of the stabilizing agent on the activity of Pt nanoparticles, alumina powder was modified using LbL deposition with either citrate- or MSA-stabilized Pt nanoparticles to prepare heterogeneous catalysts for conventional slurry reactions. Formic acid was chosen as a model compound

for this process because many organic molecules degrade to low molecular weight compounds and eventually to formic acid, which is then oxidized to CO_2 and H_2O in the final step of complete wet air oxidation (scheme 4.1).[51]

$$HCOOH + \tfrac{1}{2} O_2 \xrightarrow{\text{Catalyst}} CO_2 + H_2O$$

Scheme 4.1 Catalytic wet air oxidation of formic acid.

In wet air oxidation of formic acid with these materials, the catalyst modified with citrate-stabilized Pt nanoparticles exhibited an activity of 1.3 ± 0.2 mmol/(s*gPt) whereas the catalyst containing MSA-stabilized Pt nanoparticles had an activity of 0.7 ± 0.1 mmol/(s*gPt). The average nanoparticle size is similar for both types of particles, so differences in surface area should not account for the difference in activity. In fact, MSA-stabilized particles showed slightly smaller diameters (higher surface area per mass) in TEM images. The most likely explanation for the difference between the two types of nanoparticles is that the thiol stabilizers bind more tightly than citrate to the surface of the nanoparticle, and this stronger binding limits the number of active sites for catalysis. Previous studies of catalysis by thiol-stabilized metal nanoparticles also showed low reaction rates.[52,53]

Alumina powder modified by impregnation of $PtCl_6^{2-}$ and subsequent reduction of Pt(IV) to Pt nanoparticles had an activity of 1.0 ± 0.1 mmol/s*gPt, which is again lower than that of the catalyst containing citrate-stabilized nanoparticles. Thus, the LbL deposition with citrate-stabilized nanoparticles provides catalysts with comparable or better activities than traditional methods of

catalyst preparation. Furthermore, these data suggest that the polyelectrolyte multilayer does not inhibit the activity of the Pt nanoparticles. To maximize catalytic activity, the following studies with tubular membranes modified by method 1 utilized citrate-stabilized PtNPs rather than MSA-stabilized PtNPs.

4.3.3 Oxidation of Formic Acid with Disk-shaped Membranes

In initial studies of membrane-based oxidation, solutions sparged with O_2 were passed through an alumina membrane coated with a PAA/PAH/PtNP film. At initial formic acid concentrations < 2 mM, nearly all of the formic acid was oxidized to CO_2 and water during passage through the membrane because at these concentrations, formic acid was the limiting reactant. However, at formic acid concentrations > 10 mM the amount of oxidation was essentially constant because O_2 was the limiting reagent. The solubility of O_2 in water at 1 atm of O_2

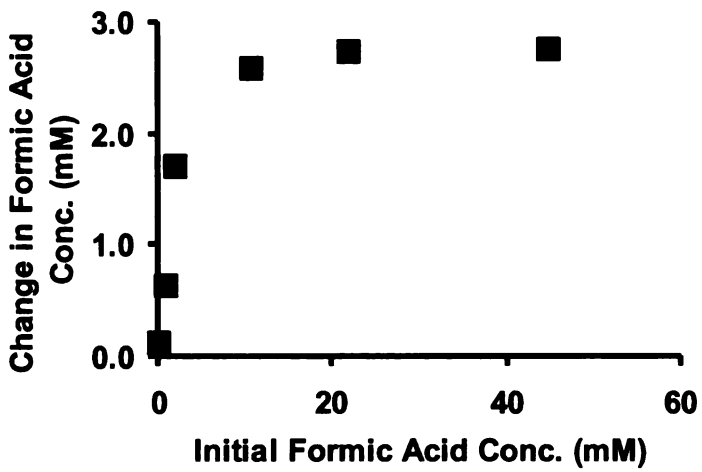

Figure 4.11 Change in formic acid concentration in membrane-catalyzed oxidation with several initial formic acid concentrations. Solutions were sparged with O_2, and the flux through the porous alumina membrane modified with citrate-stabilized Pt nanoparticles (method 1) was 0.023 mL/cm^2-sec.

is roughly 1.25 mM,[54] which would correspond to a concentration of 2.5 mM formic acid that could be oxidized. This is similar to the maximum change in formic acid concentration shown in Figure 4.11.

Alumina membranes modified with Pt, Au, Pd, and Ru nanoparticles were all tested for the oxidation of formic acid using the flow-through mode with multiple passes through the membrane. In all experiments, the initial formic acid concentration was 21.7 mM (1000 mg/L). Solutions were saturated with oxygen by bubbling O_2 into the solution for 2 min and then passing the solution through the membrane at a flow rate of 0.023 mL/cm^2-sec. The plot in Figure 4.12 shows the change in formic acid concentration through 6 passes for each of the nanoparticle-modified membranes.

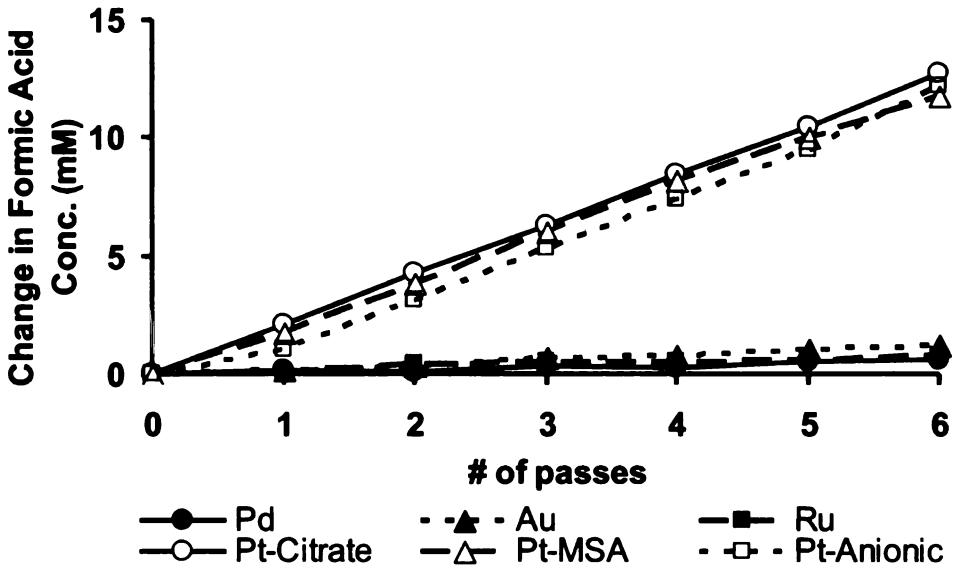

Figure 4.12 Cumulative change in formic acid concentration in membrane-catalyzed oxidation after multiple passes through alumina membranes modified with either Pt, Au, Pd, or Ru nanoparticles. Solutions were sparged with O_2, and the flux through the metal nanoparticle-containing membranes was 0.023 mL/cm^2-sec.

The membranes containing Pt nanoparticles all exhibited changes in formic acid concentration of 2 to 2.5 mM with each pass through the membrane, which is again consistent with the expected solubility of O_2 in aqueous solutions. This suggests that essentially all of the O_2 was consumed when passing the solution through the Pt-containing membranes. Membranes containing metals other than Pt did not effectively oxidize formic acid. In fact, the average change in formic acid concentration for each pass was 0.20, 0.11, and 0.13 mM for Au, Pd, and Ru nanoparticle-modified membranes respectively. The low activity of these other metals suggests that Pt catalysts are ideal for wet air oxidation reactions. In these experiments, membranes containing MSA-stabilized Pt nanoparticles performed as well as those containing citrate-stabilized Pt nanoparticles. The membranes modified by anionic impregnation with Pt also had similar formic acid conversion. This shows that even though the three types of Pt nanoparticles have different activities in slurry reactions, the difference in activities is not observed in membrane reactions using the conditions described above because the reaction is limited by the solubility of O_2. In order to see differences in the activity of the three Pt-containing membranes, the oxidation reactions should be performed at higher flow rates.

Nevertheless, for oxygen-sparged solutions containing 10.8 mM formic acid, increasing the flux through the citrate-stabilized Pt nanoparticle-modified membrane from 0.023 to 0.12 mL/cm^2sec did not significantly affect the reduction in formic acid concentration that occurred upon passing the solution through the membrane (Figure 4.13). This suggests that the reaction is still limited by the

amount of O_2 in the solution at high flow rates. If the reaction were kinetically limited, we would expect less reduction of the formic acid concentration at higher flow rates due to lower residence times in the membrane. In most fast gas/liquid reactions with flow-through contactors, the solubility of the gas in solution will limit the reaction rate unless high gas pressures are employed. For this reason, tubular interfacial gas/liquid contactors are often more attractive than flow-through contactors for membrane-catalyzed gas/liquid reactions such as wet air oxidation.

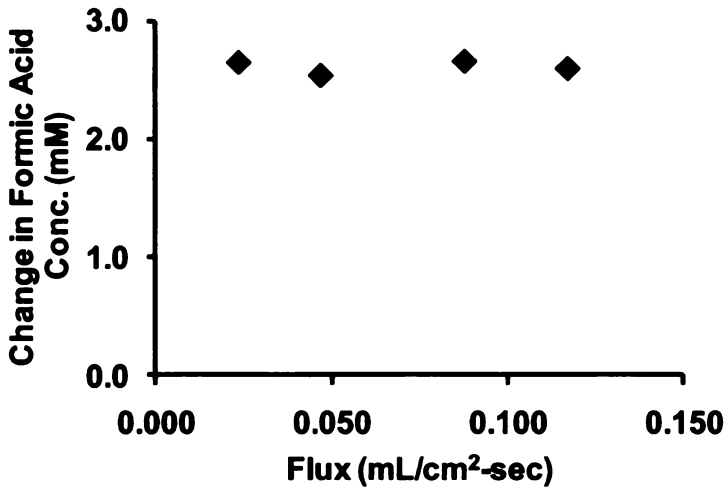

Figure 4.13 Change in formic acid concentration during membrane-catalyzed oxidation as a function of flux through a Pt nanoparticle-modified disk-shaped alumina membrane prepared by method 1. The initial formic acid concentration was 10.8 mM, and solutions were sparged with O_2 before passing through the membrane.

4.3.4 Wet Air Oxidation with Tubular Membranes

This section compares the catalytic activities of five types of tubular interfacial contactor membranes (Figures 4.3 - 4.7) in sequential studies of the oxidation of formic acid, acetic acid, and phenol. Experiments were performed

on at least two membranes modified by each method. Because catalyst deactivation often occurs during phenol oxidation,[55-57] membranes were again tested in the oxidation of formic acid after experiments with phenol to see if catalyst deactivation occurred.

4.3.4.1 Wet Air Oxidation of Formic Acid

Initially, formic acid oxidation was examined at 0.2, 1, 2, 3, 4, and 4.3 bar of air overpressure to determine the effect of overpressure on reaction rates. High air overpressures increase the solubility of O_2 in the solution, but more importantly, they shift the location of the gas/liquid interface so that it is closer to the inner layer where there should be a larger amount of catalyst. The highest activity in formic acid oxidation occurs at 4 or 4.3 bar of overpressure because the gas/liquid interface is closest to the inner layer of the tube where most of the catalyst is located. However, in some cases much of the air begins to come through the defects in the membrane at an overpressure of 4.3 bar. As a result, the catalytic activity sometimes starts to decrease at 4.3 bar because the gas/liquid interface is no longer well-maintained in the catalytic layer of the membrane. This is consistent with previous results.[28] Figure 4.14 shows the increase in activity as the air overpressure increases. Furthermore, when N_2 is used as the gas instead of air for oxidation reactions, no reaction occurs, which shows that the change in formic acid concentration due to adsorption to the polyelectrolyte/PtNP film is negligible.

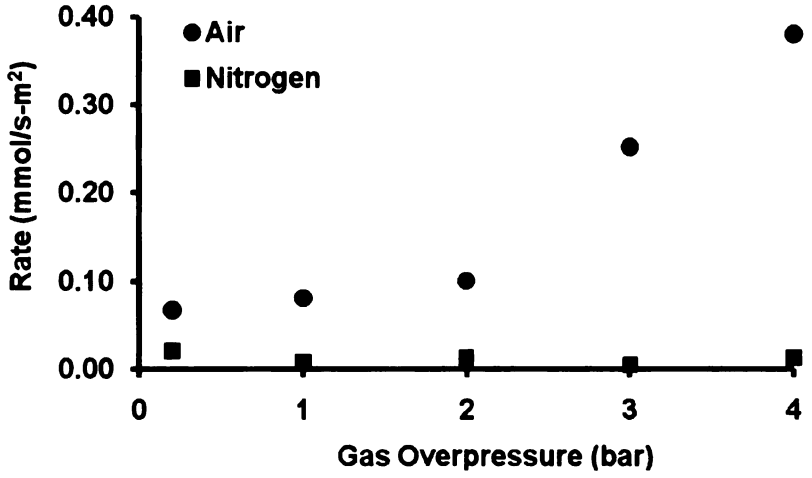

Figure 4.14 Normalized rate of formic acid oxidation vs. air or N_2 overpressure for a tubular membrane modified with a PAA/PAH/PtNP film. Normalization was performed with respect to the area of the internal wall of the membrane.

The activities of membranes prepared by all 5 methods of modification were compared with respect to membrane area and Pt loading. Each membrane exhibits the expected trend of increasing activity with increasing air overpressures. Membranes prepared by methods 1 and 2 exhibit similar activities (normalized to membrane area) for formic acid oxidation and similar specific activities (normalized to Pt content) as well (Figure 4.15). Membranes prepared by method 3 show a similarly high reaction rate (Figure 4.15a), but because the Pt content of these membranes is higher than that of all other membranes (Table 4.1), their specific activity at overpressures >3 bar is lower than for membranes prepared by methods 1 and 2 (Figure 4.15b). This is not surprising because in method 3, the initial Pt deposition occurs throughout the membrane, not just in the surface layer. Only the Pt that is near the gas/liquid interface is efficiently used for formic acid oxidation. In Figure 4.15a, the

relatively high activities at low overpressures for the membranes prepared by method 3 likely occur because at low overpressures the gas/liquid interface is deeper in the membrane, and these membranes still have significant amounts of Pt in these locations.

Membranes prepared by method 4 show a high rate of formic acid oxidation (Figure 4.15a) but a lower activity per gram of Pt (Figure 4.15b) than methods 1 and 2. This suggests that method 4 deposits the platinum deeper into

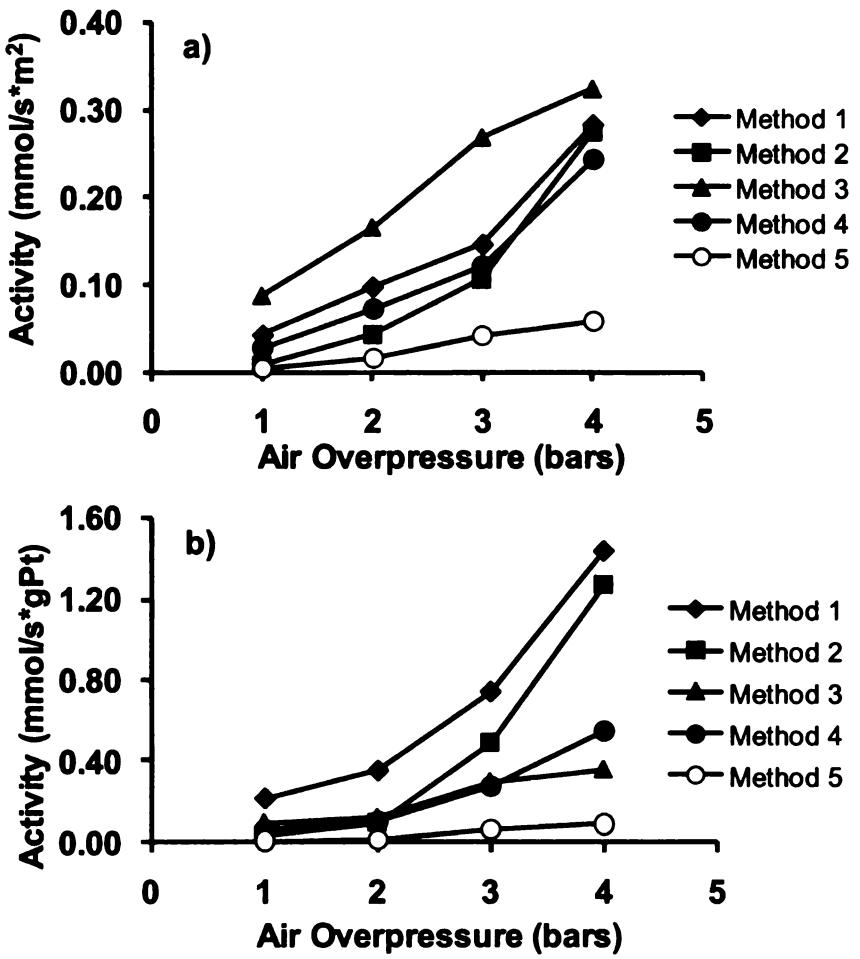

Figure 4.15 Normalized rate of formic acid oxidation vs. air overpressure for Pt-containing membranes prepared by the methods shown in Figures 4.3-4.7. Normalization was performed with respect to a) the area of the internal wall of the membrane and b) the amount of Pt in the membrane.

the membrane than methods 1 and 2, and therefore the specific activity with method 4 membranes is low at the higher air overpressures because all of the platinum is not being used effectively. On the other hand, the membranes prepared by method 5 exhibit a much lower activity than those prepared by the other four methods. This is expected because Pt does not bind well to the surface of ZrO_2 and is easily removed during the nitric acid rinsing step. Therefore, the Pt is mostly bound to regions that were not washed well with nitric acid. Since these regions are most likely located away from the gas/liquid interface, the method 5 membranes should have relatively low activity.

When comparing the LbL-modified membranes (methods 1-3) with membranes described in the literature,[26] the rate per membrane area is only $^1/_3$ to $^1/_2$ as high as published values. On the other hand, the rate is 5 times higher than published values when normalizing to Pt content. The rate is also ~50% higher than previous values obtained with "low-loading" membranes, which had Pt contents similar to the membranes prepared in this study.[26] The specific activities of membranes prepared by method 4 are similar to past results with "low-loading" membranes. Additional formic acid oxidation experiments were also performed with tubular membranes containing a PAA/PAH/AuNP film. At room temperature no formic acid oxidation was observed. However, Au is typically an inactive oxidation catalyst at low temperatures. When performing formic acid oxidation at higher temperatures, (feed temperature = 80 °C) some oxidation occurs with the Au nanoparticles, but the activity at 4 bar air (0.07

mmol/s*m^2) overpressure is still significantly lower than with the Pt-containing membranes.

4.3.4.2 Wet Air Oxidation of Acetic Acid

Acetic acid is a much more refractory compound to oxidize (scheme 2) than formic acid and is often an intermediate produced in the oxidation of oxygenated compounds like phenol or other carboxylic acids.[14,58,59] Supported Ru or Pt catalysts are often used at high temperatures to oxidize acetic acid and other short chain carboxylic acids completely to CO_2 and H_2O.[60-62] However, carbonate species are commonly formed on the catalyst surface, which results in catalyst poisoning and reduced performance.[63,64]

Though the exact mechanism of acetic acid oxidation is not known, it is generally believed that short chain carboxylic acids undergo oxidation through a free radical mechanism.[65-68] In general, for compounds containing 3 or more carbon atoms, hydrogen abstraction occurs at a C-H bond to form a free radical R•, which then reacts with oxygen to form an alkylperoxyl radical (ROO•). This unstable radical then undergoes decarboxylation or other decomposition reactions to form shorter chain intermediates. Propagation of the free radicals continues rapidly until acetic acid is formed. Duprez et al. proposed that in the presence of a catalyst, acetic acid is oxidized through formation of an acetate radical followed by decarboxylation and formation of a methyl radical that forms a peroxyl radical and is broken down into CO_2 and water.[66] Scheme 4.2 shows the proposed pathway for this series of reactions.

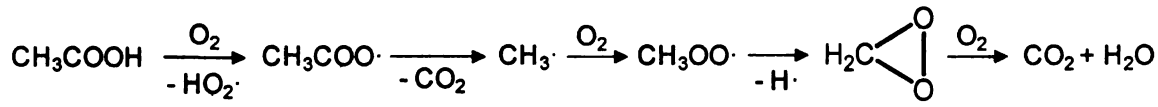

Scheme 4.2 Proposed mechanism for catalytic wet air oxidation of acetic acid. Adapted from Duprez et al.[66]

In this work, we performed oxidation of acetic acid under conditions similar to those used in formic acid oxidation. Analogous to results with formic acid, the rate of acetic acid oxidation at room temperature is highest at 4 or 4.3 bar (Figure 4.16). The oxidation rate is determined by TOC analysis and thus tells how much of the acetic acid is completely oxidized to CO_2 and H_2O. It does not account for any partial conversion to other intermediate species that may also form.

Figure 4.16a shows that membranes prepared by methods 1 and 2 have a much higher activity for room temperature acetic acid oxidation than membranes prepared by the other 3 methods. The membranes prepared by method 3 show a small specific activity, but membranes prepared by methods 4 and 5 exhibit essentially no activity for acetic acid oxidation at room temperature. At 60 °C, membranes prepared by methods 1-4 exhibit higher activity than at room temperature, as expected. In the case of membranes prepared by methods 1 and 2, on increasing the temperature from 23 °C to 60 °C the activity increases by about 60 percent and 90 percent, respectively. In contrast, the activities of membranes prepared by methods 3 and 4 increase by factors of 9 and 10, respectively. Even with this large increase in activity, the membranes prepared by methods 3 and 4 still have a 3-fold lower activity at 60 °C and 4 bars air than

the membranes prepared by the first two methods. The membranes prepared by method 5 show low activities even at the higher temperature.

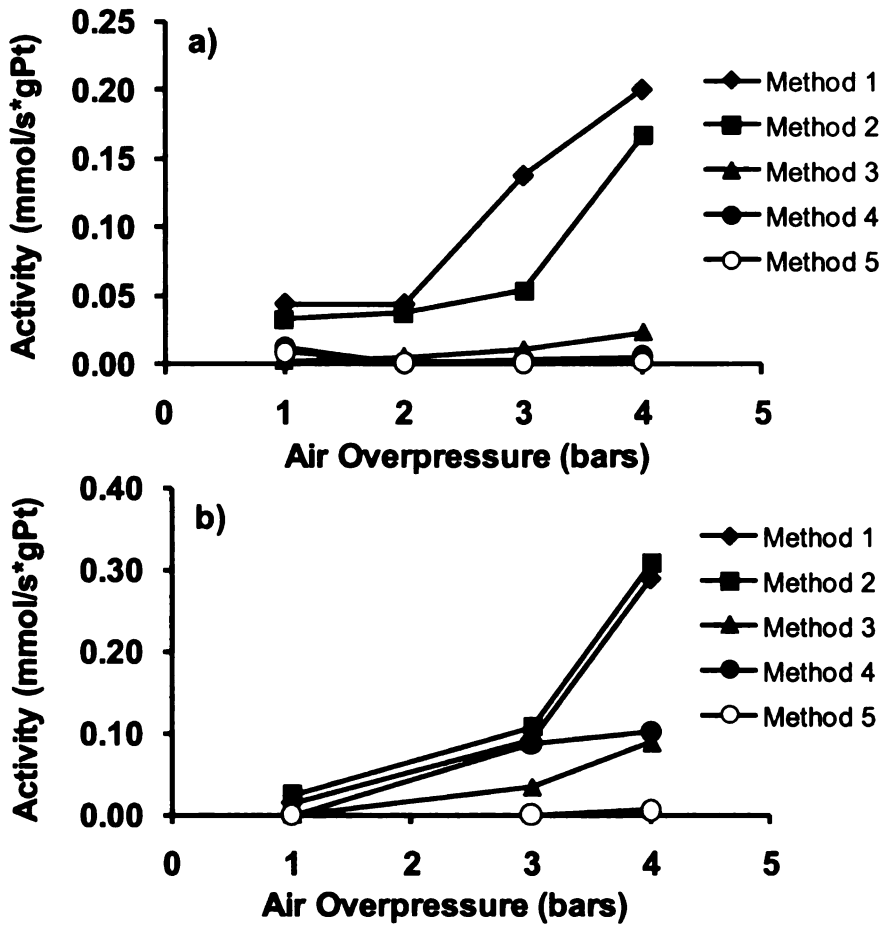

Figure 4.16. Normalized rates of membrane-catalyzed acetic acid oxidation vs. air overpressure for different membrane types at a) room temperature and b) 60 °C. Oxidation rates were normalized to the amount of Pt in the membrane.

4.3.4.3 Wet Air Oxidation of Phenol

Like acetic acid, phenol can be very difficult to oxidize, but it is a common compound for testing catalyst stability in wet air oxidation of organic pollutants.[14,57,69-71] We expect phenol oxidation to occur via a free radical mechanism in which phenoxy and phenoxyperoxyl radicals are formed and undergo further reactions to form smaller intermediates.[72] Though the

mechanism of wet air oxidation of phenol is not necessarily the same for all catalysts, previous studies showed similar intermediate and product formation during oxidation with several catalysts.[66,73,74] In general, phenol first undergoes oxidation to form intermediate ring compounds such as catechol and hydroquinone. These ring compounds then undergo ring opening reactions to form 6-carbon dicarboxylic acids, which are oxidized further to form short chain carboxylic acids and eventually CO_2. Scheme 4.3 shows a proposed oxidation pathway.

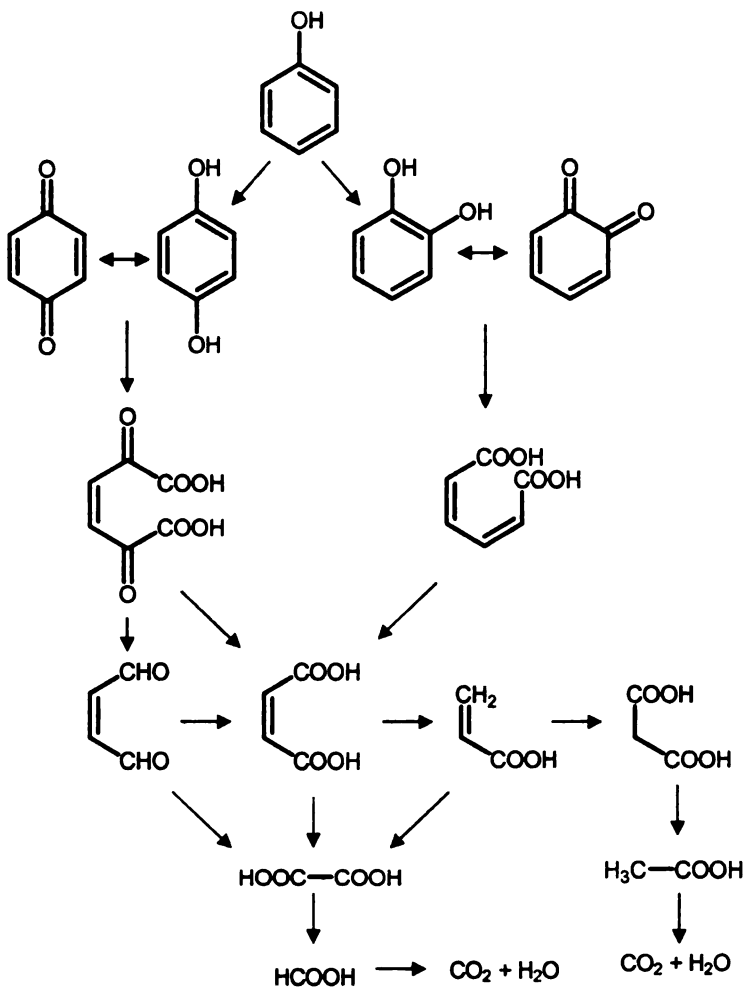

Scheme 4.3 Proposed pathway for wet air oxidation of phenol, adapted from Devlin et al.[74]

In phenol oxidation experiments, samples were collected at 1, 3, and 4 bar overpressure and subsequently analyzed by both TOC and HPLC. In TOC analysis, activities are determined from the difference in organic carbon content between the inlet and outlet solutions. In HPLC analysis, activities are determined from the decrease in phenol concentration. Similar to previous experiments involving oxidation of formic acid and acetic acid, the highest activity occurs at air overpressures of 4 bar.

Tables 4.2 and 4.3 show that, again, the highest activity occurs with membranes prepared by methods 1 and 2, and that membranes prepared by method 5 show little or no activity for the oxidation of phenol. Membranes prepared by methods 3 and 4 exhibit more than 4-fold lower specific activities than membranes prepared by the first two methods, even at higher temperature. Oxidation experiments performed at 60 °C result in higher activities (two times higher or more) than experiments performed at room temperature. We would expect to achieve even higher activities with temperatures in excess of 150 °C,[14,55] but these high temperatures are not compatible with the experimental apparatus (Figure 4.8) used in this study. Furthermore, these high temperatures may also lead to film deformation and possible sintering of the catalyst. Future studies need to explore the stability of polyelectrolyte/metal nanoparticle films at temperatures at or above 150 °C.

Table 4.2 Catalytic activities of several tubular membranes in phenol oxidation at room temperature with 4 bar air overpressure.

Preparation method	Activity	
	[a]mmol/(s*gPt)	[b]mmol/(s*gPt)
1	0.064	0.13
2	0.050	0.11
3	0.006	0.015
4	0.000	0.000
5	0.003	0.012

[a]Determined by TOC analysis, [b]Determined from HPLC analysis

Table 4.3 Catalytic activities of several tubular membranes in phenol oxidation with a feed temperature of 60 °C with 4 bar air overpressure.

Preparation method	Activity	
	[a]mmol/(s*gPt)	[b]mmol/(s*gPt)
1	0.15	0.21
2	0.11	0.21
3	0.026	0.035
4	0.027	0.025
5	0.003	0.000

[a]Determined by TOC analysis, [b]Determined from HPLC analysis

The activity values determined from HPLC are generally higher than those determined from TOC (Tables 4.2 and 4.3) because TOC analysis only shows how much of the sample is transformed to CO_2 or insoluble species, whereas HPLC shows how much phenol is oxidized to any product. The higher activities seen with HPLC suggest that some phenol is oxidized to smaller organic compounds, and not completely to CO_2. Because the conversion in phenol oxidation is low (< 10%), the quantities of these other compounds in the analyzed samples are below detectable levels in HPLC. As a result, the identity and amount of each byproduct in the reaction were not determined. The activities determined by TOC analysis and HPLC are generally in better agreement at 60

°C than at room temperature, suggesting that more of the phenol is converted to CO_2 and H_2O at higher temperatures.

After phenol oxidation, the various membranes were again used to catalyze formic acid oxidation at room temperature to determine if the oxidation of refractory compounds like phenol causes catalyst deactivation. While a decrease in activity for formic acid oxidation could be due to poisoning or other effects such as nanoparticle leaching or aggregation, a constant activity may suggest that the extent of catalyst deactivation is minimal. However, if formic acid oxidation is simply limited by O_2 solubility, then catalyst deactivation would not be observed by this method. In nearly every case, there was no decrease in formic acid oxidation rates after using the membranes for phenol oxidation. However, one of the membranes prepared by method 4 showed a 40% activity decrease in formic acid oxidation after the membrane was used for phenol oxidation. The decreased activity may have been due to leaching of Pt for that specific membrane or to poisoning of the catalyst during phenol oxidation. With that exception, each membrane maintained a constant activity for formic acid oxidation.

4.3.5 Conventional Reactions with Pulverized Tubular Membranes

To show that the interfacial contactor configuration is advantageous for wet air oxidation reactions, each type of membrane was also ground into a powder that was used as a heterogeneous catalyst in a conventional stirred tank reaction. In these reactions, a solution containing 0.108 M formic acid was

continuously bubbled with oxygen while stirring rapidly. Pure oxygen was used as the oxidant instead of air to provide as much oxygen to the reaction as possible. The results in Table 4.4 show that all five types of membranes in the powder form have similar activities when normalized to the amount of Pt in the catalyst. However, the activities of different membranes operated as interfacial contactors vary significantly with the method of modification. In the case of methods 1 and 2, membranes operated as interfacial contactors at 4 bar overpressure show activities that are ~2.5 times higher than those of membrane powders used as heterogeneous catalysts. Conversely, membranes prepared by methods 3 and 4 exhibit little difference in activity between interfacial contactors and powder catalysts, and the membrane prepared by method 5 shows higher activity in the conventional reaction. These results demonstrate that the interfacial contactor configuration can be quite valuable for gas/liquid reactions, but to take full advantage of this configuration, the catalyst must be localized in the inner layer of the membrane.

Table 4.4 Catalytic activities in formic acid oxidation for tubular membranes used as interfacial contactors and as powders in conventional stirred tank reactors.

Modification Method	Activity (mmol/s*gPt)	
	Interfacial Contactor[a]	Conventional Reactor[b]
1	1.5 ± 0.3	0.6 ± 0.05
2	1.3 ± 0.2	0.5 ± 0.03
3	0.5 ± 0.1	0.7 ± 0.1
4	0.7 ± 0.2	0.5 ± 0.03
5	0.1 ± 0.03	0.5 ± 0.1

[a]activity at air overpressure = 4 bar, [b]Pure O_2 was sparged into the reaction mixture.

4.4 Conclusions

The overall objective of this study was to compare the catalytic activity of membranes prepared using layer-by-layer deposition methods with the activity of membranes prepared by the traditional methods of evaporation/recrystallization/ reduction and anionic impregnation/reduction. Although the rate of formic acid oxidation with LbL-modified membranes was 50% lower than previous results when normalized to membrane surface area, the rate when normalized to Pt content was 5 times greater than previous results. In this study, the Pt content for all membranes was less than 5 mg of Pt per membrane.

Membranes prepared by LbL methods 1 and 2 exhibited the highest activity when normalized to the Pt content inside the membranes, most likely because of strong localization of the Pt in the inner layer of the membrane. Conversely, the other three methods deposit Pt on the entire surface of the membrane, which means that any Pt that gets deposited on the support layer or intermediate layer is most likely not being utilized when performing oxidation at higher air overpressures.

The biggest limitation to the methods involving LbL deposition is the low loading of Pt. Since the support is quite expensive, the cost of Pt is not as much of a concern as in other systems; however, Pt cost cannot be disregarded. In the future, low loading with the LbL method can be overcome by optimizing the LbL deposition procedure or by depositing multiple layers. Further studies should also include examination of catalytic activity in continuous experiments over longer periods of time to learn more about the catalyst stability. Experiments in

this study were typically performed only for a few hours. Layer-by-layer modification is quite versatile and could also be applied to polymeric hollow fiber supports, which are much less expensive than the traditional ceramic supports. This should result in a more cost-effective system for wet air oxidation of wastewater as long as the polymer membrane is sufficiently stable.

4.5 References

(1) Luck, F. *Catal. Today* **1999**, *53*, 81-91.

(2) Mishra, V. S.; Mahajani, V. V.; Joshi, J. B. *Ind. Eng. Chem. Res.* **1995**, *34*, 2-48.

(3) Zimmerman, F. J. *Chem. Eng.* **1958**, *65*, 117-20.

(4) Guibelin, E. *Water Sci. Technol.* **2004**, *49*, 209-216.

(5) Kim, B. J.; Qi, S.; Shanley, R. S. *Water Environ. Res* **1994**, *66*, 440-55.

(6) Adriaens, P.; Vogel, T. M. In *Microbial Transformation and Degradation of Toxic Organic Chemicals*; Young, L. Y., Cerniglia, C. E., Eds.; Wiley: New York, 1995, p 435-486.

(7) Fewson, C. A. *Trends Biotechnol.* **1988**, *6*, 148-53.

(8) Matatov-Meytal, Y. I.; Sheintuch, M. *Ind. Eng. Chem. Res.* **1998**, *37*, 309-326.

(9) Jeworski, M.; Heinzle, E. *Biotechnology annual review* **2000**, *6*, 163-96. .

(10) Debellefontaine, H.; Foussard, J. N. *Waste Manage.* **2000**, *20*, 15-25.

(11) Luck, F. *Catal. Today* **1996**, *27*, 195-202.

(12) Levec, J.; Pintar, A. *Catal. Today* **2007**, *124*, 172-184.

(13) Pham Minh, D.; Gallezot, P.; Azabou, S.; Sayadi, S.; Besson, M. *Appl. Catal., B* **2008**, *84*, 749-757.

(14) Pintar, A.; Batista, J.; Tisler, T. *Appl. Catal., B* **2008**, *84*, 30-41.

(15) Julbe, A.; Farrusseng, D.; Guizard, C. *J. Membr. Sci.* **2001**, *181*, 3-20.

(16) Dalmon, J.-A.; Cruz-Lopez, A.; Farrusseng, D.; Guilhaume, N.; Iojoiu, E.; Jalibert, J.-C.; Miachon, S.; Mirodatos, C.; Pantazidis, A.; Rebeilleau-Dassonneville, M.; Schuurman, Y.; Van Veen, A. C. *Appl. Catal., A* **2007**, *325*, 198-204.

(17) Dittmeyer, R.; Svajda, K.; Reif, M. *Top. Catal.* **2004**, *29*, 3-27.

(18) Bengtson, G.; Fritsch, D. *Desalination* **2006**, *200*, 666-667.

(19) Lange, C.; Storck, S.; Tesche, B.; Maier, W. F. *J. Catal.* **1998**, *175*, 280-293.

(20) Purnama, H.; Kurr, P.; Schmidt, A.; Schomäcker, R.; Voigt, I.; Wolf, A.; Warsitz, R. *AIChE J.* **2006**, *52*, 2805-2811.

(21) Schmidt, A.; Haidar, R.; Schomäcker, R. *Catal. Today* **2005**, *104*, 305-312.

(22) Schmidt, A.; Schomäcker, R. *J. Mol. Catal. A: Chem.* **2007**, *271*, 192-199.

(23) Reif, M.; Dittmeyer, R. *Catal. Today* **2003**, *82*, 3-14.

(24) Pera-Titus, M.; Miachon, S.; Dalmon, J.-A. *AIChE J.* **2009**, *55*, 434-441.

(25) Iojoiu, E. E.; Landrivon, E.; Raeder, H.; Torp, E. G.; Miachon, S.; Dalmon, J.-A. *Catal. Today* **2006**, *118*, 246-252.

(26) Iojoiu, E. E.; Miachon, S.; Dalmon, J.-A. *Top. Catal.* **2005**, *33*, 135-139.

(27) Iojoiu, E. E.; Miachon, S.; Landrivon, E.; Walmsley, J. C.; Raeder, H.; Dalmon, J.-A. *Appl. Catal., B* **2007**, *69*, 196-206.

(28) Iojoiu, E. E.; Walmsley, J. C.; Raeder, H.; Miachon, S.; Dalmon, J.-A. *Catal. Today* **2005**, *104*, 329-335.

(29) Miachon, S.; Perez, V.; Crehan, G.; Torp, E.; Raeder, H.; Bredesen, R.; Dalmon, J. A. *Catal. Today* **2003**, *82*, 75-81.

(30) Raeder, H.; Bredesen, R.; Crehan, G.; Miachon, S.; Dalmon, J.-A.; Pintar, A.; Levec, J.; Torp, E. G. *Sep. Purif. Technol.* **2003**, *32*, 349-355.

(31) Vospernik, M.; Pintar, A.; Levec, J. *Chem. Eng. Process.* **2006**, *45*, 404-414.

(32) Bercic, G.; Pintar, A.; Levec, J. *Catal. Today* **2005**, *105*, 589-597.

(33) Vospernik, M.; Pintar, A.; Bercic, G.; Levec, J.; Walmsley, J.; Ræder, H.; Eduard Emil, I.; Sylvain, M.; Jean-Alain, D. *Chem. Eng. Sci.* **2004**, *59*, 5363-5372.

(34) Perez, V.; Miachon, S.; Dalmon, J.-A.; Bredesen, R.; Pettersen, G.; Raeder, H.; Simon, C. *Sep. Purif. Technol.* **2001**, *25*, 33-38.

(35) Uzio, D.; Miachon, S.; Dalmon, J.-A. *Catal. Today* **2003**, *82*, 67-74.

(36) Braunstein, P.; Kormann, H.-P.; Meyer-Zaika, W.; Pugin, R.; Schmid, G. *Chem. Eur. J.* **2000**, *6*, 4637-4646.

(37) Daub, K.; Wunder, V. K.; Dittmeyer, R. *Catal. Today* **2001**, *67*, 257-272.

(38) Perego, C.; Villa, P. *Catal. Today* **1997**, *34*, 281-305.

(39) Centi, G.; Dittmeyer, R.; Perathoner, S.; Reif, M. *Catal. Today* **2003**, *79-80*, 139-149.

(40) Gröschel, L.; Haidar, R.; Beyer, A.; Coelfen, H.; Frank, B.; Schomäcker, R. *Ind. Eng. Chem. Res.* **2005**, *44*, 9064-9070.

(41) Xu, J.; Dozier, A.; Bhattacharyya, D. *J. Nanopart. Res.* **2005**, *7*, 449-467.

(42) Decher, G.; Schlenoff, J. B. *Multilayer Thin Films: Sequential Assembly of Nanocomposite Materials*; Wiley-VCH: Weinheim, Germany, 2003.

(43) Chen, S.; Kimura, K. *J. Phys. Chem. B* **2001**, *105*, 5397-5403.

(44) Brugger, P. A.; Cuendet, P.; Graetzel, M. *J. Am. Chem. Soc.* **1981**, *103*, 2923-7.

(45) Brown, K. R.; Walter, D. G.; Natan, M. J. *Chem. Mater.* **2000**, *12*, 306-313.

(46) Dokoutchaev, A.; James, J. T.; Koene, S. C.; Pathak, S.; Prakash, G. K. S.; Thompson, M. E. *Chem. Mater.* **1999**, *11*, 2389-2399.

(47) Yang, J.; Lee, J. Y.; Deivaraj, T. C.; Too, H.-P. *J. Colloid Interface Sci.* **2004**, *271*, 308-312.

(48) Bhattacharjee, S.; Bruening, M. L. *Langmuir* **2008**, *24*, 2916-2920.

(49) Kidambi, S.; Dai, J.; Li, J.; Bruening, M. L. *J. Am. Chem. Soc.* **2004**, *126*, 2658-2659.

(50) Kidambi, S.; Bruening, M. L. *Chem. Mater.* **2005**, *17*, 301-307.

(51) Harmsen, J. M. A.; Jelemensky, L.; Van Andel-Scheffer, P. J. M.; Kuster, B. F. M.; Marin, G. B. *Appl. Catal., A* **1997**, *165*, 499-509.

(52) Alvarez, J.; Liu, J.; Roman, E.; Kaifer, A. E. *Chem. Commun.* **2000**, 1151-1152.

(53) Eklund, S. E.; Cliffel, D. E. *Langmuir* **2004**, *20*, 6012-6018.

(54) Wilde, F. D. *Field Measurements: U.S. Geological Survey Techniques of Water-Resources Investigations* book 9, chap. A6, http://pubs.water.usgs.gov/twri9A/ Accessed February 6, 2009.

(55) Nousir, S.; Keav, S.; Jr., J. B.; Bensitel, M.; Brahmi, R.; Duprez, D. *Appl. Catal., B* **2008**, *84*, 723-731.

(56) Taboada, C. D.; Batista, J.; Pintar, A.; Levec, J. *Appl. Catal., B* **2009**, *89*, 375-382.

(57) Liotta, L. F.; Gruttadauria, M.; Di Carlo, G.; Perrini, G.; Librando, V. *J. Hazard. Mater.* **2009**, *162*, 588-606.

(58) Levec, J.; Pintar, A. *Catal. Today* **1995**, *24*, 51-58.

(59) Oliviero, L.; Barbier, J.; Duprez, D.; Wahyu, H.; Ponton, J. W.; Metcalfe, I. S.; Mantzavinos, D. *Appl. Catal., B* **2001**, *35*, 1-12.

(60) Dükkanci, M.; Gündüz, G. *Catal. Commun.* **2009**, *10*, 913-919.

(61) Wang, J.; Zhu, W.; He, X.; Yang, S. *Catal. Commun.* **2008**, *9*, 2163-2167.

(62) Mikulová, J.; Rossignol, S.; Barbier Jr, J.; Mesnard, D.; Kappenstein, C.; Duprez, D. *Appl. Catal., B* **2007**, *72*, 1-10.

(63) Mikulová, J.; Barbier Jr, J.; Rossignol, S.; Mesnard, D.; Duprez, D.; Kappenstein, C. *J. Catal.* **2007**, *251*, 172-181.

(64) Mikulová, J.; Rossignol, S.; Barbier Jr, J.; Duprez, D.; Kappenstein, C. *Catal. Today* **2007**, *124*, 185-190.

(65) Barbier, J. J.; Delanoë, F.; Jabouille, F.; Duprez, D.; Blanchard, G.; Isnard, P. *J. Catal.* **1998**, *177*, 378-385.

(66) Duprez, D.; Delanoë, F.; Barbier, J.; Isnard, P.; Blanchard, G. *Catal. Today* **1996**, *29*, 317-322.

(67) Imamura, S.; Nakamura, M.; Kawabata, N.; Yoshida, J.; Ishida, S. *Ind. Eng. Chem. Prod. Res. Dev.* **1986**, *25*, 34-37.

(68) Nikolaou, N.; Abatzoglou, N.; Gasso, S.; Chornet, E. *Can. J. Chem. Eng.* **1994**, *72*, 522-533.

(69) Cybulski, A.; Trawczynski, J. *Appl. Catal., B* **2004**, *47*, 1-13.

(70) Yang, S.; Zhu, W.; Li, X.; Wang, J.; Zhou, Y. *Catal. Commun.* **2007**, *8*, 2059-2063.

(71) Wang, J.; Zhu, W.; Yang, S.; Wang, W.; Zhou, Y. *Appl. Catal., B* **2008**, *78*, 30-37.

(72) Rivas, F. J.; Kolaczkowski, S. T.; Beltrán, F. J.; Mclurgh, D. B. *Chem. Eng. Sci.* **1998**, *53*, 2575-2586.

(73) Quintanilla, A.; Casas, J. A.; Mohedano, A. F.; Rodríguez, J. J. *Appl. Catal., B* **2006**, *67*, 206-216.

(74) Devlin, H. R.; Harris, I. J. *Ind. Eng. Chem. Fundam.* **1984**, *23*, 387-392.

Chapter 5: Conclusions and Future Work

5.1 Conclusions

The first goal of this dissertation is to show that polyelectrolyte multilayer films provide an excellent means for immobilizing metal nanoparticles on porous supports while still allowing access to the catalytic surface of the metal nanoparticles. Chapter 2 clearly shows that preformed citrate-stabilized Au nanoparticles exhibit the same catalytic activity when immobilized on 100 mesh alumina powder and when they are unsupported, semi-homogeneous catalysts. These data demonstrate that the polyelectrolyte does not inhibit the nanoparticle catalysis. Moreover, synthesizing the nanoparticles prior to immobilization on a support allows control over important properties including nanoparticle size, shape, composition, surface charge, and stabilizing ligand.

Chapter 3 presents in-situ synthesis of nanoparticles through layer-by-layer (LbL) deposition with polyelectrolyte solutions containing Pd^{2+} ions and subsequent reduction of these ions using $NaBH_4$. This method is advantageous in that it typically yields smaller particle sizes than formation of nanoparticles in solution. Additionally, the in situ technique is applicable to a variety of metal ions (eg. Pd^{2+}, Au^{3+}, Pt^{2+}, Ag^{+}, etc.), and affords control over particle size by simply changing the concentration of the metal ion in the polyelectrolyte deposition solution. Pd nanoparticles formed in this way show high catalytic activities in the hydrogenation of allylic compounds with size-dependent selectivity in the hydrogenation of mono vs. disubstituted double bonds.

In addition to alumina powder supports, LbL modification readily allows modification of porous membrane supports. The catalytic activity of Au nanoparticles in the reduction of 4-nitrophenol was the same for nanoparticles immobilized on alumina, nylon, and polycarbonate membranes despite the differences in material, pore size, and pore morphology. More importantly, the normalized rate constants of Au nanoparticles immobilized in membranes were the same as Au nanoparticles in solution. These results demonstrate the versatility of LbL deposition and provide further confirmation that LbL immobilization of nanoparticles does not result in a decrease in catalytic activity.

The second goal of this dissertation is to show that porous membranes are attractive supports for catalytic nanoparticles. Chapter 2 demonstrates that membranes operated as flow-through contactors facilitate contact between liquid phase reactants and the solid catalyst and eliminate diffusion limitations. These membranes achieved >99% conversion of 4-nitrophenol to 4-aminophenol at fluxes as high as 0.53 mL/cm^2-sec, and conversion was controlled by adjusting the flow rate of solution through the membrane. Control over reaction conversion was most apparent in the reduction of substituted nitroaromatics such as 2-nitrotoluene, where the ratio of nitroso to amine products was greatly affected by the residence time of the solution in the membrane. These nanoparticle-containing membranes also selectively reduced nitro groups in nitroaromatic compounds containing other reducible functionalities.

In an effort to find greener applications and milder reaction conditions for membrane catalysts, we examined hydrogenation reactions in chapter 3.

Membranes modified with citrate-stabilized Pd nanoparticles effectively catalyzed the hydrogenation of allyl alcohol and several nitroaromatic compounds when operated as flow-through contactors. In these reactions, the extent of conversion was primarily limited by the solubility of hydrogen rather than the reaction kinetics, which was demonstrated by the negligible decrease in conversion when increasing the flow rate by a factor of five.

Chapter 4 shows that the interfacial contactor configuration can overcome this solubility limitation to some extent. Tubular ceramic membranes modified with citrate-stabilized Pt nanoparticles showed high activities in the wet air oxidation of several model pollutants. This high activity is due in part to the ability to control the location of the gas/liquid interface within the membrane, which leads to a high surface area for contact between the gaseous and liquid reactants and the solid catalyst. The LbL technique provides more control over Pt location, limiting deposition to the skin layer where there is a higher surface area for catalyst loading and thus more area for contact between all three phases.

This work has primarily applied LbL deposition to effectively immobilize catalytic noble metal nanoparticles on a wide variety of support materials with a major focus on membranes. Though the systems explored thus far are attractive, there are many more potential applications for LbL deposition of nanoparticle catalysts. Furthermore, many characteristics of these nanoparticle systems are not completely understood and thus require further investigation into reaction mechanisms and nanoparticle properties. The remainder of this chapter

discusses some promising directions for this research. Some potential new directions include the development of novel membrane materials for large-scale catalytic applications, further utilization of membrane properties or nanoparticle size to achieve selective product formation in hydrogenation reactions, and in-situ hydrogen generation with conductive nanoparticle-containing membranes to overcome H_2 solubility limitations in flow-through reactions.

5.2. Future Work

5.2.1 Modification of Polymeric Hollow Fiber Membranes for Catalytic Reactions

One of the primary limitations to working with disk-shaped membranes is the difficulty of using the membranes in large scale applications. Because flow rate and the amount of material that can be processed are directly related to the surface area of the membrane, it is important to use membrane geometries with a high surface area. Thus, polymeric hollow fiber membranes are often utilized for high-throughput applications. Hollow fiber membranes have a higher surface area per module volume than flat-sheet membranes and thus can allow extremely high fluxes in flow-through applications. Modules consisting of polymeric hollow fibers also cost much less than tubular ceramic membranes and typically have lower operating costs.

The advantages associated with polymeric hollow fiber membranes make them attractive for a wide variety of membrane applications, and as a result they are extensively used in industry for processes such as gas separation,

hydrocarbon separation, water purification, and kidney dialysis. However, relatively few studies exist in which hollow fibers act as metal nanoparticle supports for catalytic applications. The work of Vincent and Guibal focused on the use of chitosan hollow fiber membranes loaded with Pd nanoparticles for degradation of nitrophenol and nitroaniline by sodium formate.[1,2] These studies utilized hollow fiber membranes in the liquid-liquid contactor configuration. The relatively small amount of previous research in this area leaves much room to develop novel hollow fiber materials for catalytic applications.

5.2.2 Catalytic Selectivity with Pd-Containing Membranes

Chapter 3 demonstrates that Pd containing membranes work well in hydrogenation of a variety of substrates including allylic and nitroaromatic compounds. However, we did not use these membranes for selective hydrogenation of similar substrates. Even though hydrogen solubility limits the conversion in these reactions, it could be beneficial to perform hydrogenation studies on substrates containing multiple reducible functionalities. In many hydrogenation reactions, the desired product is an intermediate that we want to produce with high selectivity while still having a high conversion of substrate. In order to achieve the desired product, we want to control the reaction time and use a catalyst that preferentially reduces one functional group over another.

The interfacial contactor configuration is commonly used for hydrogenation reactions because it is easy to flow liquid through the inside of the tube, while passing gas around the outside of the tube or vice versa. There are

also a number of commercial modules available that can hold multiple tubular membranes for these reactions. Previous studies utilized interfacial contactors for hydrogenation of nitrate and nitrite,[3] α-methylstyrene,[4] nitrobenzene,[5] cinnamaldehyde,[6] and methylenecyclohexane.[7] Interfacial contactors still suffer from mass transport limitations due to diffusion into the pores, and the catalyst needs to be at or close to the phase boundary in order to be used efficiently. Interfacial contactors also offer less control over contact time, making them less effective in achieving selective product formation.

Operating membranes in flow-through mode can overcome these limitations, but it requires passing the solution through the membrane multiple times and reincorporating hydrogen into the solution between each pass. So far, only a limited number of publications describe this method for hydrogenation reactions. Schomäcker and coworkers have done the most work in this area with previous studies including the flow-through hydrogenation of α-methylstyrene, 1,5-cyclooctadiene, 1-octyne, phenyl acetylene, and geraniol with Pd-containing polymeric membranes.[8,9] In each case, the membranes demonstrated selectivity for the singly reduced products. They also studied the flow-through hydrogenation of sunflower oil[10] and 1,5-cyclooctadiene[11] with tubular ceramic membranes. Bottino and coworkers studied methylenecyclohexane under flow-through conditions with flat PVDF and tubular ceramic membranes.[7] In both cases, the isomerization product was selectively produced over the hydrogenated species. The membranes used in these previous studies still have some disadvantages including: plugging of the

membrane pores,[12] low catalyst loading (~0.6 wt%),[8] and low catalyst accessibility (< 16% of nanoparticle surface area).[13] The problem of pore plugging is not common with the membrane pore sizes used in our studies. Our method of membrane preparation also offers a simple strategy to have high catalyst loading with uniform dispersity and easy access to the catalyst sites.

Due to the limited amount of work concerning hydrogenation with catalytic membranes operated in flow-through mode, there are a wide variety of potential applications for these membranes. Chemoselective reduction of nitro groups in the presence of other reducible functional groups is an important reaction in organic synthesis. Although the hydrogenation of simple aromatic nitro compounds readily occurs with traditional commercial catalysts, the hydrogenation of nitro groups in the presence of other reducible functional groups is more challenging. Flow-through membrane hydrogenations could provide the control over residence time necessary to facilitate reduction of the nitro group to the amine while not allowing enough time for the reduction of other functionalities. The primary limitation of these flow-through reactions is the low solubility of H_2, but this can be overcome by flowing solutions at much faster flow rates. Studying the effect of flow rate on conversion and selectivity could provide insight into the kinetics of these reactions. Likewise, nanoparticle composition, size, and stabilizer may also play a role in selectivity. When studying compounds that can be selectively reduced, comparing the activity/selectivity of membrane reactors with that of slurry reactors would help show if the selectivity is only due to the catalyst properties or if the support also plays a role. Selective

hydrogenation of olefins is another important industrial process that should also be investigated.

5.2.3 Catalytic Selectivity as a Function of Nanoparticle Size

The results in chapter 3 demonstrate the strong dependence of catalyst selectivity on particle size. Future studies should focus on understanding the origin of these size effects and their applicability to other reactions. A number of literature studies suggest that selectivity may result from different substrates reacting at different sites on the nanoparticle.[14,15] For example, compounds with monosubstituted double bonds may react preferentially at edge sites while compounds with disubstituted double bonds react at terrace sites. As the nanoparticle diameter decreases, the fraction of edge sites increases relative to the number of terrace sites, particularly if the particles become defective and are not regular cubooctahedra.

The competitive hydrogenation studies in chapter 3 suggest that compounds with mono and disubstituted double bonds react at the same sites on the nanoparticles. Thus, there are two possible explanations for the enhanced selectivities with the smaller nanoparticles. First, adsorption of the surrounding polyelectrolyte to the nanoparticle may provide more steric hindrance to binding of the double bond to the particle when the nanoparticles are small. Second, changes in the electronic structure of the nanoparticles with decreasing diameter may greatly favor the binding of the monosubstituted double bond. Bhattacharjee and coworkers showed that the latter hypothesis is more likely

because the high size-dependent selectivity in hydrogenation occurs with a range of different catalyst systems including: $[PAA\text{-}Pd(0)/PEI]_3$ films on alumina, a solution containing a PAA-Pd(0)/PEI complex, and reduced $PdCl_4^{2-}$/PEI films.[16] There should be less steric constraints with the complex in solution because of more conformational freedom. Similarly, reduced $PdCl_4^{2-}$/PEI films should be less tightly packed and show less steric hindrance to binding.

Using nanoparticle systems with a range of sizes, hydrogenation of a number of different compounds can help to elucidate the origins of size-dependent selectivity. For example, adding additional substituent groups to the double bond on allyl alcohol should offer insight into the effect of steric hindrance on reactivity and selectivity with different particle sizes. Figure 5.1 shows several compounds that could be used to probe steric effects of nanoparticles in hydrogenation. Comparison of the cis and trans forms of crotyl alcohol could offer insight into the orientation of the double bond as it interacts with the nanoparticle surface. Furthermore, comparison of the hydrogenation TOFs of disubstituted double bonds with methyl, ethyl, and isopropyl substituents should provide the most information. Single substrate experiments would be useful for determining the differences in reactivity/selectivity of different substrates; however, mixed substrate experiments would be necessary to determine if different substrates react on the same catalyst sites.

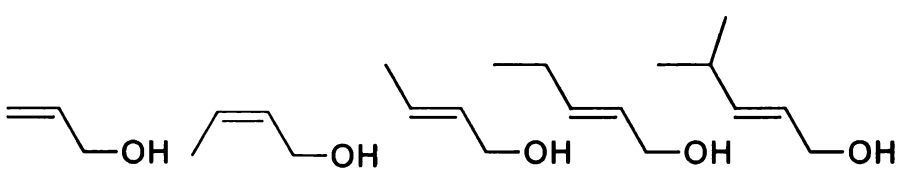

Figure 5.1 Compounds that could be used to probe steric effects in hydrogenation as a function of nanoparticle size.

The method of in-situ nanoparticle formation in polyelectrolyte multilayer films provides some control over nanoparticle size, but the size distribution is relatively wide compared to other methods. To more conclusively demonstrate size-dependent selectivity, other nanoparticle systems should be investigated. Unfortunately, the methods that produce reactive nanoparticles with diameters less than 3 nm are rare. The citrate reduction method typical yields particles with diameters > 5 nm,[17-19] whereas the Brust method gives smaller nanoparticles,[20,21] but the Brust particles are capped with thiols that decrease catalytic activity.[22,23] Dendrimer-encapsulated particles provide several advantages over the citrate or Brust methods,[24,25] the first of which is that the particles are relatively monodisperse in size, which allows for more effective evaluation of reactivity as a function of particle diameter.

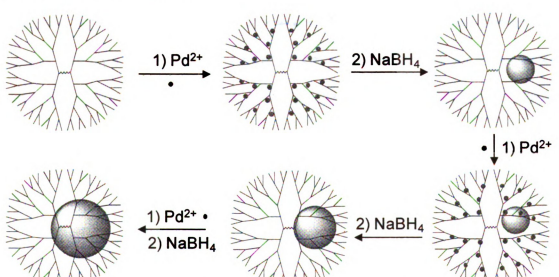

Figure 5.2 Synthesis of relatively large nanoparticles in dendrimers using multiple cycles of metal-ion loading and reduction. Higher generation dendrimers could be employed in the actual nanoparticle formation.

Diameters of nanoparticles in dendrimers are typically 1 to 3 nm, which is in the region of interest for selective hydrogenation of monosubstituted double bonds, but it would also be useful to produce larger particles to have a wider size range. Synthesis of larger particles would likely require a technique in which the nanoparticles are prepared in a multistep process as shown in Figure 5.2. The metal ions can be loaded in the dendrimer with an approximate binding ratio of 1 metal ion per tertiary amine group and then reduced with $NaBH_4$ to form nanoparticles. After dialysis to remove the reducing agent, repetition of this process several times should produce larger particles in a controlled fashion. Dendrimer-containing nanoparticles can be deposited in polyelectrolyte films or used directly in solution. Previous work by Crooks and coworkers suggests that TOFs may decline slightly for particles less than 2 nm in diameter,[25,26] but selectivities for hydrogenation of mono and multisubstituted double bonds have not been investigated with these systems. Several studies suggest that there is an optimum nanoparticle size to achieve high reactivity, but relatively few studies have investigated selectivity.[27,28]

Regardless of whether steric or electronic effects are dominant in altering reactivities, the selectivity of nanoparticles as a function of size should extend to a number of reactions. Again, chemoselective hydrogenation of nitroaromatic compounds offers an interesting reaction to study. It would be beneficial to determine if nanoparticle size plays a role in which groups are more easily reduced. Initial results by Bhattacharjee suggest that even relatively large nanoparticles show high selectivity in the reduction of nitrobenzaldehyde to

aminobenzaldehyde.[29] With a [PAA-Pd(0)/PEI]$_3$ film containing 3.4 nm diameter Pd nanoparticles, 94% of the nitrobenzaldehyde is converted to aminobenzaldehyde. In contrast, with Pd on carbon, the doubly reduced species accounts for 60% of the product. Future studies should investigate the selectivity as a function of nanoparticle size for a number of different nitroaromatic compounds.

5.2.4 Electrocatalytic Hydrogenation with Pd-Containing Membranes

We are particularly interested in using Pd-containing membranes for liquid-phase hydrogenation because these reactions have fast kinetics and are used in a wide range of applications in the pharmaceutical, petrochemical, fine chemical, and wastewater treatment industries.[30-32] Membrane-based hydrogenation is attractive for minimizing mass-transport limitations and performing continuous reactions, but the low solubility of H_2 limits conversion. Above, we mentioned the two most common methods for overcoming this limitation: passing the solution through the membrane multiple times with reincorporation of hydrogen into the solution between each pass and using an interfacial contactor configuration. The former case doesn't really solve the problem unless extremely high flow rates are used. The interfacial contactor configuration is attractive, but reactions are still likely to be limited by mass transport of substrate to the catalyst, and the catalyst loading may be small.

In-situ hydrogen generation could offer a better solution for overcoming this limitation as it would provide a constant supply of hydrogen inside the

membrane pores during the reaction. If the hydrogen generation occurs faster than the reaction kinetics, then flow-through hydrogenation reactions would no longer have H_2 solubility limitations. To generate hydrogen in-situ, Pd nanoparticle-containing membranes must be conductive, and the hydrogen should be produced at the surface of the nanoparticles where the hydrogenation will take place.

Electrocatalytic hydrogenation occurs when hydrogen is produced at the surface of an electrode by electrolysis of water or reduction of protons.[33-35] In addition to avoiding the need for high hydrogen pressures, electrocatalytic hydrogenation has the potential to be environmentally friendly because it uses ambient temperature, aqueous solutions, and electrons rather than chemical reducing agents. In conventional electrode systems, hydrogen production occurs at the working electrode, but additional stirring and/or diffusion of the substrate to the electrode surface is necessary to facilitate the reaction.[36-43] Pintauro and coworkers examined the electrochemical hydrogenation of vegetable oil using fuel cell membranes to supply electrochemically generated hydrogen.[44-47] Remarkably, when H_2 was fed to the anode and hydrogen was subsequently generated at the cathode, the fraction of H_2 that hydrogenated fatty acid double bonds ranged from 45 to 97%.[46] Thus, electrochemically generated hydrogen can, in principle, be used very efficiently for hydrogenation. Performing flow-through electrocatalytic hydrogenation with catalytic membranes (Figure 5.3) will have the same advantages as traditional electrocatalytic hydrogenation plus the added benefits of using convective transport through membrane pores.

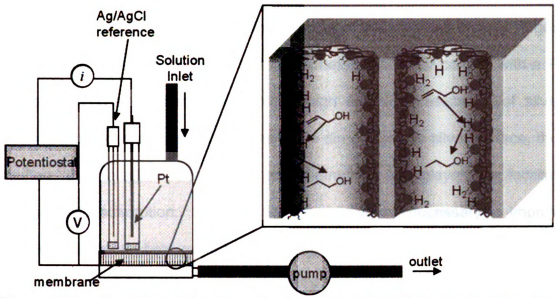

Figure 5.3 Experimental setup for examining flow-through electrocatalytic hydrogenation in Pd nanoparticle-containing membranes. Hydrogen is electrochemically generated in the conductive, nanoparticle-containing membrane. The hydrogenation of allyl alcohol to 1-propanol is shown as an example reaction.

The first step toward performing electrocatalytic hydrogenation in membranes is the development of a porous, conductive electrode capable of electrochemically producing hydrogen in aqueous media. Most synthetic membranes consist of polymeric or ceramic materials that have minimal electrical conductivity and are thus not suitable for electrochemical hydrogenation. As a test system for electrochemical hydrogenation, we investigated silver membranes (obtained from SPI supplies), which were developed primarily for other applications because of their chemical resistance and bactericidal properties. The silver membranes are highly conductive, but clean silver does not catalyze dissociation of H_2, and the activity of Ag is orders of magnitude less than the activity of Pt in the hydrolysis of water.[48,49] After modifying the surface of a silver

membrane with a monolayer of mercaptoundecanoic acid, we deposited a uniform PEI/Pd nanoparticle film inside the pores of the silver membrane. Figure 5.4 shows SEM images of silver membranes before and after coating with a Pd nanoparticle-containing film. Due to the high chemical resistance of silver, polyelectrolyte adsorption does not take place directly on the silver surface, thus requiring the initial formation of an alkanethiol monolayer to facilitate polyelectrolyte adsorption. Shorter alkanethiols may be necessary to improve the electrical contact between the electrode (Ag membrane) surface and the Pd nanoparticles.

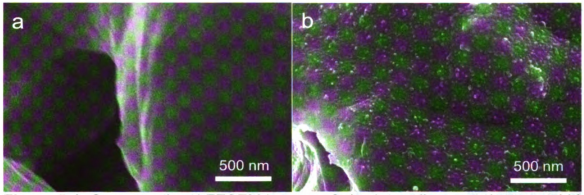

Figure 5.4 Cross-sectional FESEM images of a) a bare silver membrane and b) a silver membrane coated with a mercaptoundecanoic acid/PEI/PdNP film.

As an initial experiment to test the capability of Pd-containing Ag membranes for electrochemical hydrogen production, we performed electrocatalytic hydrogenation of allyl alcohol. To facilitate hydrogen formation and provide a conductive solution, 0.1 M HCl served as the supporting electrolyte. However, electrolytes that contain Cl^- may lead to catalyst poisoning,[50,51] so future experiments should utilize other supporting electrolytes that do not contain Cl^-. When passing a 5 mM solution of allyl alcohol through

the membrane at a flux of 0.01 mL/cm^2-sec, more than 20% of the allyl alcohol was electrocatalytically hydrogenated to 1-propanol. This is comparable to results obtained in the traditional hydrogenation reaction (bubbling the solution with H_2) with the same membrane. We obtained similar conversions in the electrocatalytic hydrodehalogenation of 4-bromophenol to phenol. Unmodified silver membranes did not allow electrochemical or traditional hydrogenation to take place.

Future studies should focus on understanding the mechanism of electrocatalytic hydrogenation in membranes so that these systems can be utilized for room-temperature hydrogenation at low pressures and higher substrate concentrations (> 0.1 M). The first step in this future work is to investigate the electrochemical generation of H_2 using disk electrodes that can be readily characterized. An important question to answer is whether H_2 is generated primarily at the nanoparticles or the electrode surface. Ideally, H_2 generation will occur exclusively at the nanoparticles because the efficiency of hydrogen utilization should be much greater if electrochemically generated hydrogen atoms could be used for hydrogenation prior to H_2 formation. This would not occur if H_2 was generated primarily at the Ag surface, because Ag is not an efficient hydrogenation catalyst.[52,53] Future studies could instead utilize carbon membranes because carbon is well known to have a relatively high overpotential for H_2 generation.

Additional studies could look at the effect of multiple nanoparticle layers on the rate of hydrogen generation. Deposition of additional layers is

straightforward on both membranes and electrodes, and chapter 2 showed that additional layers of nanoparticles increase the rates of membrane catalysis. Moreover, other studies showed that at least for the first four or five layers, the nanoparticles in polyelectrolyte films are electrochemically active.[54-57] Coverage of the Ag with multilayers of polyelectrolytes should also decrease the rate of H_2 generation at the underlying electrode.[58] Addition of a substrate such as allyl alcohol to the solution may also affect the generation of hydrogen on nanoparticle electrodes. The added substrate may shift the potential for hydrogen generation, which could be helpful in developing more energy-efficient reactions.

Both the generation of hydrogen and the rate of hydrogenation likely depend on the nanoparticle composition and size. Therefore, a study of different nanoparticle materials and sizes could be beneficial. Though Pd is most common for hydrogenation reactions,[31,59] generation of hydrogen may occur more readily at a Pt surface.[60-62] Once the ideal nanoparticle system is chosen, catalytic studies should investigate conversion and current efficiency as a function of overpotential, substrate concentration, and flow rate through the membrane. In aqueous flow-through hydrogenation reactions, hydrogen is the limiting reactant at substrate concentrations > 1 mM, but this will not likely be the case with electrochemical generation of hydrogen and high mM substrate concentrations. Higher substrate concentrations and flow rates should increase the current efficiency (utilization of adsorbed hydrogen).

5.3 Summary

In summary, polyelectrolyte multilayer films provide a convenient platform for immobilizing active and highly accessible metal nanoparticles for catalysis. Porous membranes are especially attractive supports for polyelectrolyte-stabilized metal nanoparticles as they demonstrate many advantages over conventional catalyst supports. We've demonstrated that membranes containing catalytically active metal nanoparticles effectively catalyze reduction, hydrogenation, and oxidation reactions, but they also show great promise for a number of other catalytic applications.

5.4 References

(1) Vincent, T.; Guibal, E. *Environ. Sci. Technol.* **2004**, *38*, 4233-4240.

(2) Thierry, V.; Francisco, P.; Eric, G. *J. Appl. Polym. Sci.* **2004**, *94*, 1634-1642.

(3) Centi, G.; Dittmeyer, R.; Perathoner, S.; Reif, M. *Catal. Today* **2003**, *79-80*, 139-149.

(4) Cini, P.; Harold, M. P. *AIChE J.* **1991**, *37*, 997-1008.

(5) Peureux, J.; Torres, M.; Mozzanega, H.; Giroir-Fendler, A.; Dalmon, J. A. *Catal. Today* **1995**, *25*, 409-15.

(6) Pan, X. L.; Liu, B. J.; Xiong, G. X.; Sheng, S. S.; Liu, J.; Yang, W. S. *Catal. Lett.* **2000**, *66*, 125-128.

(7) Bottino, A.; Capannelli, G.; Comite, A.; Di Felice, R. *Desalination* **2002**, *144*, 411-416.

(8) Schmidt, A.; Haidar, R.; Schomäcker, R. *Catal. Today* **2005**, *104*, 305-312.

(9) Purwanto, P.; Deshpande, R. M.; Chaudhari, R. V.; Delmas, H. *J. Chem. Eng. Data* **1996**, *41*, 1414-1417.

(10) Schmidt, A.; Schomäcker, R. *J. Mol. Catal. A: Chem.* **2007**, *271*, 192-199.

(11) Schmidt, A.; Wolf, A.; Warsitz, R.; Dittmeyer, R.; Urbanczyk, D.; Voigt, I.; Fischer, G.; Schomäcker, R. *AIChE J.* **2008**, *54*, 258-268.

(12) Reif, M.; Dittmeyer, R. *Catal. Today* **2003**, *82*, 3-14.

(13) Gröschel, L.; Haidar, R.; Beyer, A.; Reichert, K.-H.; Schomäcker, R. *Catal. Lett.* **2004**, *95*, 67-75.

(14) Freund, H. J.; Baumer, M.; Libuda, J.; Risse, T.; Rupprechter, G.; Shaikhutdinov, S. *J. Catal.* **2003**, *216*, 223-235.

(15) Silvestre-Albero, J.; Rupprechter, G.; Freund, H. J. *J. Catal.* **2006**, *240*, 58-65.

(16) Bhattacharjee, S.; Dotzauer, D. M.; Bruening, M. L. *J. Am. Chem. Soc.* **2009**, *131*, 3601-3610.

(17) Turkevich, J.; Kim, G. *Science* **1970**, *169*, 873-9.

(18) Turkevich, J.; Miner, R. S., Jr.; Babenkova, L. *J. Phys. Chem.* **1986**, *90*, 4765-7.

(19) Turkevich, J.; Stevenson, P. C.; Hillier, J. *Discussions of the Faraday Society* **1951**, *No. 11*, 55-75.

(20) Brust, M.; Walker, M.; Bethell, D.; Schiffrin, D. J.; Whyman, R. *J. Chem. Soc., Chem. Commun.* **1994**, 801-2.

(21) Brust, M.; Fink, J.; Bethell, D.; Schiffrin, D. J.; Kiely, C. *J. Chem. Soc., Chem. Commun.* **1995**, 1655-1657.

(22) Alvarez, J.; Liu, J.; Roman, E.; Kaifer, A. E. *Chem. Commun.* **2000**, 1151-1152.

(23) Eklund, S. E.; Cliffel, D. E. *Langmuir* **2004**, *20*, 6012-6018.

(24) Kim, Y.-G.; Oh, S.-K.; Crooks, R. M. *Chem. Mater.* **2004**, *16*, 167-172.

(25) Niu, Y.; Yeung, L. K.; Crooks, R. M. *J. Am. Chem. Soc.* **2001**, *123*, 6840-6846.

(26) Oh, S.-K.; Niu, Y.; Crooks, R. M. *Langmuir* **2005**, *21*, 10209-10213.

(27) Doyle, A. M.; Shaikhutdinov, S. K.; Freund, H.-J. *Angew. Chem. Int. Ed.* **2005**, *44*, 629-631.

(28) Valden, M.; Lai, X.; Goodman, D. W. *Science* **1998**, *281*, 1647-1650.

(29) Bhattacharjee, S. PhD Dissertation, Michigan State University, 2008.

(30) Bond, G. C. *Chem. Ind.* **1967**, 2018-25.

(31) Molnar, A.; Sarkany, A.; Varga, M. *J. Mol. Catal. A: Chem.* **2001**, *173*, 185-221.

(32) Hoelderich, W. F. *Catal. Today* **2000**, *62*, 115-130.

(33) Chapuzet, J. M.; Lasia, A.; Lessard, J. *Electrocatalysis* **1998**, 155-196.

(34) Fuchigami, T.; Tajima, T. *Electrochemistry* **2006**, *74*, 585-589.

(35) Lessard, J. *Chemical Industries* **2005**, *104*, 3-17.

(36) Cirtiu, C. M.; Brisach-Wittmeyer, A.; Menard, H. *J. Catal.* **2006**, *245*, 191-197.

(37) Cirtiu, C. M.; Brisach-Wittmeyer, A.; Menard, H. *Catal. Commun.* **2007**, *8*, 751-754.

(38) Cirtiu, C. M.; Hassani, H. O.; Bouchard, N.-A.; Rowntree, P. A.; Menard, H. *Langmuir* **2006**, *22*, 6414-6421.

(39) Dalavoy, T. S.; Jackson, J. E.; Swain, G. M.; Miller, D. J.; Li, J.; Lipkowski, J. *J. Catal.* **2007**, *246*, 15-28.

(40) Vago, M.; Williams, F. J.; Calvo, E. J. *Electrochem. Commun.* **2007**, *9*, 2725-2728.

(41) Chen, G.; Wang, Z.; Yang, T.; Huang, D.; Xia, D. *J. Phys. Chem. B* **2006**, *110*, 4863-4868.

(42) Do Amaral Ferraz Navarro, D. M.; Navarro, M. *J. Chem. Educ.* **2004**, *81*, 1350-1352.

(43) Korotaeva, L. M.; Rubinskaya, T. Y. *Electrochemistry* **2005**, 1-22.

(44) An, W.; Hong, J. K.; Pintauro, P. N. *J. Appl. Electrochem.* **1998**, *28*, 947-954.

(45) An, W.; Hong, J. K.; Pintauro, P. N.; Warner, K.; Neff, W. *J. Am. Oil Chem. Soc.* **1999**, *76*, 215-222.

(46) Pintauro, P. N.; Gil, M. P.; Warner, K.; List, G.; Neff, W. *Ind. Eng. Chem. Res.* **2005**, *44*, 6188-6195.

(47) Warner, K.; Neff, W. E.; List, G. R.; Pintauro, P. *J. Am. Oil Chem. Soc.* **2000**, *77*, 1113-1117.

(48) Mohammad, A. B.; Yudanov, I. V.; Lim, K. H.; Neyman, K. M.; Rosch, N. *J. Phys. Chem. C* **2008**, *112*, 1628-1635.

(49) Uchida, T.; Mogami, H.; Yamakata, A.; Sasaki, Y.; Osawa, M. *J. Am. Chem. Soc.* **2008**, *130*, 10862-+.

(50) Mendyka, B.; Musialik-Piotrowska, A.; Syczewska, K. *Catal. Today* **1992**, *11*, 597-610.

(51) Rasmussen, S. B.; Kustov, A.; Due-Hansen, J.; Siret, B.; Tabaries, F.; Fehrmann, R. *Appl. Catal., B* **2006**, *69*, 10-16.

(52) Emmett, P. H.; Skau, N. *J. Am. Chem. Soc.* **1943**, *65*, 1029-35.

(53) Sarkany, A.; Revay, Z. *Appl. Catal., A* **2003**, *243*, 347-355.

(54) Chirea, M.; Garcia-Morales, V.; Manzanares, J. A.; Pereira, C.; Gulaboski, R.; Silva, F. *J. Phys. Chem. B* **2005**, *109*, 21808-21817.

(55) Cho, J.; Caruso, F. *Chem. Mater.* **2005**, *17*, 4547-4553.

(56) Zhao, J.; Bradbury, C. R.; Fermin, D. J. *J. Phys. Chem. C* **2008**, *112*, 6832-6841.

(57) Zhao, J.; Wasem, M.; Bradbury, C. R.; Fermin, D. J. *J. Phys. Chem. C* **2008**, *112*, 7284-7289.

(58) Harris, J. J.; Bruening, M. L. *Langmuir* **2000**, *16*, 2006-2013.

(59) Tungler, A.; Fogassy, G. *J. Mol. Catal. A: Chem.* **2001**, *173*, 231-247.

(60) Lofrano, R. C. Z.; Queiroz, J. V.; Romero, J. R. *J. Mol. Catal. A: Chem.* **2001**, *174*, 231-238.

(61) Machida, M.; Sato, K.; Ishibashi, I.; Abul Hasnat, M.; Ikeue, K. *Chem. Commun.* **2006**, 732-734.

(62) Pontolio, J. O. S.; Purgato, F. L. S.; Romero, J. R. *Quim. Nova* **2004**, *27*, 550-554.

MICHIGAN STATE UNIVERSITY LIBRARIES
3 1293 03063 2651